

PHOTOCOPIED FROM THE ORIGINAL

© 1975

YEN-SHENG EDMUND SUN

ALL RIGHTS RESERVED

PROXIMITY EFFECT IN Ag-Pb ALLOYS

Thesis by
Yen-Sheng Edmund Sun

In Partial Fulfillment of the Requirements
For the Degree of
Doctor of Philosophy

California Institute of Technology
Pasadena, California

1975
(Submitted August 19, 1974)

To Jane and my parents

ACKNOWLEDGMENTS

The author wishes to express his deepest appreciation to Professor Pol Duwez and Doctor Chang Chyi Tsuei for their highly inspirational advice and never-ending understanding and encouragement throughout this work. Technical assistance from C. Geremia, S. Kotate, H. H. So, J. A. Wysocki, F. Youngkin, and M. Yung is also gratefully acknowledged. The author also wants to thank Mrs. A. Bressan for typing the thesis drafts and Mrs. Virginia Conner and Mrs. Roberta Duffy for typing the final thesis.

This work was made possible by grants from the United States Atomic Energy Commission.

Last, but not least, the author wishes to express his sincere gratitude to his wife, Jane, for her encouragement during the course of this work.

ABSTRACT

The superconducting properties and the microstructure of the $\text{Ag}_{100-x}\text{Pb}_x$ alloys, $1 \leq x \leq 5$, prepared by rapid quenching from the liquid state with and without subsequent heat treatments, have been studied. The x-ray diffraction measurements show that supersaturated solid solutions of Pb in Ag can be obtained up to 3.2 at. % Pb as compared to less than 0.1 at. % Pb at equilibrium. It was found that by suitable heat treatment it is possible to vary the size and distribution of the Pb precipitates in the Ag matrix and reproducible superconducting properties in the alloy can be observed. The superconducting transition temperature of these samples can be qualitatively explained by the Silvert and Singh's theoretical calculation. The theory developed for the case of layer structure can be extended to three dimensions to explain the critical current versus temperature behavior. The critical current versus field behavior of these alloys can be explained by the modification of the Josephson effect. Combining these results together with the critical magnetic field measurements and the microstructure studies of the alloys, it can be concluded that the three-dimensional proximity effect is the main mechanism for the superconductivity in the Ag-Pb alloys. Based on the Hilsch empirical formula which was based on experimental results obtained on layer structures, the experimental data in this investigation show that the electron-phonon-electron interaction in silver is attractive. The interaction parameter NV obtained is approximately 0.06, which would lead to a value of 10^{-5} °K for the superconducting transition temperature of Ag. These values are in agreement with other determinations which

were done on vapor-deposited metallic film sandwiches. Hence, the Hilsch empirical relation valid for layer structures is also valid in the three-dimensional case. Because the transition temperature and the critical current can be varied in a wide range by controlling the heat treatments, the Ag-Pb superconductors might have some useful applications.

TABLE OF CONTENTS

Part	Title	Page
I	INTRODUCTION	1
II	EXPERIMENTAL METHODS	4
	A. Material Choices	4
	B. Alloy Preparations	4
	C. Quenching Technique	5
	D. X-Ray Diffraction	5
	E. Heat Treatment	6
	F. Resistivity Measurement	6
	G. Critical Current Measurement	6
	H. Magnetoresistivity	9
	I. Superconducting Volume Fraction	9
	J. Metallographic Studies	12
III	EXPERIMENTAL RESULTS	14
	A. Lattice Parameter	14
	B. Transformation of the Supersaturated Solid Solution	16
	C. Resistivity Measurement	19
	1. Resistivity versus temperature	19
	2. Magnetoresistivity	33
	D. Critical Current Density (J_c)	35
	1. Critical current density versus temperature in earth magnetic field	35

Table of Contents (Cont'd)

Part	Title	Page
	2. Critical current density versus temperature measurement under applied magnetic field	38
	3. Critical current density versus field and the method to choose samples which exhibit proximity effect	43
E.	Superconducting Volume Fraction (SVF)	46
	1. a. c. bridge results	46
	2. Magnetization measurement results	52
F.	Metallographic Studies	55
G.	Relation Between Superconducting Transition Temperature and the Dimension of the Pb Precipitates	67
IV	DISCUSSION	70
	A. Relevant Theory about the Occurrence of Superconductivity for the Samples in this Investigation	70
	B. Critical Current and Superconducting Volume Fraction	85
	1. Model and experimental results of critical current versus temperature	85
	2. The effect of external magnetic field on critical current	97
	3. Superconducting volume fraction (SVF)	103

Table of Contents (Cont'd)

Part	Title	Page
C.	Demagnetization Effect and Critical Magnetic Field	107
	1. Demagnetization effect in H_c measurement	107
	2. Critical magnetic field (H_b)	112
D.	Determination of the Superconducting Transition Temperature and the Effective Electron-Electron Interaction Parameter in Ag	113
E.	Kinetics of Transformation of the Ag-Pb Metastable Solid Solution	117
	1. Amount of transformation and the activation energy	117
	2. The precipitation process of the phase from the Ag-Pb supersaturated solid solution	124
V	SUMMARY AND CONCLUSIONS	127
	REFERENCES	129
	APPENDIX I	134

I. INTRODUCTION

From simple quantum theory it is known that a particle (or a wave packet) can penetrate through a potential barrier. There are many examples of this kind in nature; devices have even been made by using this idea, for example, the tunnel diode. Superconductivity is due to an attractive potential between two electrons via an electron-phonon interaction, which in turn generates the electron bound pairs called Cooper pairs⁽¹⁾. It can be expected that this "pair" can also penetrate through potential barriers which have a weaker electron-phonon-electron attractive interaction or even have a repulsive interaction. This potential barrier may be an insulator, a semiconductor, or a metal. These kinds of superconductor-normal material (SN) or superconductor-normal material-superconductor (SNS) sandwiches can carry a supercurrent, provided N is thin enough and the temperature is low enough. The probability amplitude $F = \langle \psi_{\uparrow} \psi_{\downarrow} \rangle$ for finding Cooper pairs is expected to decay exponentially in the barrier, as is the case of a single particle (wave packet) in the potential barrier.

Theories indicate that this is indeed a good approximation⁽²⁻⁴⁾. If the barrier is an insulator, this pair tunneling effect is called the Josephson effect⁽⁵⁻⁷⁾, which has many interesting characteristics⁽⁷⁻⁹⁾. If the barrier is a normal metal, this pair tunneling effect is called the "proximity effect." The penetration depth of a Cooper pair in an insulator is usually of the order of 20 - 50 Å, while in normal metals the distance is typically 1000 Å and can be made even larger if desired⁽¹⁰⁾. Because the penetration depth of a Cooper pair is so large in normal metals, it is convenient to work with metallic

films of rather large thicknesses where the chemical composition and the metallurgical structure can be controlled with reasonable accuracy. The first "proximity effect" experiment was performed by H. Meissner⁽¹¹⁾ in 1960. Since then, there has been a large amount of work done on the theories and measurements of superconducting transition temperatures and on supercurrents of vapor-deposited metallic film sandwiches⁽¹²⁻³³⁾. Besides the pair tunneling phenomenon in the proximity junction, theories^(3, 16) also suggest that by measuring the superconducting transition temperature or critical current, the effective electron-phonon-electron interaction can be obtained.

The NS or SNS sandwiches are effectively a one-dimensional structure in terms of the pair tunneling effect. Studies have very rarely been done in other dimensions. The first three-dimensional proximity junctions were manufactured by Raub and Raub in 1965⁽³⁶⁾ by simply annealing the electrolytic supersaturated solid solution of Cu-Pb. By electron-microscopic investigation they observed that Pb particles were distributed throughout the Cu matrix. By changing the annealing temperature and annealing time they could control the particle size. Unfortunately, they only measured the T_c with the magnetic induction method, electrical measurements such as electrical resistivity versus temperature; critical current and critical field measurements are missing. Also, some of their annealing temperatures are higher than the Pb melting temperature. This might lead to a superconducting short circuit of Pb filaments in the sample. Besides Raub and Raub, Tsuei and Newkirk⁽³⁸⁾ have tried using materials like Cu-Nb in the as-cast state to study the three-dimensional

proximity effect. They did measure the T_c electrically. However, it is hard to control the size of the superconducting particle and interparticle distance in the as-cast state.

In this investigation, the $Ag_{100-x}Pb_x$ system where $1 \leq x \leq 5$ was studied. The technique to convert the alloy into a suitable proximity junction will be presented in the next chapter. Electrical resistivity measurements, critical current measurements, critical field measurements, and superconducting volume measurements were performed to study the superconducting properties. X-ray diffraction and SEM metallographic studies were used to study the process of precipitation of Pb in the Ag matrix. Results show the size of the Pb particles and interparticle distance can be controlled; therefore, the transition temperature and critical current can be controlled. Models based on the extension of one-dimensional theories were used to explain the experimental results. An effective electron-phonon-electron interaction in Ag was estimated, which was found comparable with other investigators' results. Finally, the advantage of using a three-dimensional structure as compared to a one-dimensional structure in utilizing the proximity effect is shown in Appendix I.

II. EXPERIMENTAL METHOD

A. Material Choices

The $\text{Ag}_{100-x}\text{Pb}_x$ system with $1 \leq x \leq 5$ was chosen in this investigation for the following reasons.

(a) The maximum mutual solid solubility of Pb and Ag (0.1 at. % Ag in Pb and 0.1 at. % Pb in Ag at 200°C) is quite low. The maximum solid solubility of Pb in Ag obtainable by quenching was found to be about 3 at. %. By subsequent annealing, it was then possible to control the interparticle size and distance of the Pb precipitates in the Ag matrix which is necessary for creating a proximity junction.

(b) It is possible to establish an inherent electrical contact, because of the metallurgical bonding between Pb and Ag.

(c) The dimensions of the quenched sample can be accurately measured. This leads to an accurate measurement of the resistivity, which in turn gives an estimation of the mean free path in the sample.

(d) Pb has a conveniently high superconducting transition temperature.

B. Alloy Preparations

All the alloys used in this investigation were prepared by induction melting of appropriate amounts of the following constituents:

<u>Element</u>	<u>Source of Supply</u>	<u>Purity</u>
Ag	Englehard Industries, Inc.	99.99%
Pb	Johnson Matthey and Co.	99.9995%

The elements for each alloy were placed in a fused quartz crucible, evacuated, flushed with argon, and refilled to atmospheric pressure with argon (99.99% purity), then melted in an induction

furnace. After final weighing, the alloys were cast into 2 mm rod using quartz tubing. The weight loss following melting was less than 0.2%, so the nominal alloy compositions were taken as the actual ones.

C. Quenching Technique

The supersaturated solid solution of Pb in Ag was obtained by "piston and anvil technique" developed by Pietrokowski⁽³⁵⁾. The foils produced by this technique were about 1 to 2 cm in diameter and 50 μm to 100 μm thick.

D. X-ray Diffraction

Since it is difficult to file these samples into a powder, a foil was first cut into a rectangular shape about 1 mm \times 6 mm with a Debye-Scherrer camera. Typical exposure time is about 4 hours at 45 KV and 20 mA in nickel-filtered copper radiation. Exposed films are developed according to the standard procedure. The films were then read on a film reader. The lattice parameter and its estimated uncertainty were determined by the Nilson-Riley extrapolation function. By scanning electron-microscopic and further x-ray diffraction studies, the grain size in sample foils was estimated to be about 10 μm or less. Therefore, using a foil instead of a powder in the Debye-Scherrer camera to determine the lattice spacing was justified. The intensity of the Pb (111) line and the Ag (111) line of annealed foils was determined by using the Norelco diffractometer in $\text{CuK}\alpha$ radiation at an angular displacement of 0.05° (2θ) in 150 seconds.

For very accurate measurement of the width intensity and position of the peak, an angular displacement of 0.001° (2θ) in 30 seconds was used.

E. Heat Treatment

Samples which need to be heat-treated were sealed in an evacuated pyrex glass tube, then put into a furnace in which the temperature was controlled to within 5°C by using a controlled and a chromel versus alumel thermocouple as reference.

F. Resistivity Measurement

Resistivity versus temperature experiments were performed using the standard four point probe method. Samples were cut into an approximately $0.8\text{ cm} \times 0.2\text{ cm}$ rectangular shape. Pure platinum wire was then spot-welded on the specimens. The samples were then mounted on a low temperature probe. Current was supplied by a PAR voltage/current reference source (model TC-100 2BRC) with an accuracy of $\pm 0.005\%$ (range from 0 - 200 mA) or a HP 6177B d. c. current source (accuracy $\pm 1\%$, range 0 - 500 mA). The current and potential were measured by a Dana 5800 DVM with an accuracy of $\pm 0.1\ \mu\text{v}$. Only the potential was measured, the current being obtained from the potential drop across a standard resistor of $0.05\ \Omega$. Thermal gradient effects were minimized by current reversal. The temperature was measured by a calibrated Ge crystal (useful range from 1.2°K to 77°K) and a copper - constantan thermocouple (useful range from 77°K to room temperature).

G. Critical Current Measurement

(a) Critical current versus temperature at earth magnetic field. The experimental set-up of this measurement is the same as the resistivity measurement except that the current was allowed to vary. The critical current was defined as the current which gave rise

to a potential difference of $1 \mu\text{v}$ between the contacts. By changing this voltage criterion by an order of magnitude, the critical current changed by less than a factor of two.

(b) Critical current versus temperature with magnetic field applied and critical current versus field measurement. For these experiments, the specimen was mounted on a probe as shown in Fig. 1. The specimen and the current leads were mounted between two heaters which were made of copper and were hemispherical in cross section. The heater wires were wound non-inductively on the copper pieces.

A calibrated GaAs temperature sensor made by Lake Shore Cryogenics was placed under the specimen. Wood's metal was used to seal the entire heater-specimen assembly in a cylindrical canister. The canister was evacuated and back-filled to a partial pressure with He gas to improve the heat exchange with the liquid He bath. A temperature controller was used to control the temperature of the heater-specimen assembly to within 0.1°K . The probe was then centered in a Varian 12" magnet. The magnetic field was measured by a Bell 640 incremental Gaussmeter and a Varian proton resonance device.

The sample was measured with the magnetic field both perpendicular and parallel to the current flow. Current in the range from 0 to 500 mA was supplied by the same current supply used in the resistivity measurements. In addition, a Kepco d. c. power supply was used to obtain higher current values. Voltage across the sample was measured by a Dana 5800 DVM with a resolution of $\pm 0.1 \mu\text{v}$.

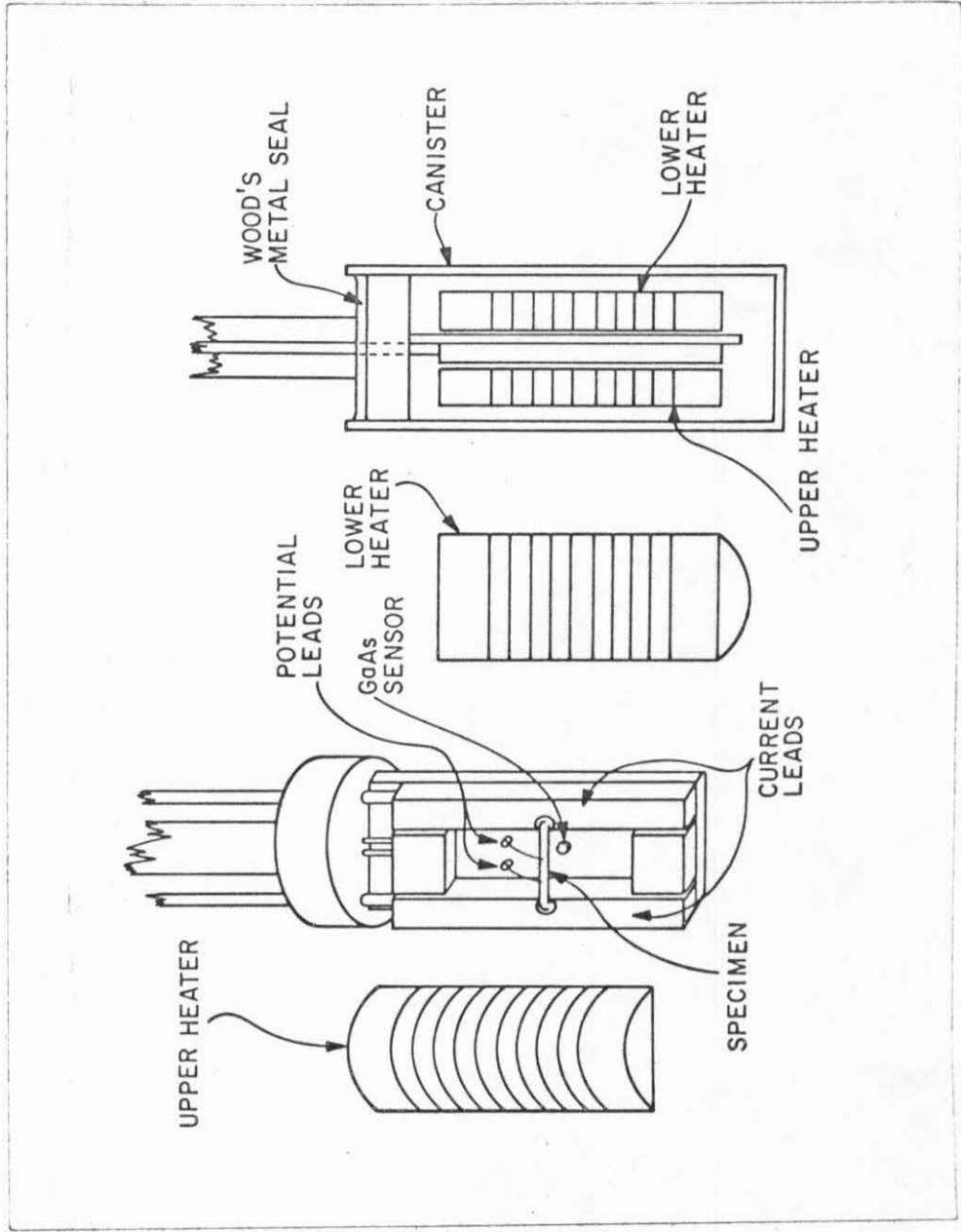


Fig. 1. Schematic diagram of the probe used for measuring critical current density as a function of both field and temperature.

Again, the critical current was defined as the current which gave rise to a potential difference of $1 \mu\text{v}$.

H. Magnetoresistivity

The experimental apparatus for the magnetoresistivity was the same as that used for the critical current versus field. However, for these measurements the current was fixed and voltage across the sample was recorded as the magnetic field was varied.

I. Superconducting Volume Fraction

(a) a. c. bridge method. The bridge circuit used in this investigation is based on the design used in the superconducting material division of Bell Telephone Laboratory. A schematic diagram of the bridge is shown in Fig. 2(a), and its equivalent circuit is shown in Fig. 2(b). a PAR lock-in amplifier was used as a null detector.

A sample in the form of small pieces and a Nb particle with a known mass were sealed into a teflon tube, which in turn was inserted into the sample coil. The bridge was balanced at 10°K . The temperature was then decreased. Because of the Meissner effect in the sample, the bridge became unbalanced at temperatures below the transition temperature. The amount of sample used in this experiment was usually about 5 mg to 20 mg, which has an equivalent volume normally about 5 per cent or less of the volume of the coil. From simple circuit analysis, the superconducting volume fraction X can be related to the unbalanced voltage as measured by the lock-in amplifier by the following formula:

$$X(T) = \frac{\text{volume of the Nb particle} \times [\Delta V \text{ (due to the sample at temperature } T)]}{\text{volume of the sample} \times [\Delta V \text{ (due to the Nb particle)]}$$

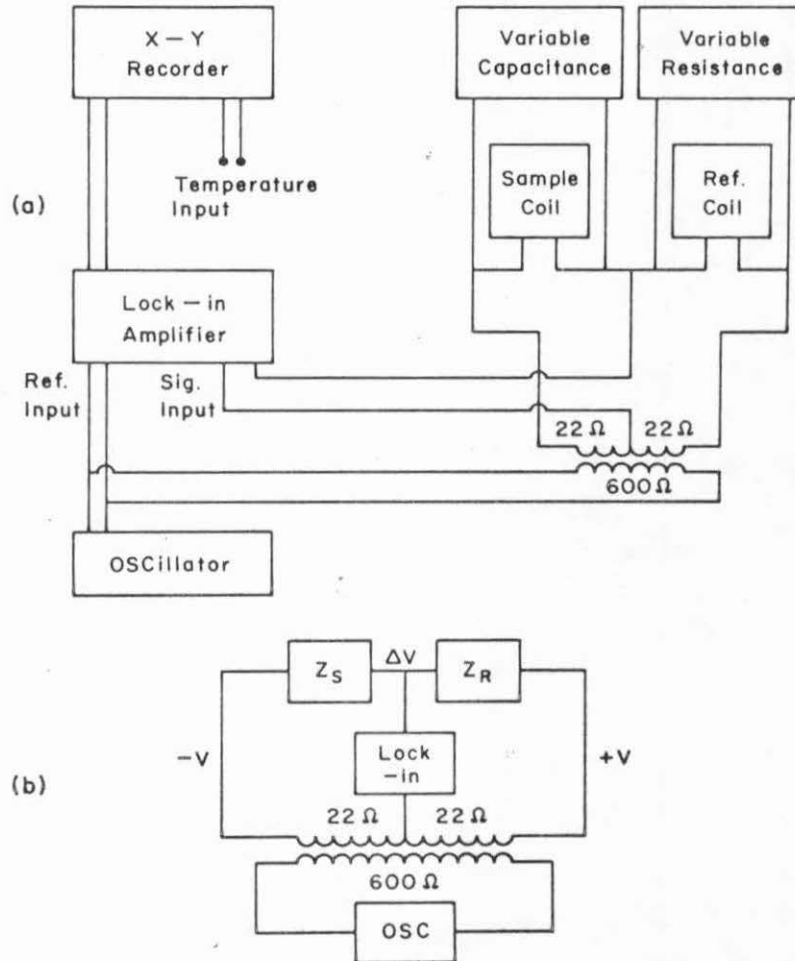


Fig. 2. (a) Block diagram of equipment used for measuring the superconducting volume fraction. (b) The equivalent circuit of (a).

where the ΔV is the unbalanced voltage which was measured by the lock-in amplifier.

(b) Magnetization measurement. Since the Ag-Pb system is a Type I superconductor in nature (see discussion, section C), $M = -\frac{X(H, T)}{4\pi} H$, where $X(H, T)$ is the superconducting volume fraction which is a function of both the magnetic field and the temperature. If M versus H can be measured at a given temperature, then x as a function of H can be obtained at that temperature. The measurements of M versus H can be deduced from the susceptibility versus H measurements. The measurements of susceptibility were made by using a 6-inch electromagnet equipped with a constant force pole cap. The force gradient was $10.25 \text{ (KOe)}^2/\text{cm}$ for 0.4 inches under a pole piece gap of 1 inch. The force exerted on the sample was measured using a Cahn null balance with a sensitivity of 5 microvolts for 0.1 microgram, at an accuracy of 10 per cent. Temperature was measured by a calibrated Ge crystal, sensitive to $\pm 0.05^\circ\text{K}$ at low temperatures ($T < 10^\circ\text{K}$).

The specimen was then chopped into fine pieces and loaded into a gelatine capsule. The capsule was then suspended from the electrobalance with a 0.003-inch quartz fiber.

The balance, under a bell jar, was in connection with a quartz tube housing the heater and thermometer, while the gelatine capsule holding the sample was hanging freely from the balance. The sample chamber was supported in a standard dewar assembly. The magnetic field was measured by a Bell 640 incremental gaussmeter. The overall accuracy of the measurement was estimated to be about

2 per cent above 1 KG (1000 Gauss) and 5 per cent below 1 KG for a sample weighing 100 mg.

J. Metallographic Studies

(a) Preparation of sample. A sample foil was first cut into a rectangular shape about 0.8 cm × 0.2 cm. The foil was then firmly clamped between two $\frac{1}{8}$ inch × $\frac{1}{2}$ inch × $\frac{3}{4}$ inch 316 stainless steel blocks. This assembly was placed in a Buehler $1\frac{1}{4}$ inch bakelite ring mold so that the foil would be on the edge, and then vacuum cast in Buehler plastic epoxide resin.

The mounted specimen was wet ground on No. 400 wet-on-dry paper, followed by No. 600 paper.

Rough polishing was done on an 8-inch wheel, covered with nylon cloth, and charged with 6 μm diamond paste. Intermediate polishing was done on an 8-inch wheel covered with Buehler microcloth and charged with 1 μm diamond paste. Final polishing was done on an 8-inch wheel covered with microcloth and charged with a distilled-water suspension of 0.05 μm gamma alumina. Etching was done by swabbing with an aqueous solution of 0.2 per cent each of H₂Cr₂O₄ and H₂SO₄; time was 20 to 30 seconds, depending on the individual specimen.

The specimen was alternately polished and etched at least 3 times to assure removal of the disturbed layer.

(b) Microscopic study. The sample was first examined with a Bausch and Lomb Metallograph at a magnification of 750×. To ensure that a thin layer of Ag was removed by the etching agent exposing the subsurface Pb particles, the specimens were then coated with a

thin carbon film by vapor evaporation to avoid the static charge induced by the electron beam bombardment in a Cambridge Scanning electron-microscope. Specimens were then examined and the identification of Ag and Pb phases was done by an EDAX (Energy Dispersive Analysis of X-rays) system. The typical magnification of the sample was in the ranges between 2,000x to 30,000x.

III. EXPERIMENTAL RESULTS

A. Lattice Parameter

The lattice parameter measurements on samples of $\text{Ag}_{100-x}\text{Pb}_x$ with $0 \leq x \leq 7$ immediately after quenching are shown in Fig. 3. From Vegard's law, it can be seen that the solid solution of Pb in Ag can be extended to about 3.2 at. % Pb. However, for a given quenched sample, because the quenching rate of different parts of the sample is not the same^(53, 69), the measured lattice parameter has a range as seen in Fig. 3. Since all the quenched samples are metastable at room temperature, it is necessary to examine the stability of these samples. The lattice spacings were measured for quenched samples which were annealed at room temperature for various times. For a given sample, if the lattice spacing remains the same for a relatively long time, it can be considered stable. For a given composition, about four to five samples were checked to make sure that samples produced by the piston and anvil techniques were reproducible. A typical result was the $\text{Ag}_{97}\text{Pb}_3$ samples in which the lattice parameter for samples immediately after quenching was observed to be the same as for samples annealed at room temperature for four months. Even for samples annealed at room temperature for two years, the lattice parameter was only changed from 4.104 \AA initially to 4.100 \AA . It can be concluded that the quenched samples are quite stable at room temperature.

For samples with more than 3.2 at. % Pb, particles of Pb will start precipitating immediately after quenching. The undissolved Pb will either form in grain boundaries or distribute throughout the Ag matrix, causing the superconducting properties to be non-uniform for

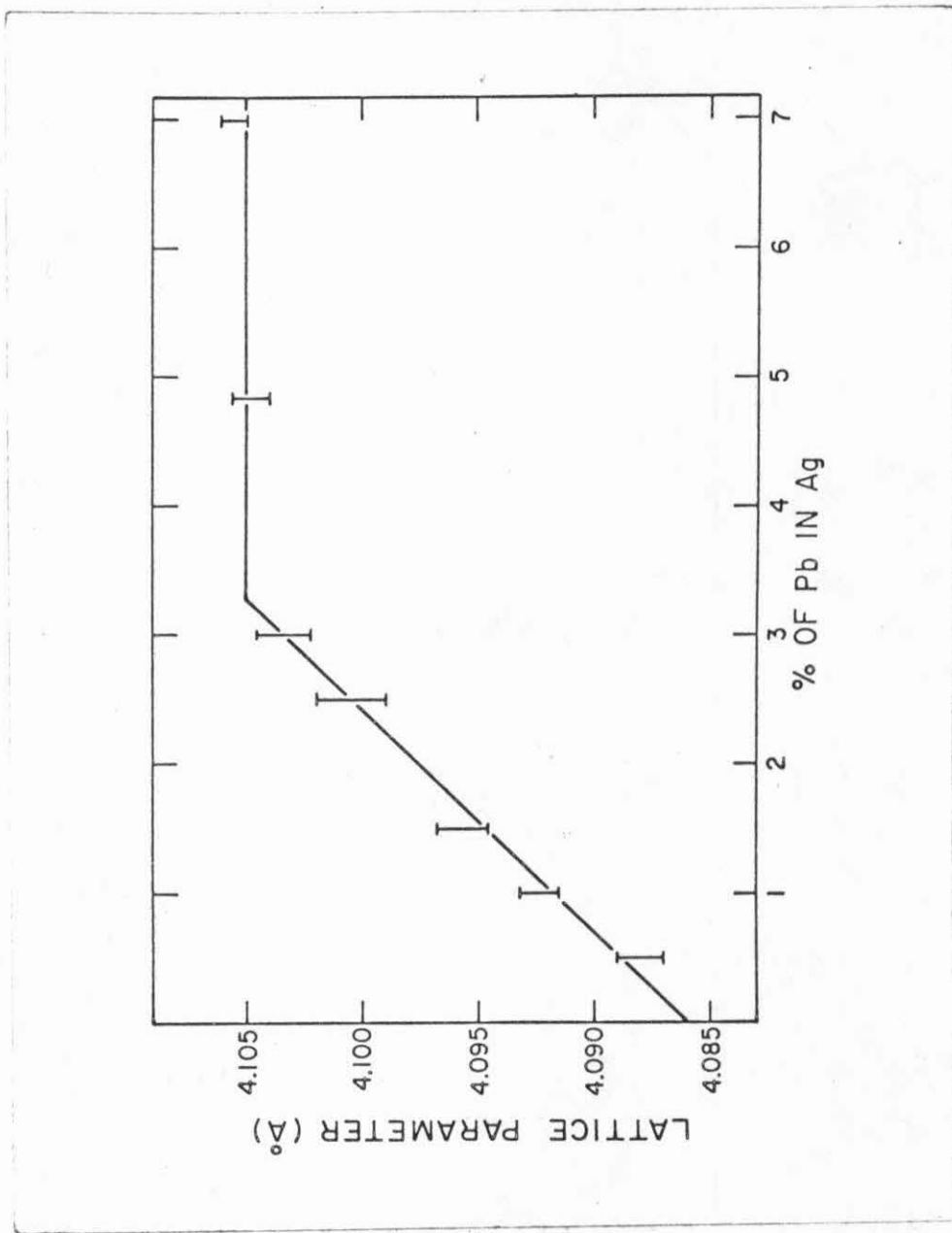


Fig. 3. Lattice parameter versus at. % Pb of the liquid quenched $Ag_{100-x}Pb_x$ alloys.

different quenched foils. With less than 3.2 at. % Pb, the precipitation of the Pb particle in the quenched samples can be controlled by annealing at temperatures below 300°C. However, as seen from the phase diagram of the Ag-Pb binary system in Fig. 59, the eutectic temperature is observed to be 304°C. Therefore, it can be expected that the diffusion rate of Pb particles in all the quenched samples annealed at 300°C will be very high. It was actually observed that for a given quenched sample annealed at 300°C for only 10 to 20 minutes, the lattice parameter experiment showed that the Ag lattice spacing had already returned to the equilibrium value. It was found that the most reasonable rate of precipitation could be obtained by annealing the quenched samples at 200°C, and that the results were highly reproducible. For example, Fig. 4 shows that the lattice spacing of Ag gradually returns to equilibrium as a function of annealing times for samples of $\text{Ag}_{97}\text{Pb}_3$ annealed at 200°C.

B. Transformation of the Supersaturated Solid Solution

By measuring the x-ray diffraction peak intensity ratio of the (111) Pb line to the (111) Ag line of the quenched and heat treated Ag-Pb alloys, the amount of transformation from the supersaturated state back to equilibrium in the alloys can be obtained. The results for the quenched $\text{Ag}_{97}\text{Pb}_3$ samples annealed at 200°C and 300°C for various times are presented in Table I. The half width of the Ag (111) line of all the quenched $\text{Ag}_{97}\text{Pb}_3$ samples has $\Delta 2\theta < 0.38^\circ$. This indicates the Ag lattice does not get distorted after quenching. For the other compositions of Pb in Ag, samples with less than 3 at. % Pb show the same transformation behavior as the quenched $\text{Ag}_{97}\text{Pb}_3$ samples.

Table I

Peak intensity ratios of the (111) Pb line to the (111) Ag line of the quenched $\text{Ag}_{97}\text{Pb}_3$ alloys annealed at 200°C , 300°C and room temperature

Annealing temperature ($^\circ\text{C}$)	Annealing time	$\frac{I_{\text{pb}}(111)}{I_{\text{Ag}}(111)}$
25	0 hours (or as quenched)	<.01
25	4 months	<.01
25	1 year	<.01
200	5 hours	0.023
200	27 hours	0.045
200	41 hours	0.046
200	67 hours	0.072
200	100 hours	0.094
200	500 hours	0.1
200	2000 hours	0.1
300	1 hour	0.099
300	337 hours	0.1

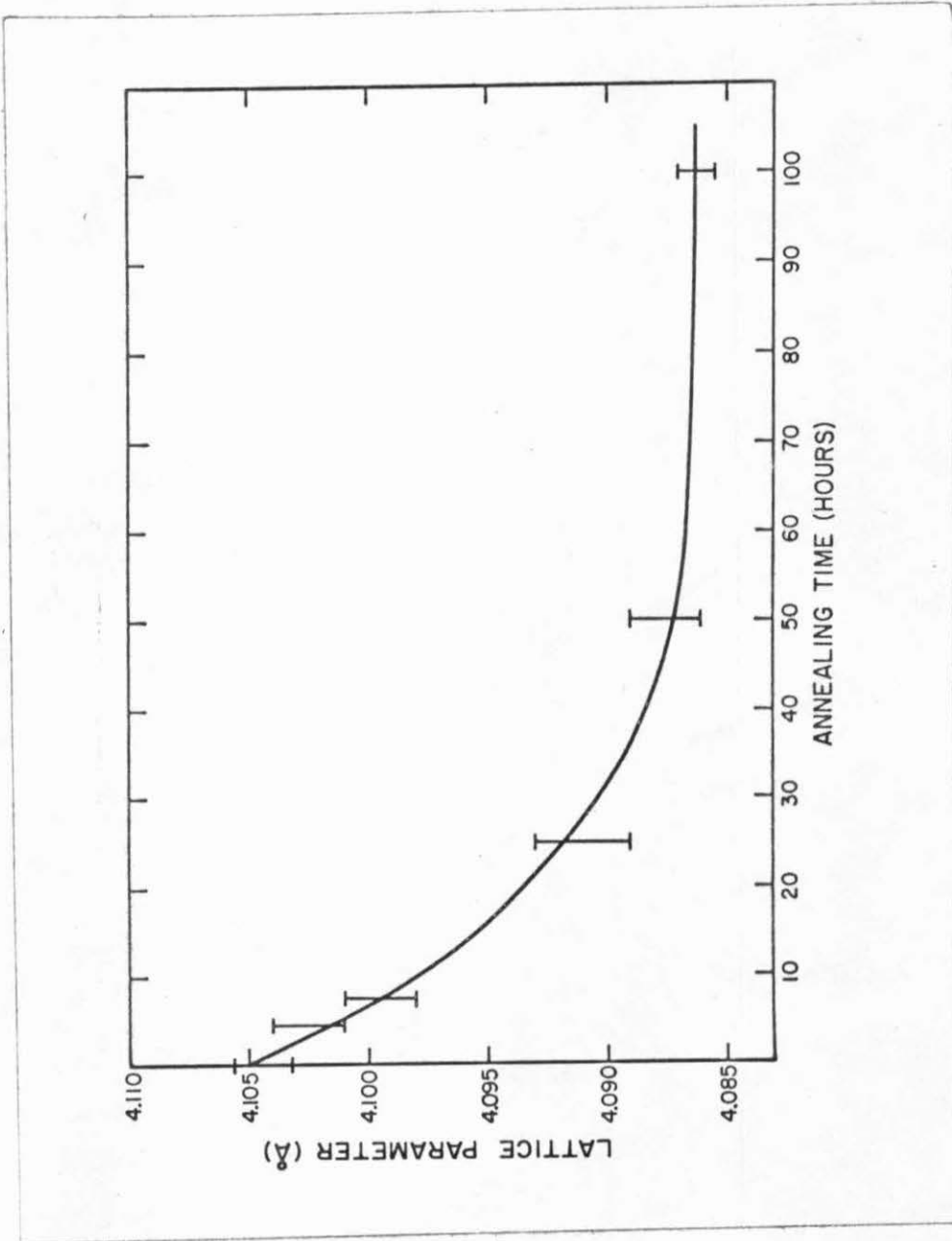


Fig. 4. Lattice parameter as a function of annealing time of quenched $\text{Ag}_{97}\text{Pb}_3$ alloys annealed at 200°C .

For samples with Pb content above 3.2 at.%, Fig. 3 has already shown that the samples are not a supersaturated solid solution anymore, but exist as two phases. Therefore, no x-ray intensity measurements for the transformation studies have been made.

C. Resistivity Measurement

1. Resistivity versus temperature. The resistivity versus temperature results of the quenched $\text{Ag}_{100-x}\text{Pb}_x$, $1 \leq x \leq 5$ samples and those with subsequent annealing can be divided into two regions.

(a) Temperature range between 7.2°K and 300°K .

All the samples in this region show typical dirty metallic alloys behavior. Some examples are shown in Fig. 5. The resistivities depend linearly with temperature for $T > 25^\circ\text{K}$; while between 7.2°K and 25°K , the residual resistivities are independent of temperature. The residual resistivity is important because it can determine the mean free path of Ag in the sample, and this mean free path in turn determines the superconducting properties of the sample. An example of the residual resistivity as a function of annealing time for a given composition and an annealing temperature is shown in Fig. 6.

(b) Temperature below 7.2°K .

This is the interesting range. The superconducting properties, if they exist in the sample, become evident. To make the resistivity versus temperature results for samples annealed at a given temperature for various times more clear, the resistivity was normalized with respect to its corresponding residue resistivity and then plotted against temperature. The results for quenched $\text{Ag}_{100-x}\text{Pb}_x$ samples

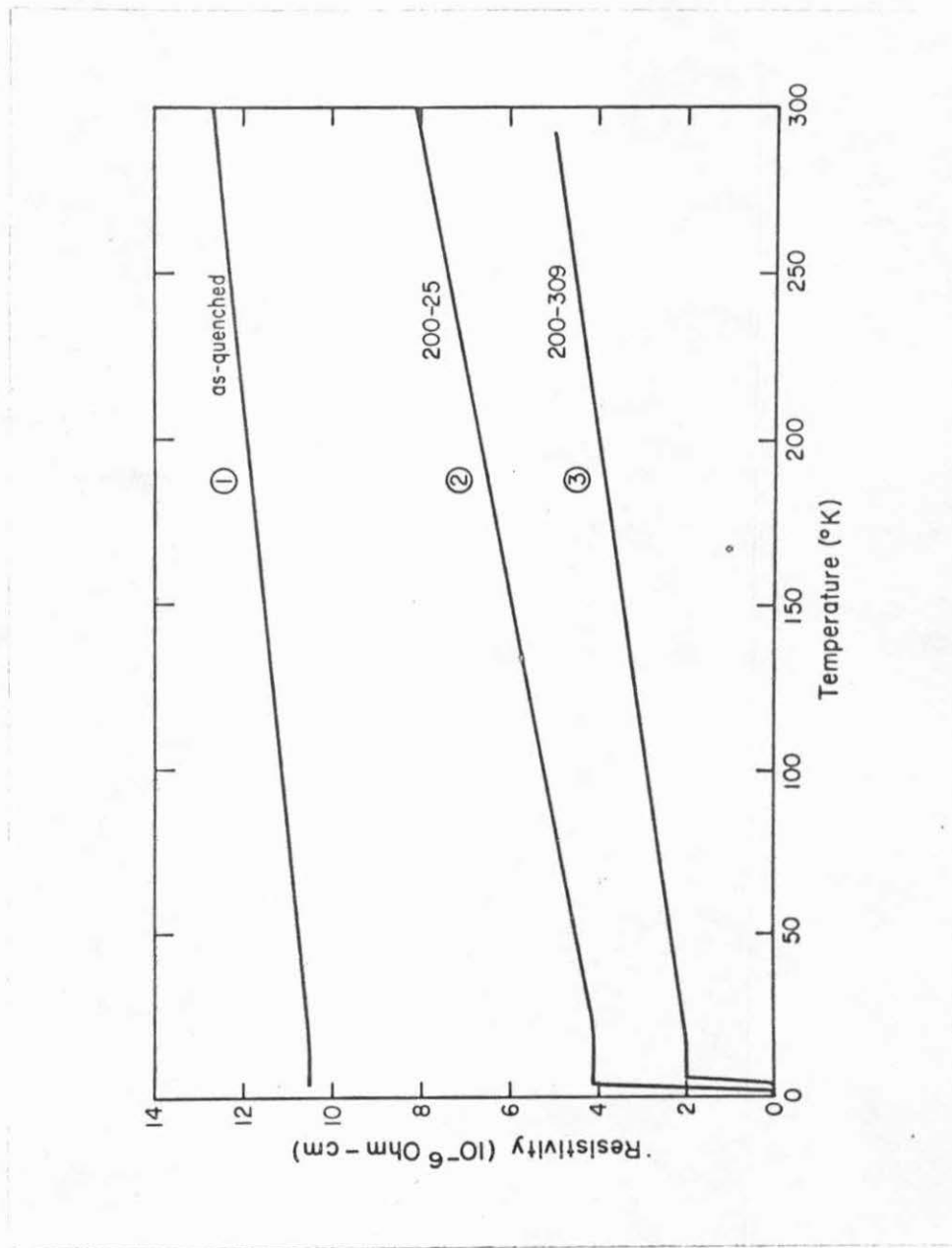


Fig. 5. Resistivity versus temperature of some $\text{Ag}_{97}\text{Pb}_3$ alloys. Curve 1 : as-quenched; Curve 2 : quenched and annealed at 200°C for 25 hours; Curve 3 : quenched and annealed at 200°C for 309 hours.

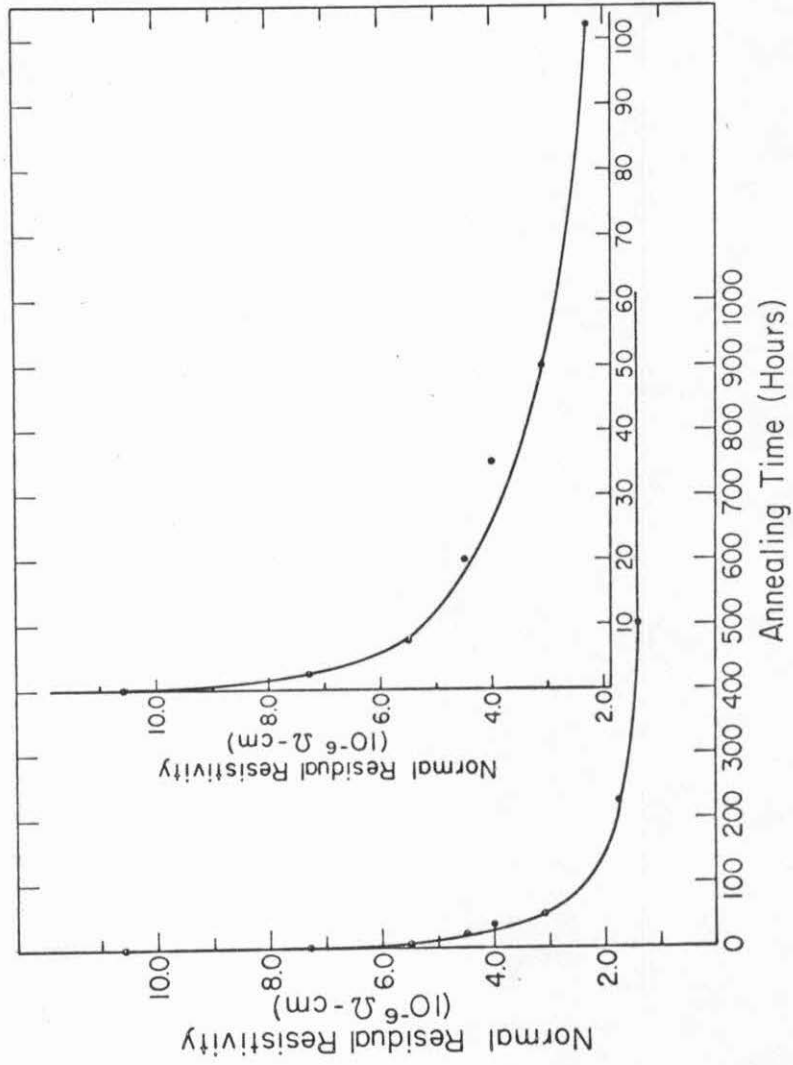


Fig. 6. Residual resistivity as a function of annealing time of quenched $\text{Ag}_{97}\text{Pb}_3$ alloys annealed at 200°C .

annealed at 200°C and 300°C for various times with $x = 5, 3, 2.5, 1.5,$ and 1 are shown in Figs. 7 through 16. All the samples were measured with current density $J \cong 20 \text{ amp/cm}^2$. In general, for a given composition and annealing temperature, the transition temperature goes up with increased annealing time.

For quenched $\text{Ag}_{95}\text{Pb}_5$ samples, as seen in Figs. 7 and 8, all the samples were superconducting. Samples in this composition show some inconsistencies; in other words, different foils which were prepared and treated in exactly the same conditions can have different transitions. For example, in Fig. 7, curves 1 and 3 are two samples which were measured immediately after quenching, but these two transitions are different. Due to this kind of non-reproducible results, it was decided that the samples with Pb content more than 3 at. % be deleted in other measurements.

For quenched $\text{Ag}_{100-x}\text{Pb}_x$ samples, $1 \leq x \leq 3$, consistent and reproducible results were obtained in different foils which were prepared and treated in exactly the same conditions. In this composition range, it can be observed from Figs. 9 through 16 that samples measured immediately after quenching and samples annealed at 200°C less than one hour are not superconducting down to 1.2°K. It can also be observed that for samples which were annealed at the same temperature for the same time, but were of different compositions, the temperatures at which the resistivities (ρ) drop to zero decrease with the Pb content in the sample; but the onset temperatures at which the ρ/ρ_n start to drop keep approximately constant with the Pb content

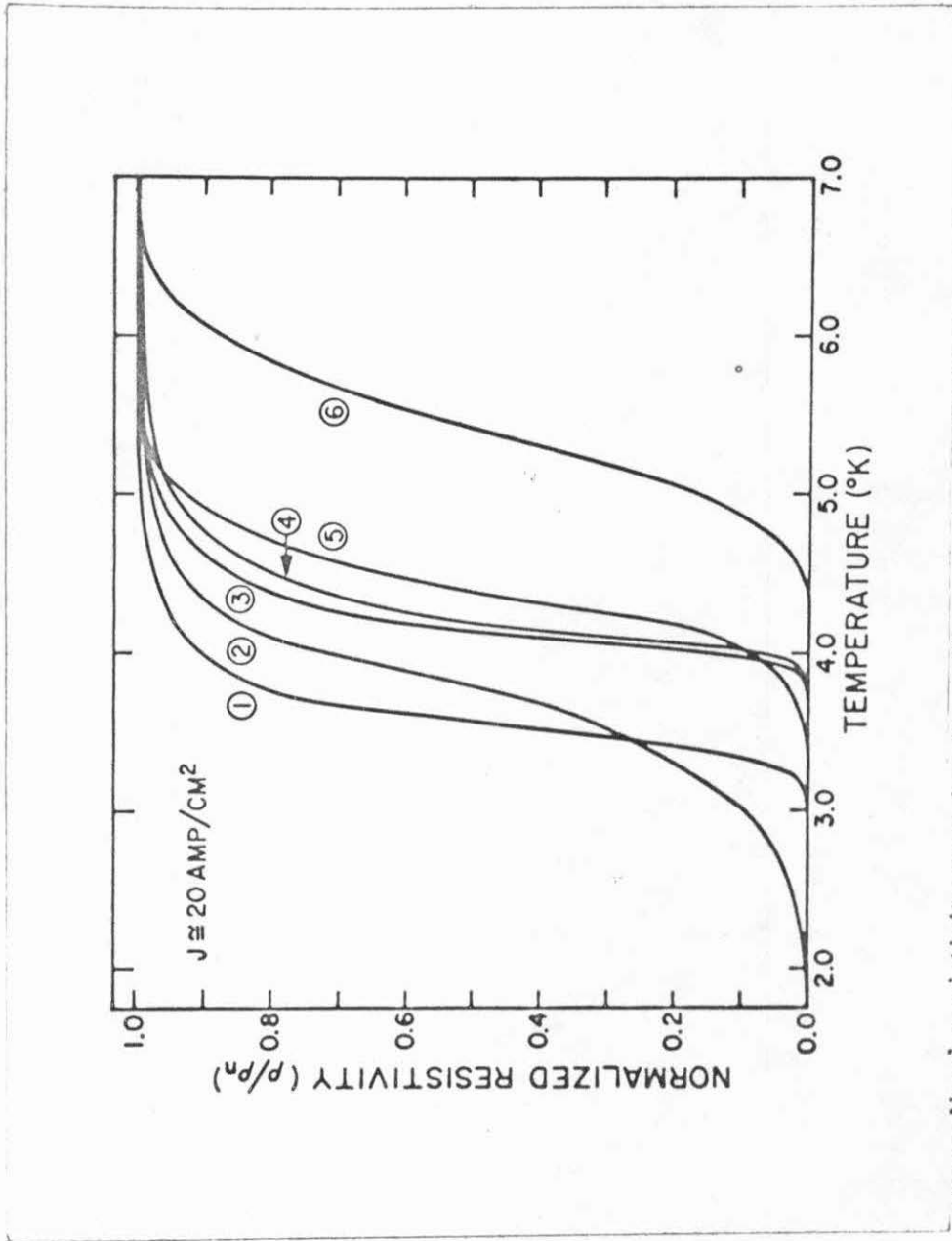


Fig. 7. Normalized resistivity as a function of temperature of the quenched Ag₉₅Pb₅ alloys annealed at 200°C: 1 as-quenched; 2 annealed for 4.5 hours; 3 another as-quenched; 4 annealed for 48 hours; 5 annealed for 100 hours; 6 annealed for 311 hours.

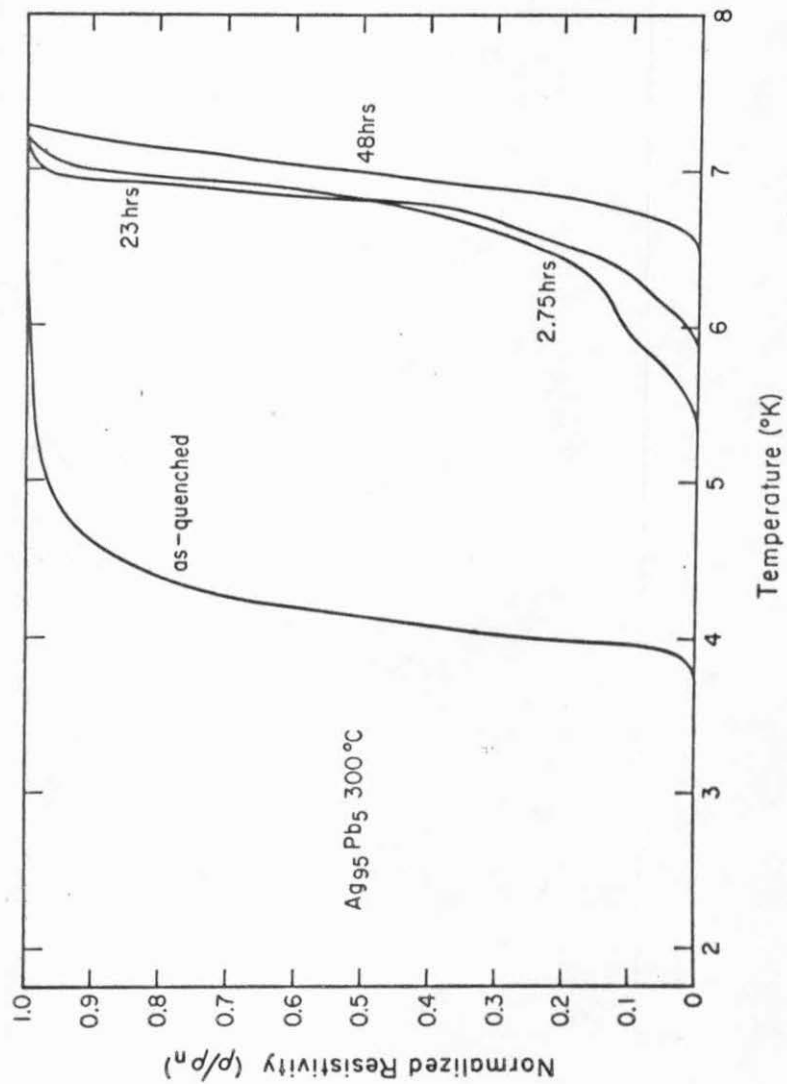


Fig. 8. Normalized resistivity as a function of temperature of the quenched Ag₉₅Pb₅ alloys annealed at 300°C.

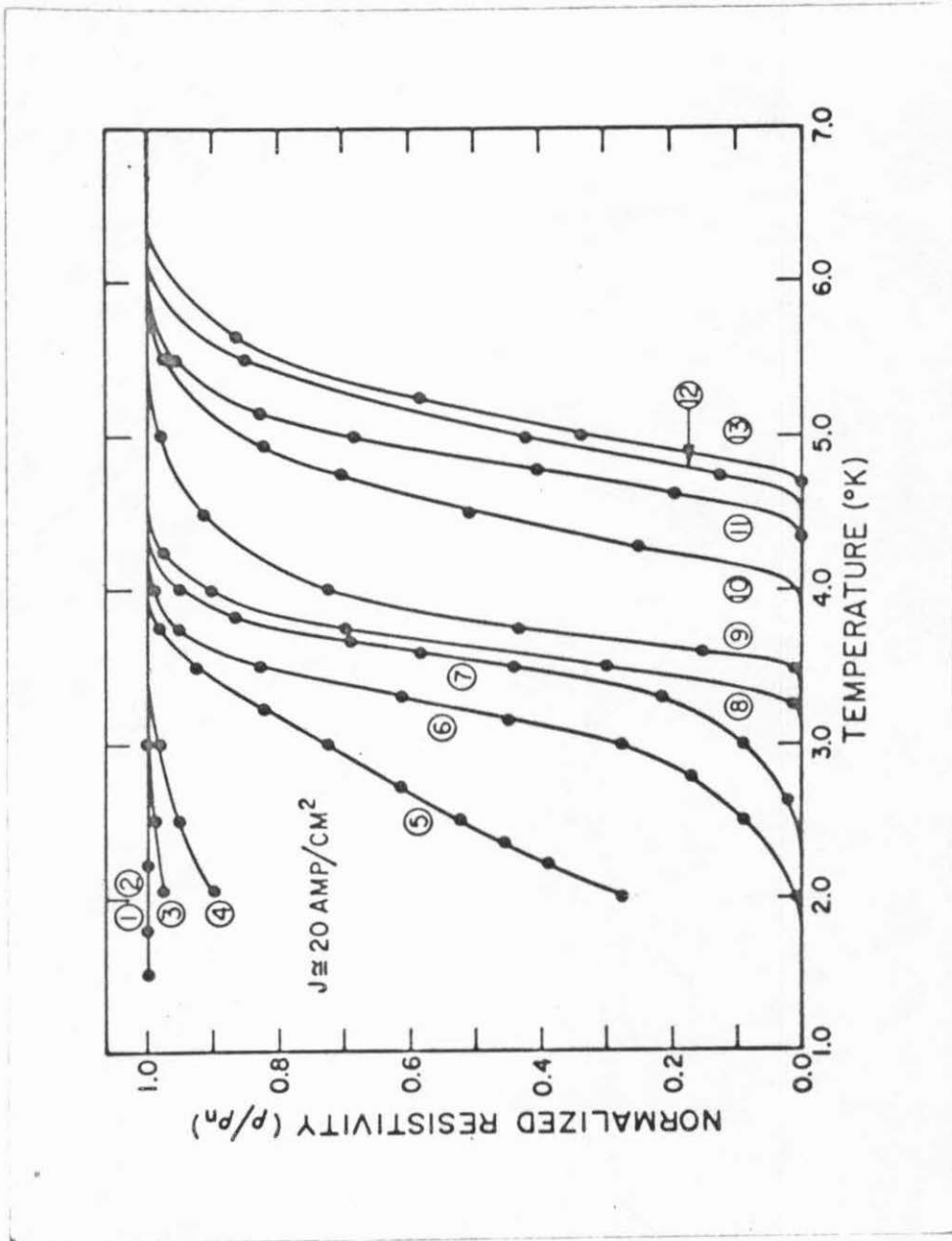


Fig. 9. Normalized resistivity as a function of temperature of the quenched Ag₉₇Pb₃ alloys annealed at 200°C. 1 as-quenched; 2 annealed for 0.33 hours; 3 annealed for one hour; 4 annealed for 2.5 hours; 5 annealed for 7.5 hours; 6 annealed for 20 hours; 7 annealed for 35 hours; 8 annealed for 102 hours; 9 annealed for 225 hours; 10 annealed for 820 hours; 11 annealed for 1050 hours; 12 annealed for 1050 hours; 13 annealed for 1050 hours.

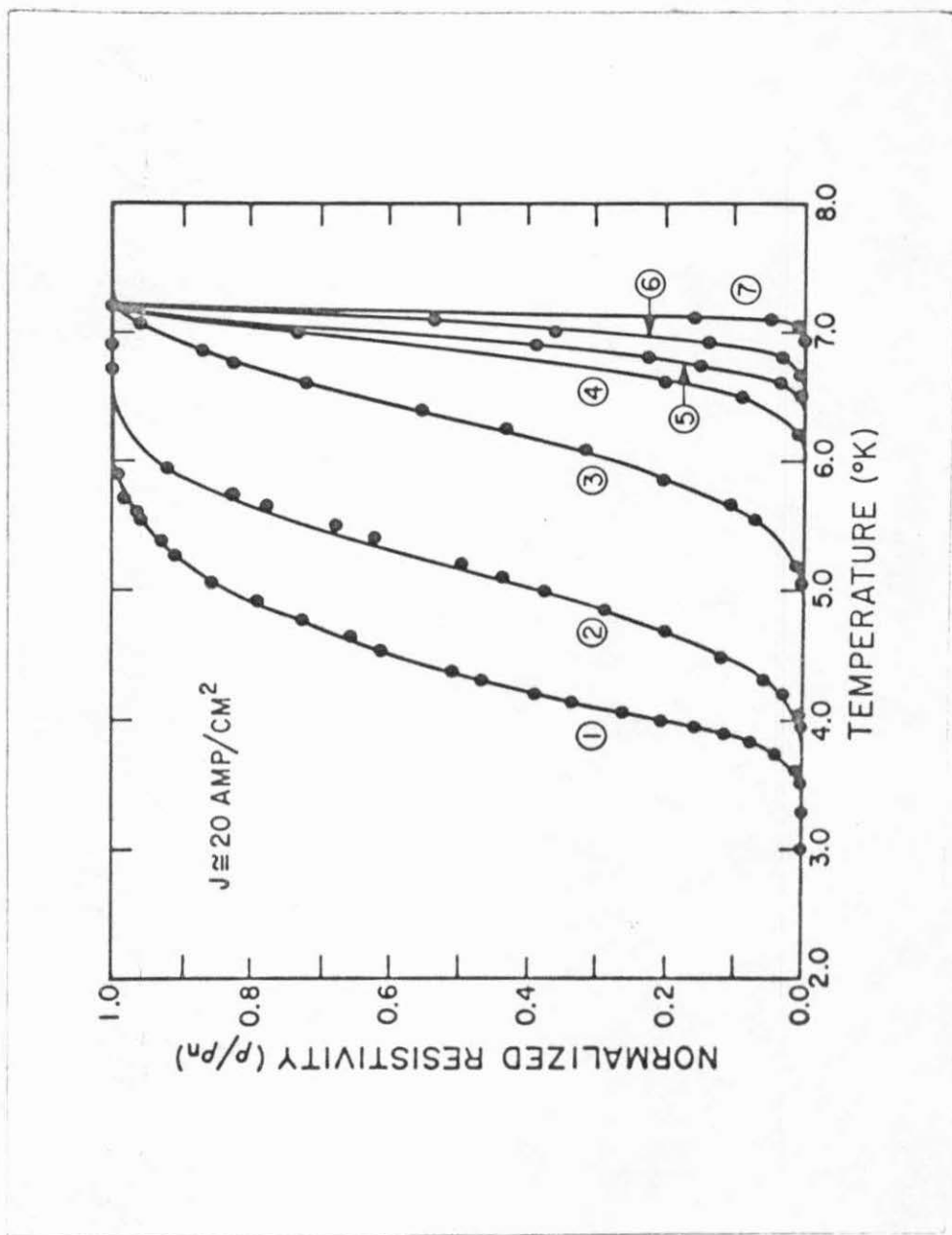


Fig. 10. Normalized resistivity as a function of temperature of the quenched Ag₉₇Pb₃ alloys annealed at 300°C: 1 annealed for 0.33 hours; 2 annealed for 1 hour; 3 annealed for 2 hours; 4 annealed for 18 hours; 5 annealed for 50 hours; 6 annealed for 100 hours; 7 annealed for 311 hours.

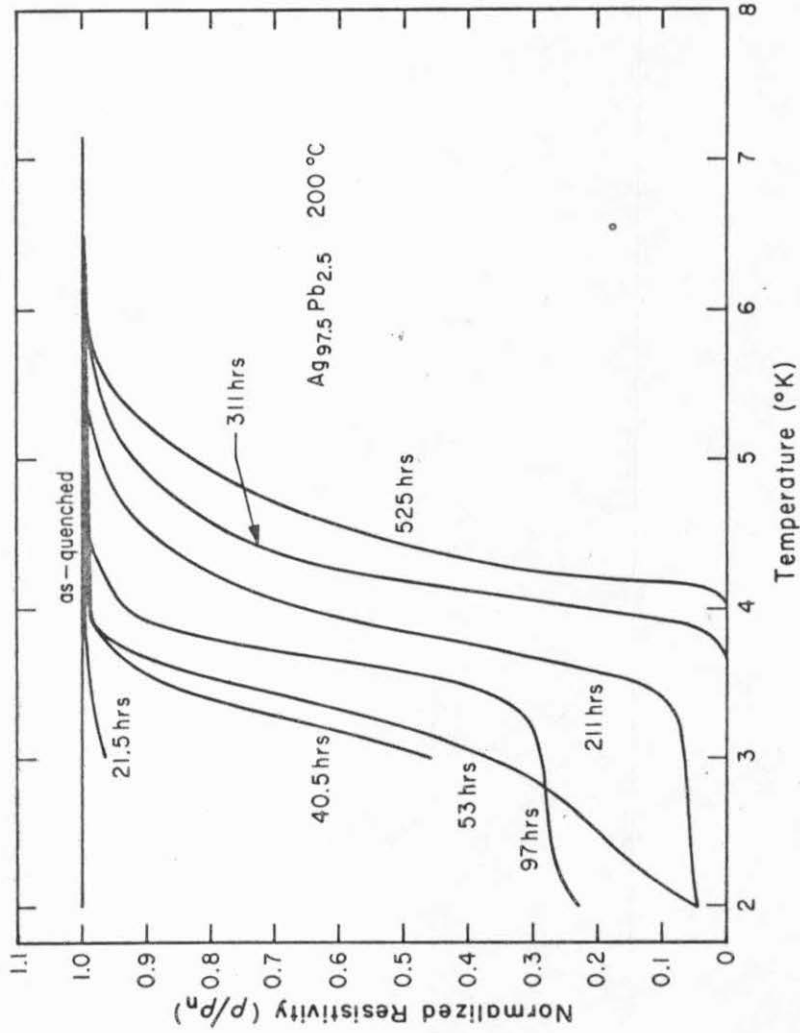


Fig. 11. Normalized resistivity as a function of temperature of the quenched $\text{Ag}_{97.5}\text{Pb}_{2.5}$ alloys annealed at 200°C .

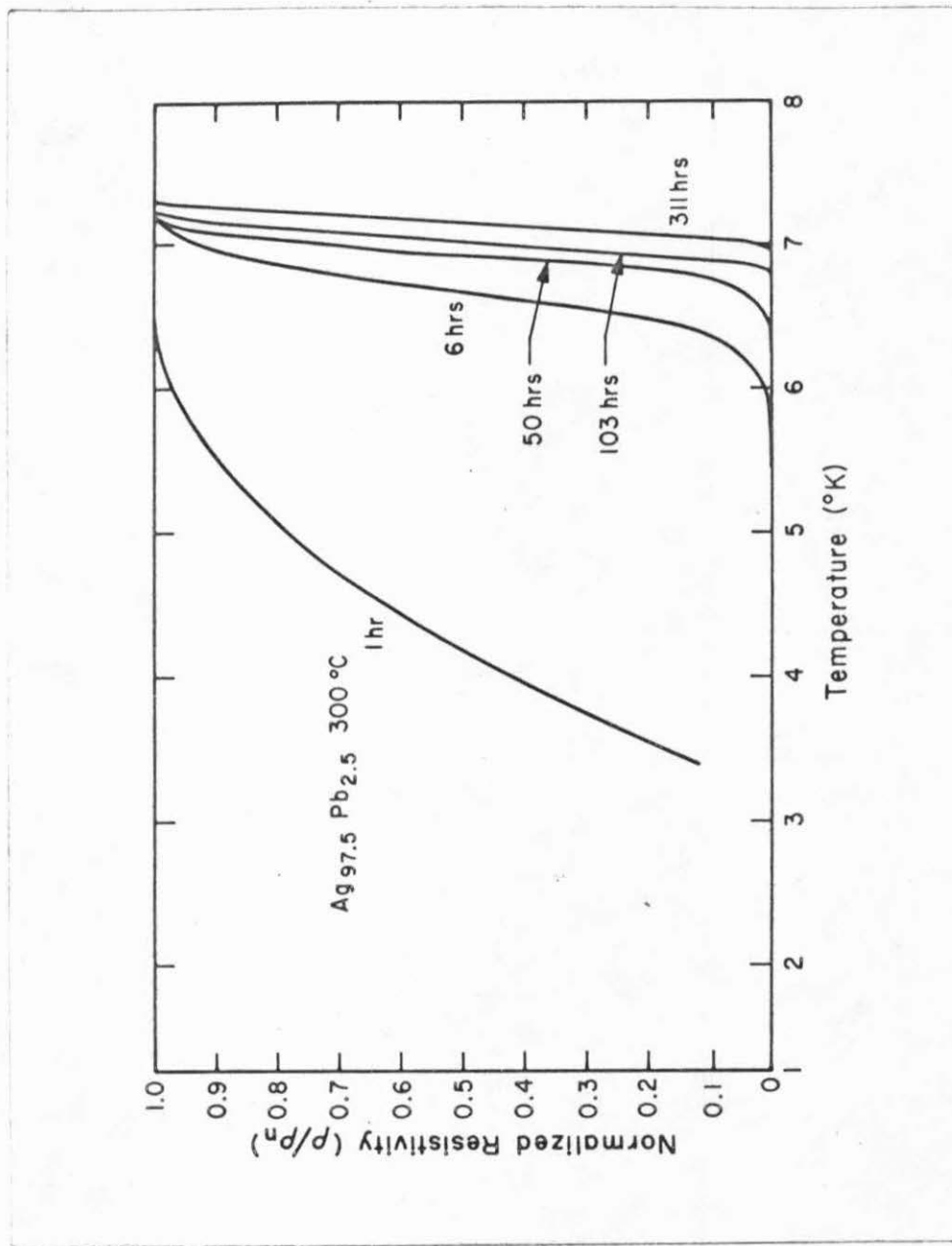


Fig. 12. Normalized resistivity as a function of temperature of the quenched $\text{Ag}_{97.5}\text{Pb}_{2.5}$ alloys annealed at 300°C .

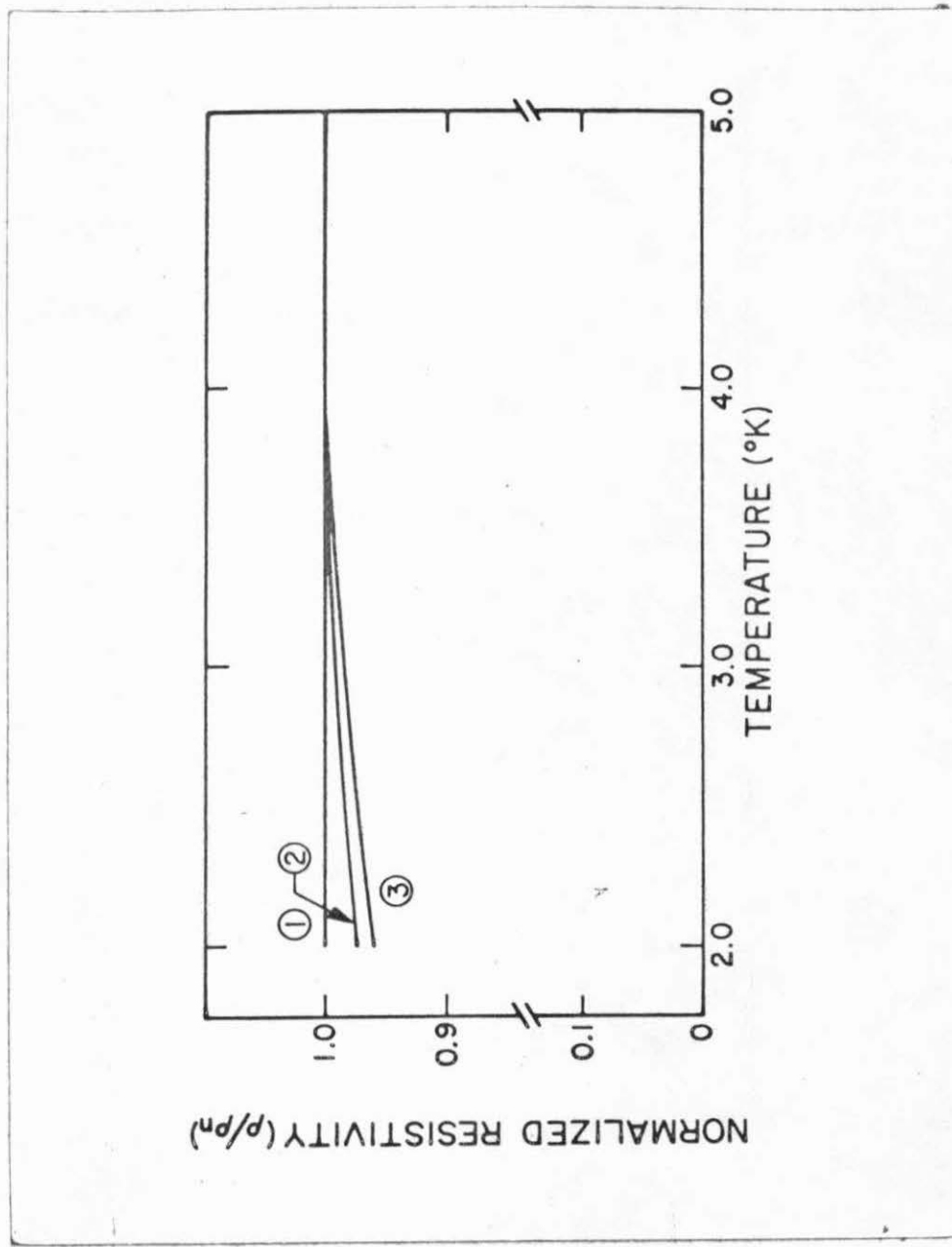


Fig. 13. Normalized resistivity as a function of temperature of the quenched $\text{Ag}_{98.5}\text{Pb}_{1.5}$ alloys annealed at 200°C . 1 as-quenched, annealed for 42.5 hours, and annealed for 72 hours; 2 annealed for 142.5 hours; 3 annealed for 306.5 hours.

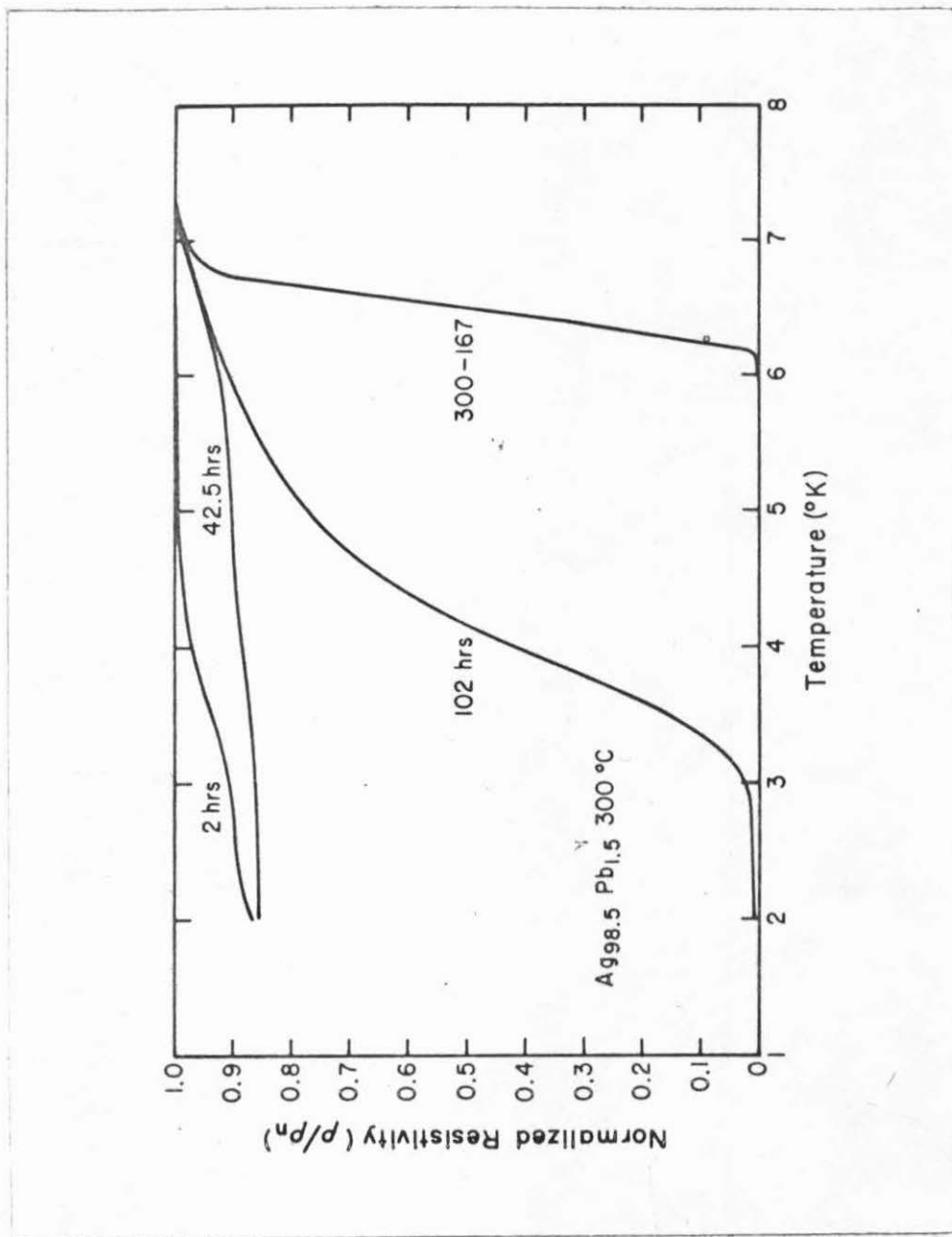


Fig. 14. Normalized resistivity as a function of temperature of the quenched $\text{Ag}_{98.5}\text{Pb}_{1.5}$ alloys annealed at 300°C .

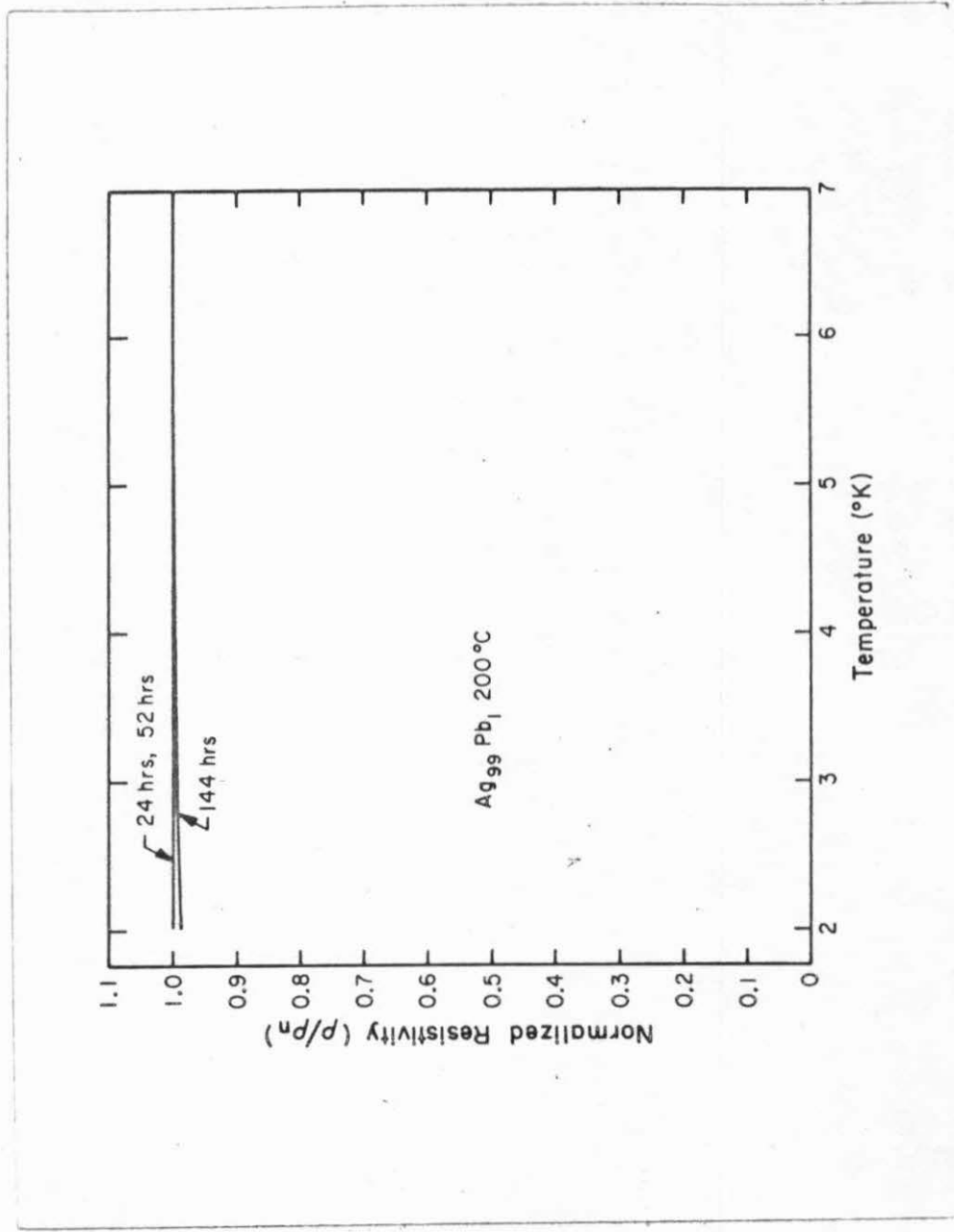


Fig. 15 Normalized resistivity as a function of temperature of the quenched Ag₉₉Pb₁ alloys annealed at 200°C.

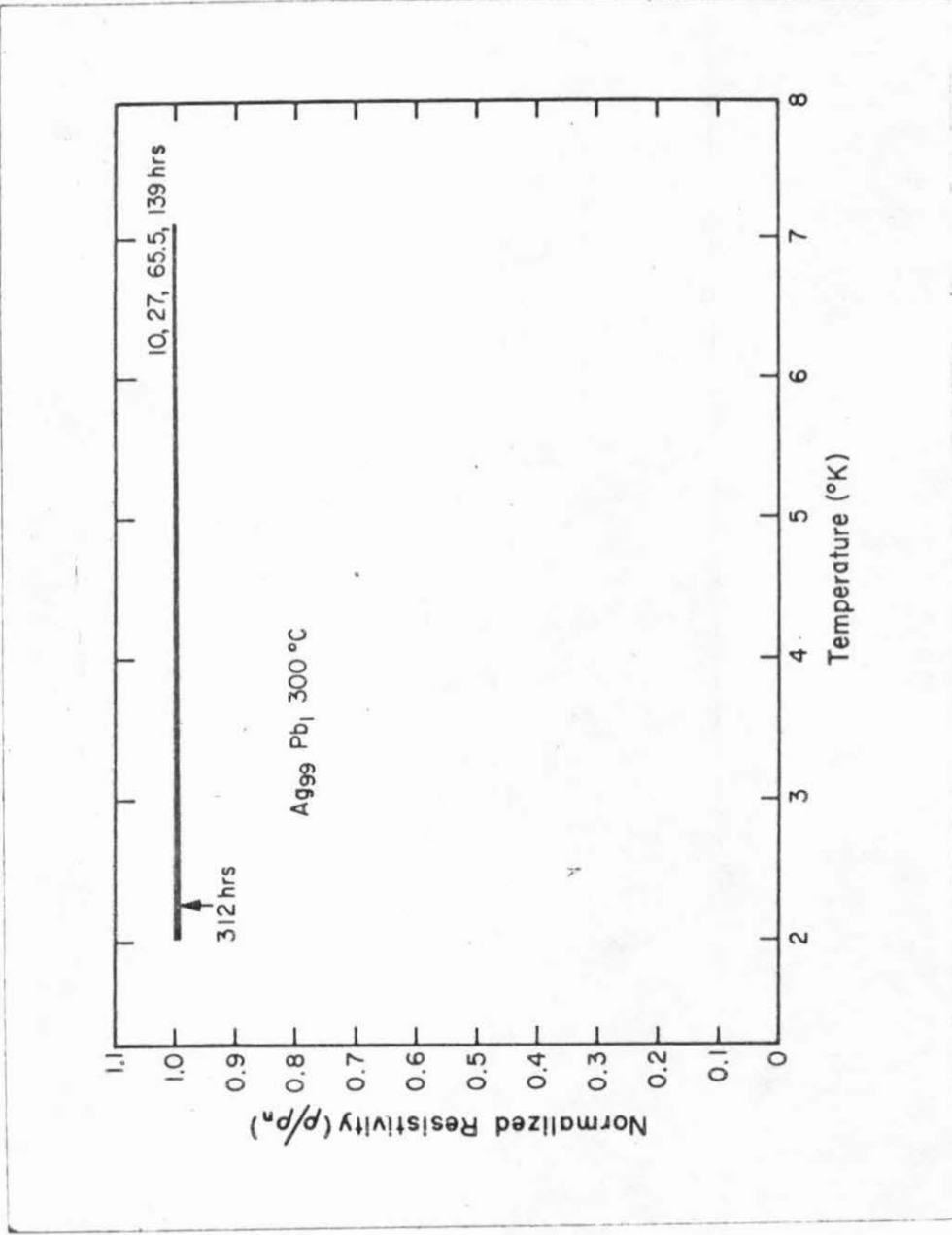


Fig. 16. Normalized resistivity as a function of temperature of the quenched Ag₉₉Pb₁ alloys annealed at 300°C.

in the sample. For quenched samples annealed at 300°C , the onset of the transition was observed to move to 7.2°K for annealing times above 5 hours except in samples with only 1 at. % Pb in Ag, in which the critical current for $T > 4^{\circ}\text{K}$ is too small to be detectable.

Some of the samples show some finite resistance at low temperatures; for example, in Fig. 11, the quenched $\text{Ag}_{97.5}\text{Pb}_{2.5}$ samples annealed at 200°C for 97 hours and 211 hours show finite residual resistances at $T < 3.5^{\circ}\text{K}$. This effect was considered to be due to the contact resistance between the spot-welded Pt wires and the samples.

In conclusion, the complete superconductivity $\rho = 0$ can be obtained most easily and reproducibly in the $\text{Ag}_{97}\text{Pb}_3$ samples annealed at 200°C for various times. Therefore, these samples are most suitable for the other kinds of measurements in proximity effect studies.

2. Magnetoresistivity. The magnetoresistivity versus temperature results are very similar to the ρ versus T cases. For example, the normalized magnetoresistivities versus temperature of the quenched $\text{Ag}_{97}\text{Pb}_3$ samples annealed at 200°C for various times with magnetic field parallel to the direction of the measuring current at $T = 1.3^{\circ}\text{K}$ are presented in Fig. 17. The results show that the magnetic field strength at which the superconducting transition occurs increases with annealing time. For samples which were annealed at the same temperature for the same amount of time, but were of different compositions, the magnetic field strength at which the resistivities (ρ) drop to zero decreases with the Pb content in the sample, but the onset temperatures at which the resistivities start to

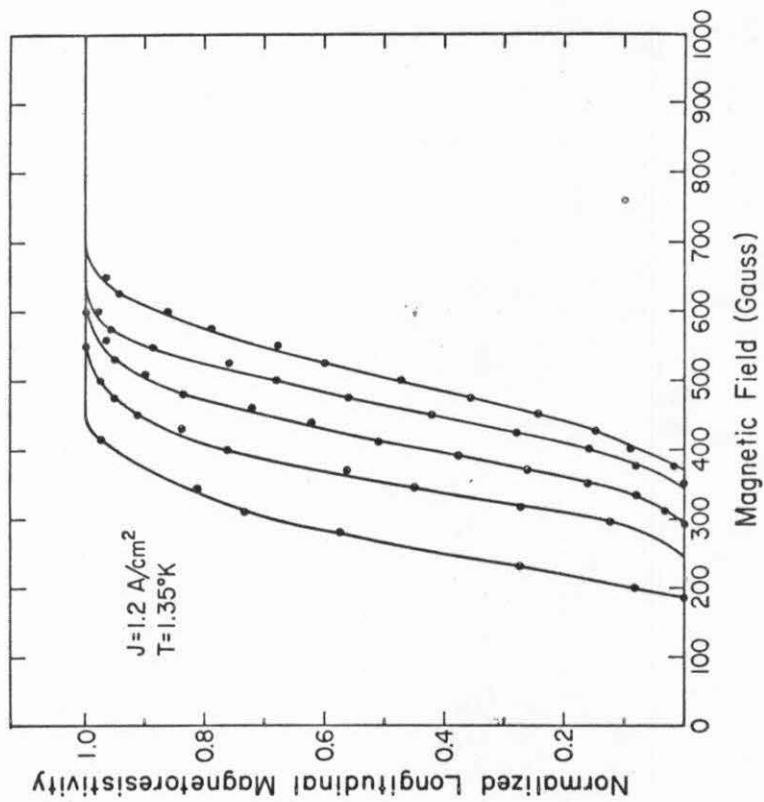


Fig. 17 Normalized longitudinal magnetoresistivity of the quenched $\text{Ag}_{97}\text{Pb}_3$ alloys annealed at 200°C : curves from left to right are for samples annealed for 54 hours, 102 hours, 225 hours, 500 hours, and 820 hours.

drop keep approximately constant with the Pb content in the sample. This behavior is similar to the ρ versus T cases.

It was found that for a given sample the transverse and longitudinal magnetoresistivities versus field are not the same. An example is shown in Fig. 18. For that particular sample, the magnetic fields at which the complete disappearance of resistance occurs have a difference of about 40 Gauss for the cases of magnetic field parallel to the direction of current and perpendicular to it.

D. Critical Current Density (J_c)

1. Critical current density versus temperature in earth magnetic field. At a given temperature, for quenched $Ag_{100-x}Pb_x$ samples, $1 \leq x \leq 3$, with the same heat treatment, the critical current density was found to decrease as x decreases. For $Ag_{98.5}Pb_{1.5}$ and $Ag_{99}Pb_1$ samples, the critical current is too small to be detectable even at very low temperature ($T \sim 1.3^\circ K$).

The critical current versus temperature for samples annealed at $200^\circ C$ for various times have approximately the same behavior. Figure 19 shows the results obtained from a quenched $Ag_{97}Pb_3$ sample which was annealed at $200^\circ C$ for various times. Since the same sample was used, the critical current can replace the critical current density in observing the differences in the qualitative behavior of the J_c versus T. It can be observed that the critical current decreases rapidly as temperature increases, and for a given temperature the critical current increases as the annealing time gets longer. This effect can lead to the fact that the resistivity versus temperature curve is dependent on the measuring current density. An example of

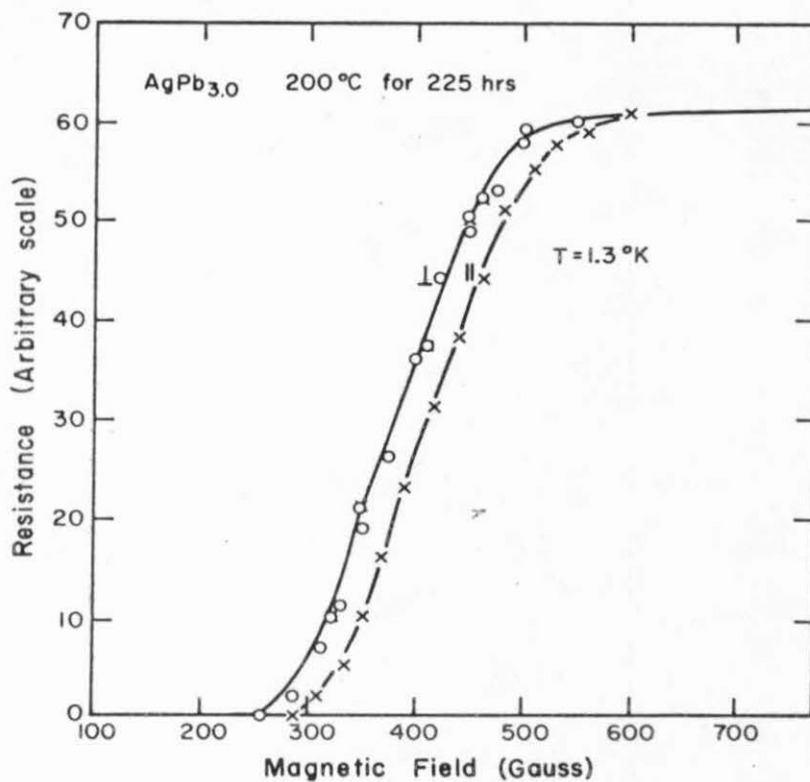


Fig. 18. Longitudinal and transverse magnetoresistance for the quenched Ag₉₇Pb₃ alloy annealed at 200 °C for 225 hours: ⊥ transverse magnetoresistivity, || longitudinal magnetoresistivity.

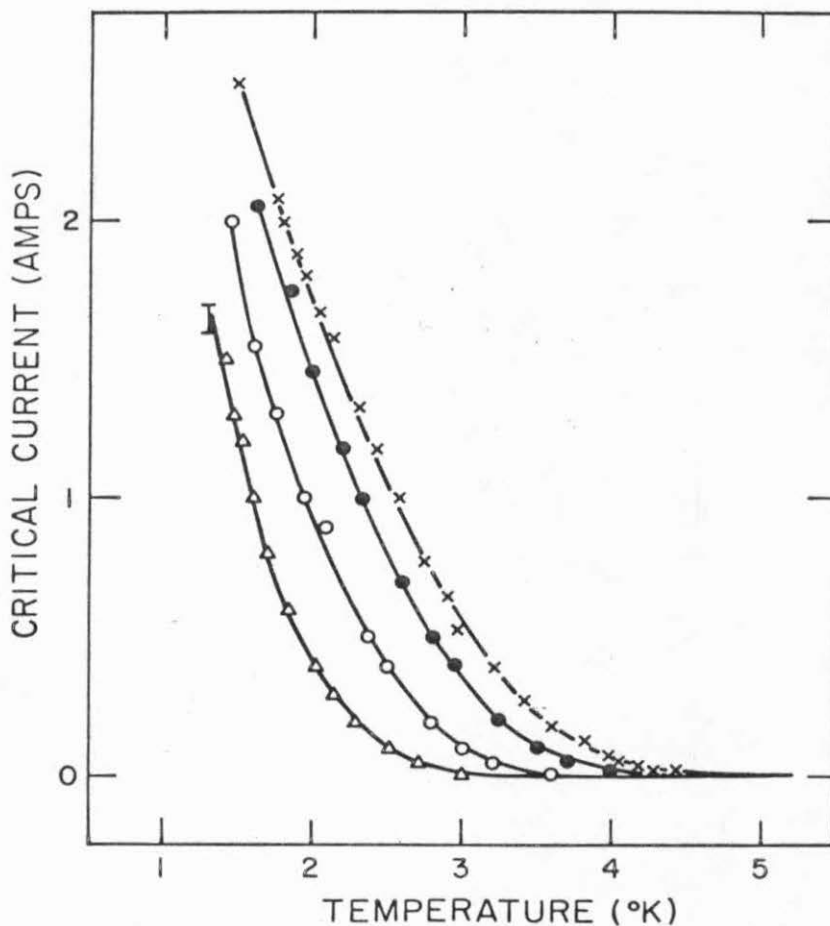


Fig. 19. Critical current as a function of temperature of a quenched $\text{Ag}_{97}\text{Pb}_3$ alloy annealed at 200°C . Δ annealed for 54 hours, \circ annealed for 102 hours, \bullet annealed for 225 hours, \times annealed for 500 hours.

this effect is shown in Fig. 20. It can therefore be expected that if the criterion for the transition temperature of the sample was defined as the temperature at which the resistivity drops to zero (as it normally is used in defining the T_c of ordinary superconducting compounds and alloys), then for the same sample, different measuring current density will give different T_c . Typical results are shown in Fig. 21. However, from Fig. 20, the onset of ρ versus T seems to be independent of the measuring current density, and it will therefore be a good choice for defining the T_c in the sample.

For quenched samples annealed at 300°C for less than 20 hours, the qualitative behavior of the critical current density versus temperature as compared to those annealed at 200°C are about the same. But as the annealing time increases, particularly with samples annealed more than 50 hours, the critical current tends to reach a finite limit at low temperature. A typical example of this behavior is shown in Fig. 22.

2. Critical current density versus temperature under applied magnetic field. The critical current versus temperature behavior for quenched $\text{Ag}_{100-x}\text{Pb}_x$ samples, $1 \leq x \leq 3$, annealed at 200°C for various times, and samples annealed at 300°C for less than 10 hours under various magnetic fields are very similar. A typical example is shown in Fig. 23. It can be seen that for a given temperature the critical current decreases as magnetic field increases, and at $T = 1.3^\circ\text{K}$ there is about 30 per cent decrease in the critical current when H only increases from earth magnetic field to about 11 Gauss for that particular sample.

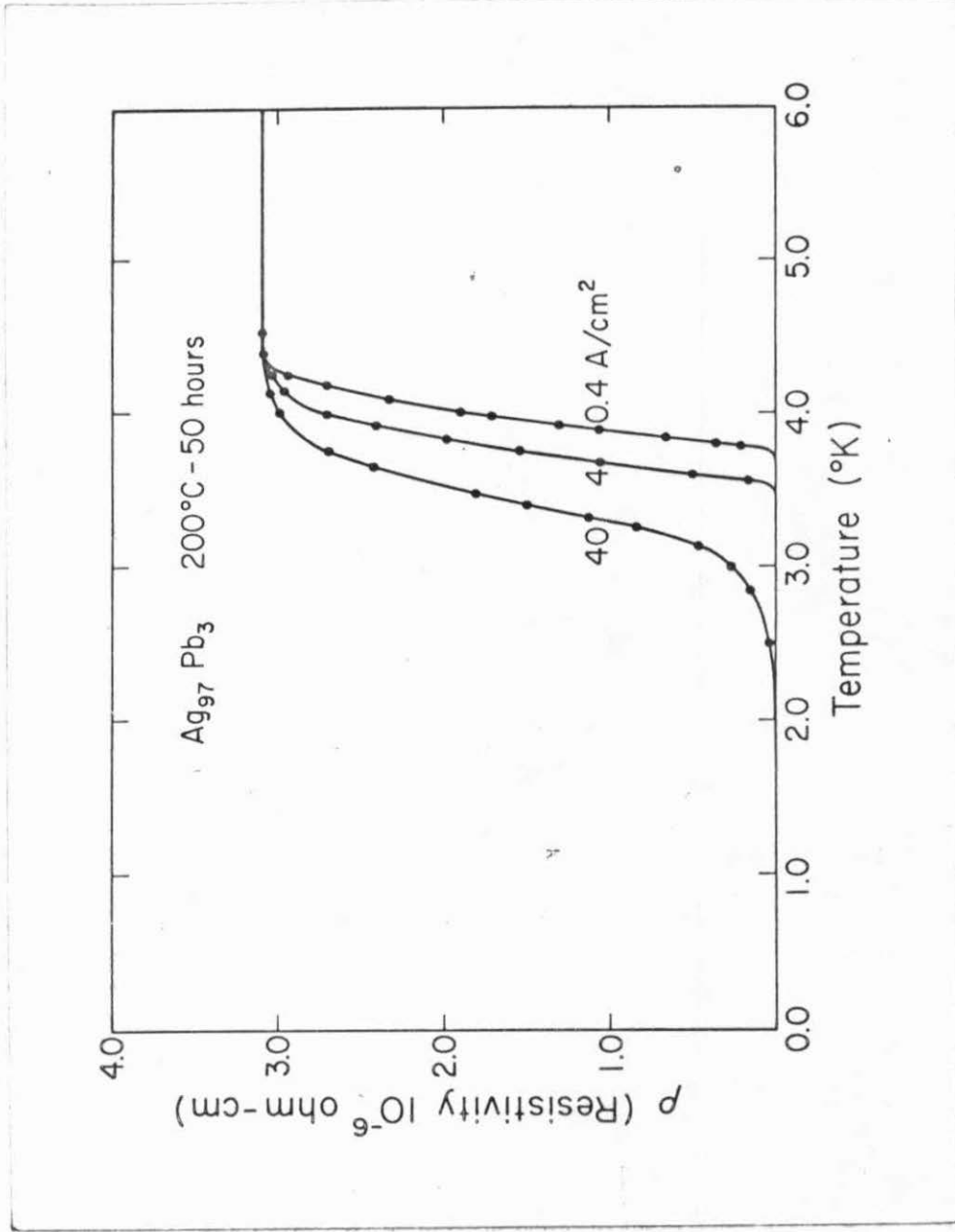


Fig. 20. Resistivity versus temperature for the quenched $\text{Ag}_{97}\text{Pb}_3$ alloys annealed at 200°C for 50 hours with different current densities.

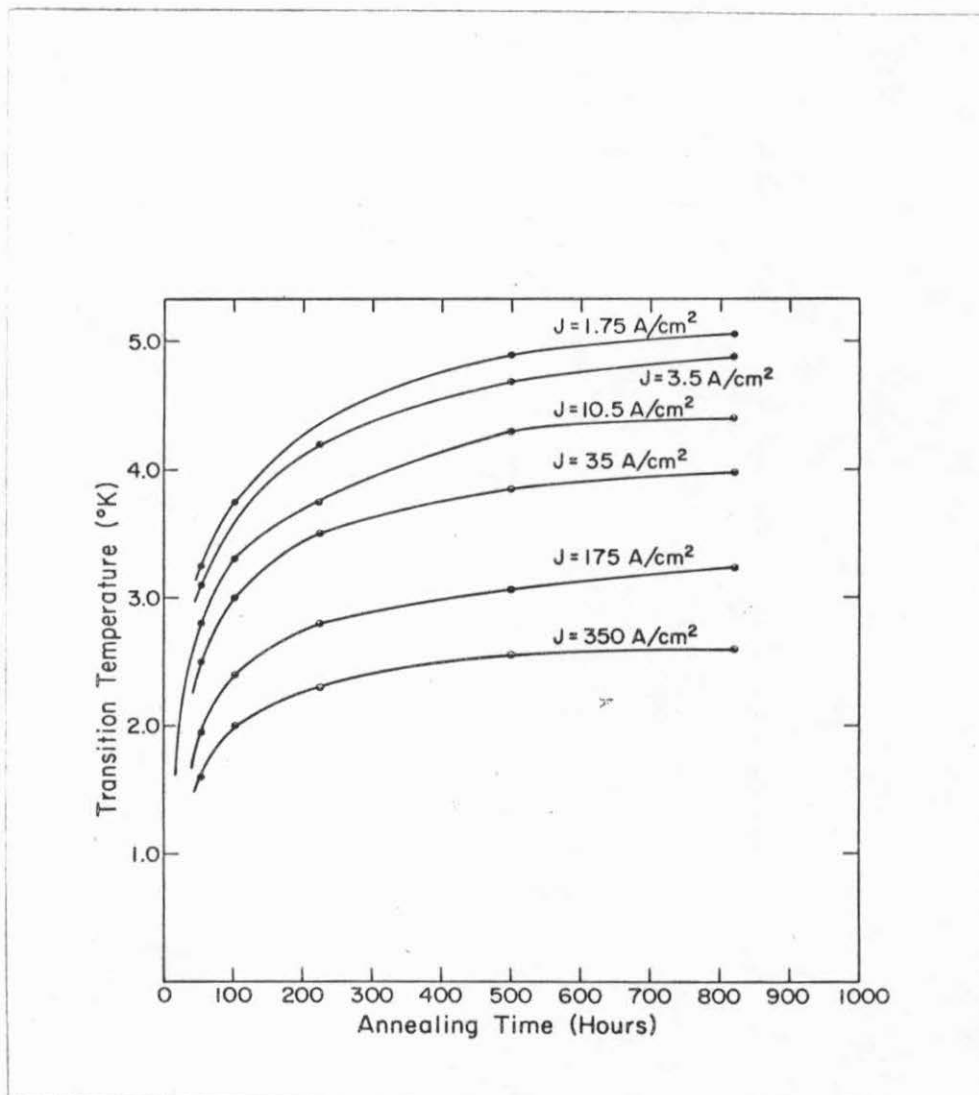


Fig. 21. Transition temperature as a function of annealing time of the quenched $\text{Ag}_{97}\text{Pb}_3$ alloys annealed at 200°C .

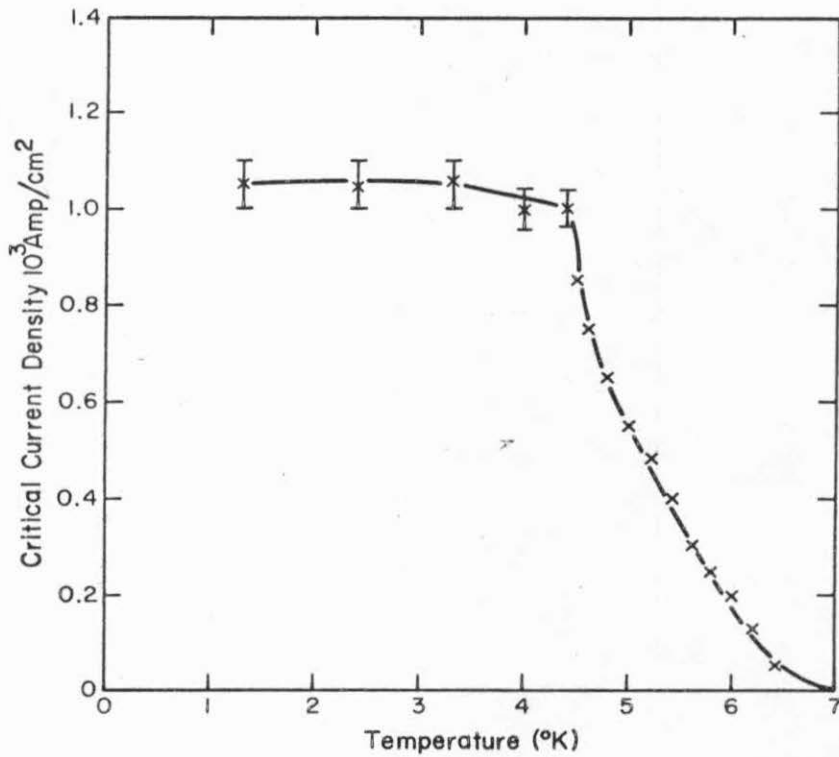


Fig. 22. Critical current density as a function of temperature of the quenched $\text{Ag}_{97}\text{Pb}_3$ alloy which was annealed at 300°C for 311 hours.

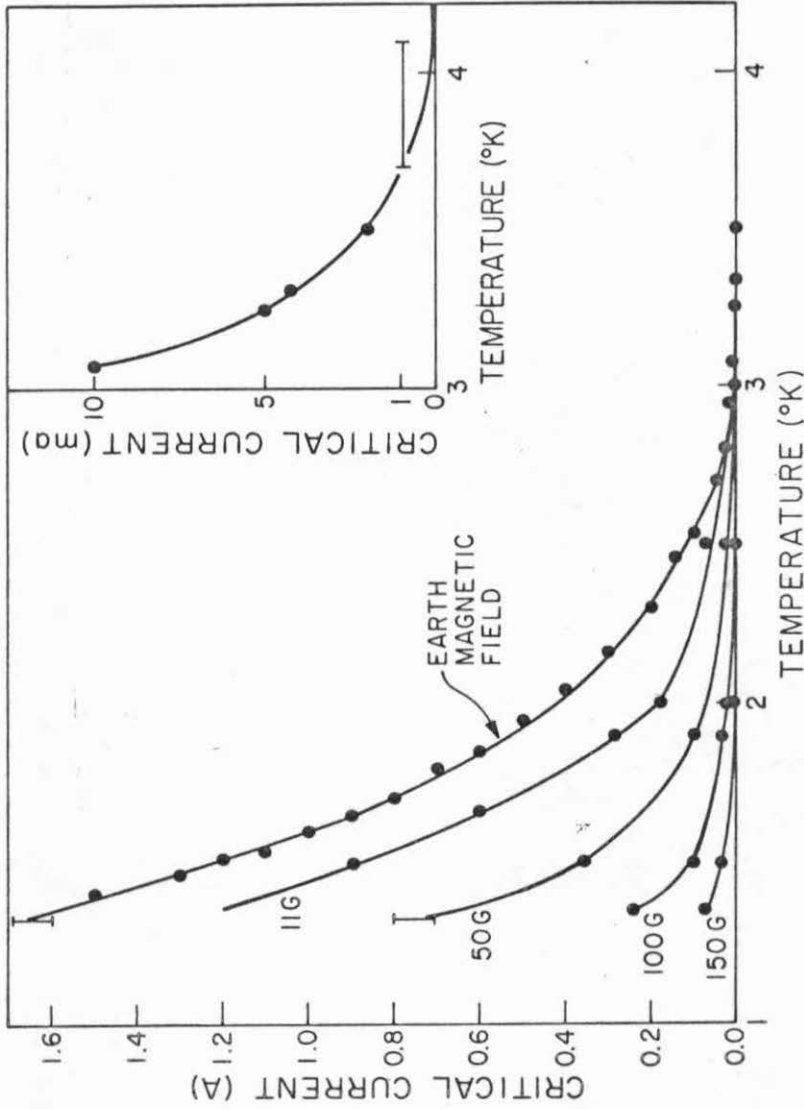


Fig. 23. Critical current as a function of temperature of a quenched $\text{Ag}_{97}\text{Pb}_3$ alloy which was annealed at 200°C for 54 hours. The smaller picture in the upper right corner is a magnification of the I_c versus T curve in the earth magnetic field between 3°K and 4°K .

The qualitative behavior of the I_c versus T curve remains the same. But for quenched samples annealed at 300°C for long times (especially $t > 50$ hours), the critical current seems independent of the strength of the magnetic field up to 150 Gauss at $T = 1.3^\circ\text{K}$.

3. Critical current density versus field and the method to choose samples which exhibit proximity effect. The critical current density (J_c) versus field (H) behavior was only performed on quenched and annealed $\text{Ag}_{97}\text{Pb}_3$ samples because, for a given field, the critical current was found to decrease rapidly as Pb content in the sample decreases, and becomes undetectable for samples with 1.5 at. % Pb or less even at $T = 1.3^\circ\text{K}$.

The I_c versus H measurement on a quenched $\text{Ag}_{97}\text{Pb}_3$ sample which was annealed at 200°C for various times at $T = 1.3^\circ\text{K}$ is shown in Fig. 24. Again, the same sample was used; therefore, the critical current can replace the critical current density in observing the differences in the qualitative behavior of the J_c versus H . As in the case of I_c versus T , the critical current decreases rapidly as temperature increases, and for a given field the critical current increases as the annealing time gets longer. This effect can lead to the fact that the resistivity versus field measurement is dependent on the measuring current density which was observed in the magnetoresistivity measurement.

For a given sample, as temperature increases, the J_c preserves the same dependence with H , except the magnitude of J_c decreases. An example is shown in Fig. 25.

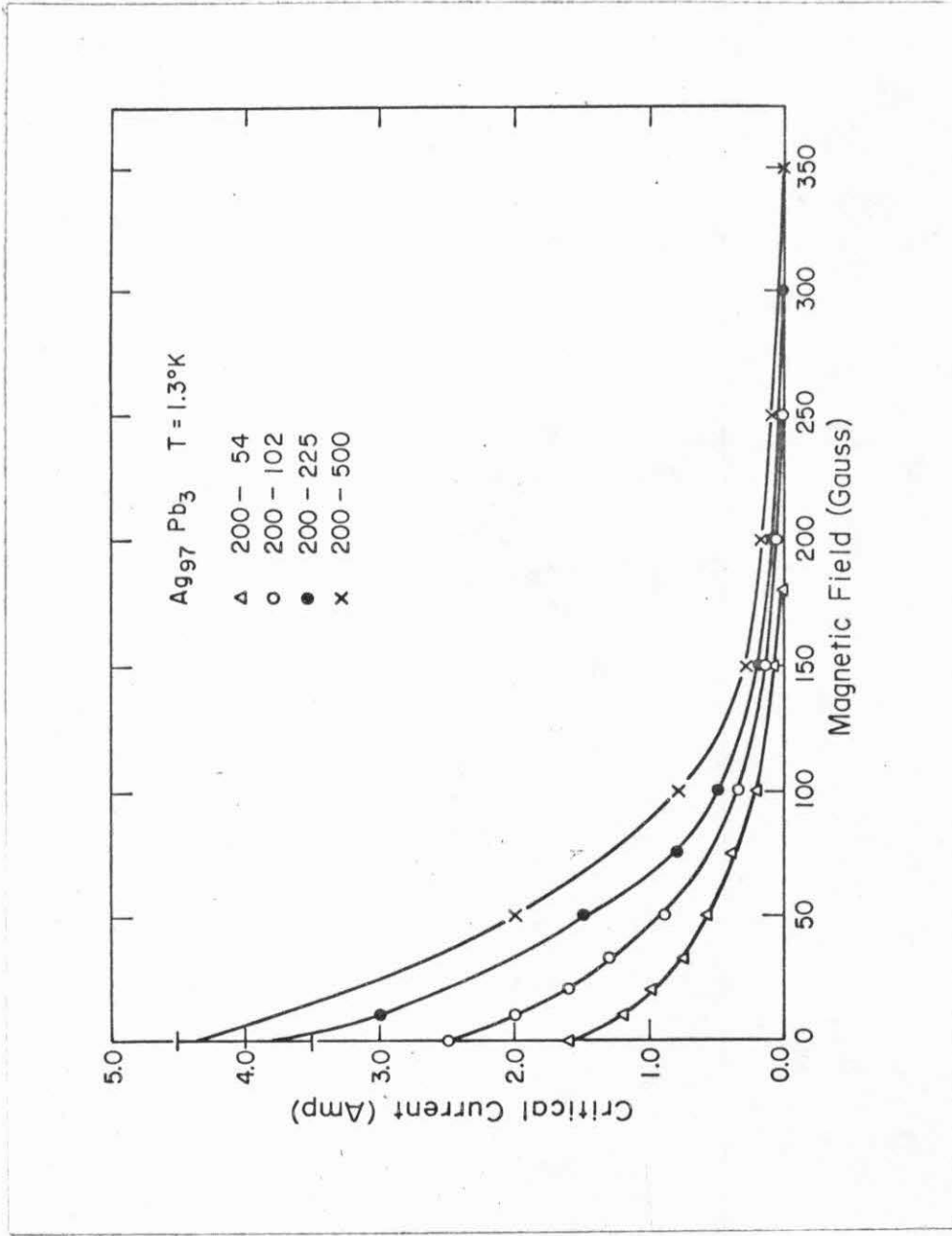


Fig. 24. Critical current versus applied field of the quenched Ag₉₇Pb₃ alloy annealed at 200°C.

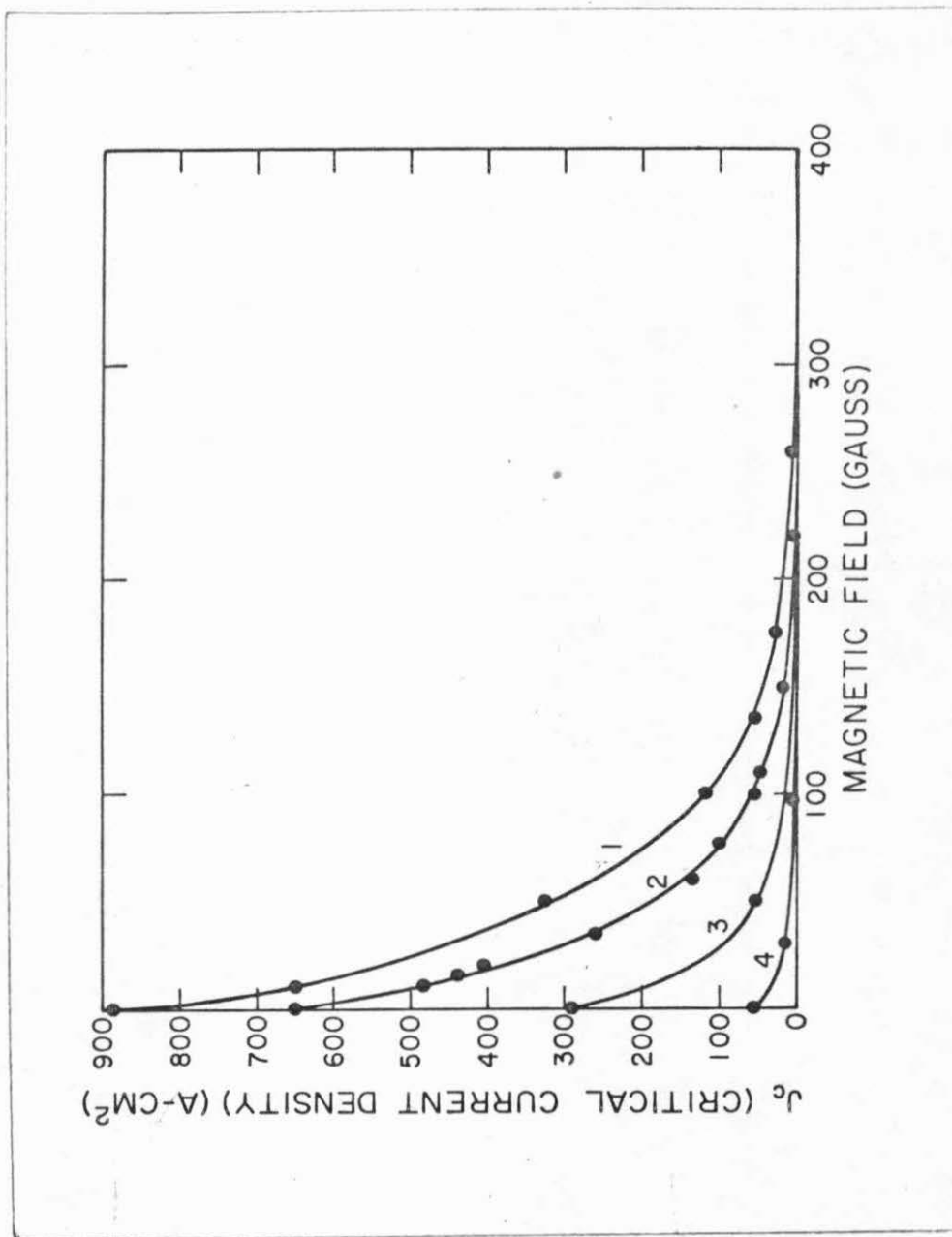


Fig. 25. Critical current density versus field of a quenched $Ag_{97}Pb_3$ alloy annealed at $200^{\circ}C$ for 54 hours at different temperatures. Curve 1: $T = 1.3^{\circ}K$; Curve 2: $T = 1.5^{\circ}K$; Curve 3: $T = 1.9^{\circ}K$; Curve 4: $T = 2.5^{\circ}K$.

Again, as in the case of I_c versus T , the I_c versus H for quenched $Ag_{97}Pb_3$ samples annealed at $300^\circ C$ for less than 20 hours is similar to the result which was obtained from samples annealed at $200^\circ C$, and samples annealed at $300^\circ C$ for more than 50 hours show the saturation of I_c at low field. An example is presented in Fig. 26. Since this kind of behavior is due to the filamentary effect of Pb in Ag that forms a superconducting short circuit across the sample, the I_c versus H or T experimental results can be used to distinguish samples which exhibit proximity effect, or the "good" samples, from samples which exhibit filamentary effect, or "bad" samples. Of course, this has to be further justified by the additional experiments like metallography studies and the superconducting volume fraction experiments. It was found that for quenched $Ag_{100-x}Pb_x$ samples with $1 \leq x \leq 3$, "good" samples were obtained and can be reproduced indefinitely times in those samples annealed at $200^\circ C$ and those samples annealed at $300^\circ C$ for less than 1.5 hours. The three-dimensional plot of the critical current density, magnetic field, and temperature for a typical "good" sample is shown in Fig. 27. For this sample, the critical surface which divides the superconducting state and the normal state is concave, which is quite different from the ordinary Type I bulk superconductors in which the critical surface is convex.

E. Superconducting Volume Fraction (SVF)

1. a. c. bridge results. As in the critical current case, the superconducting volume fraction of quenched $Ag_{100-x}Pb_x$ samples, $1 \leq x \leq 3$, was found to decrease rapidly as x decreased, and became undetectable for $x = 1.5$ and $x = 1$ even at $T = 1.3^\circ K$ after the same

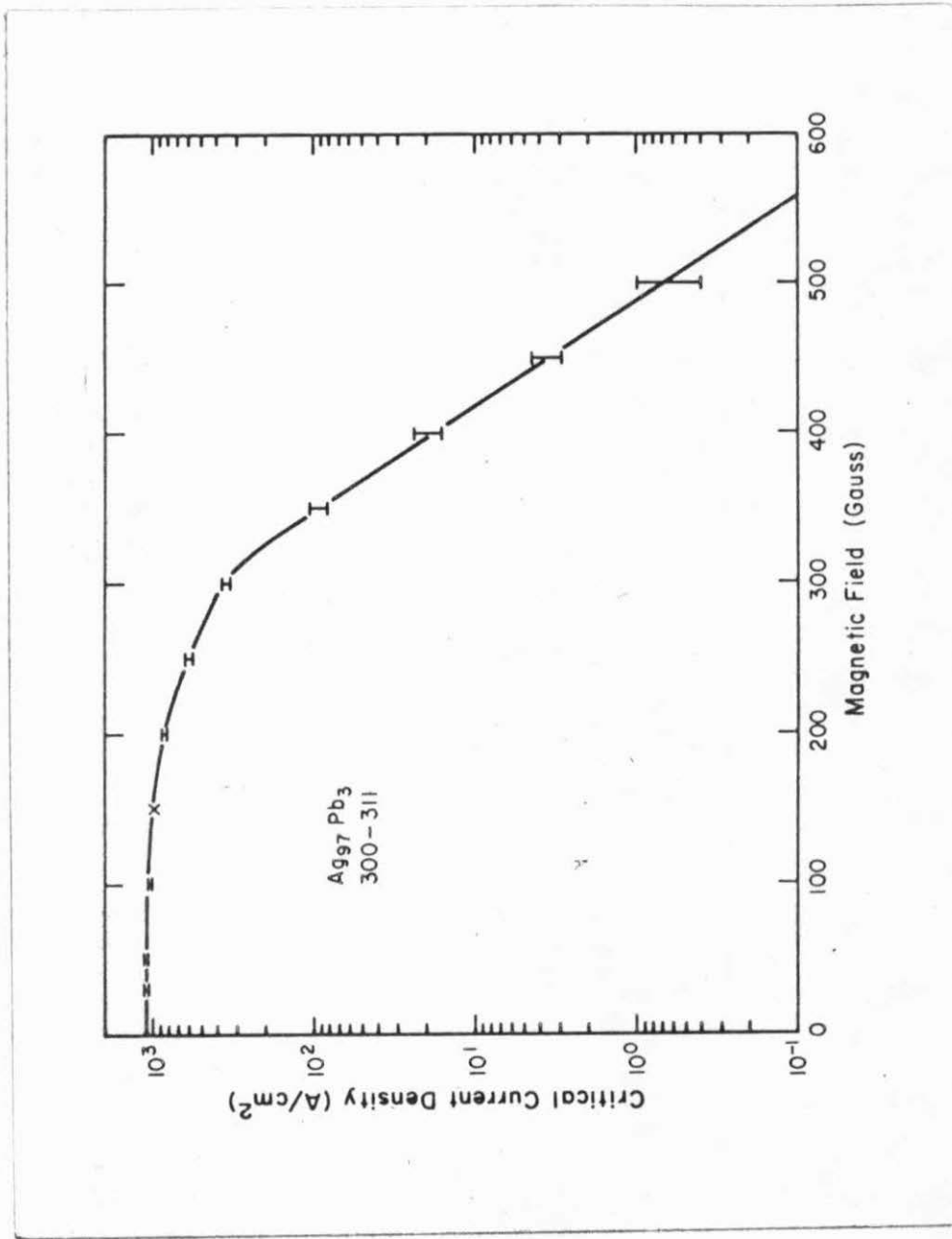


Fig. 26. Critical current density versus field of a quenched Ag97Pb₃ alloy annealed at 300°C for 311 hours at T = 1.3°K.

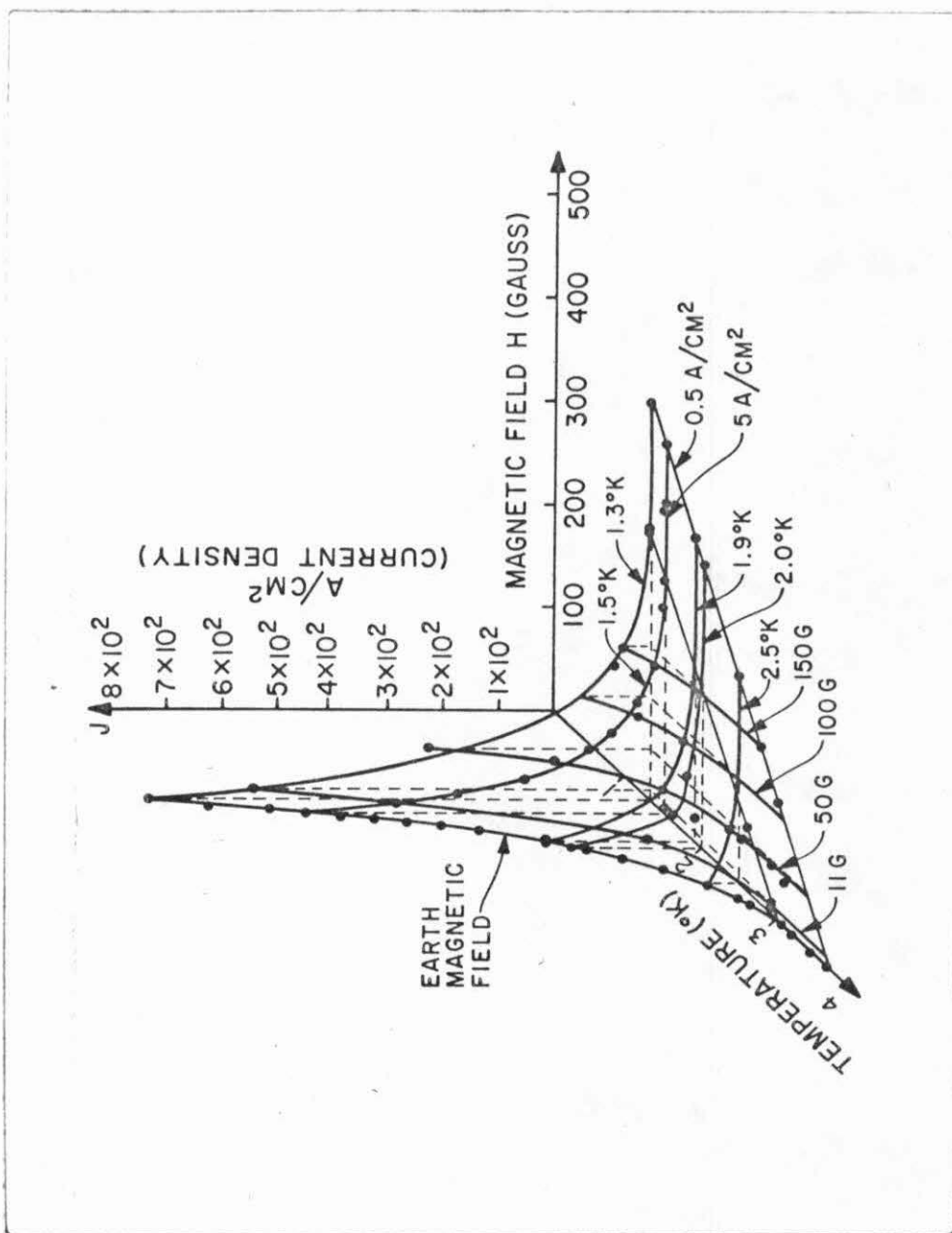


Fig. 27. Three-dimensional plot of J_c , T , and H of a quenched $Ag_{97}Pb_3$ alloy annealed at $200^\circ C$ for 54 hours.

heat treatment. Therefore, only results on quenched and annealed $\text{Ag}_{97}\text{Pb}_3$ samples are presented.

Again, similar to the case of I_c versus T , the superconducting volume fraction measured by the bridge method for quenched $\text{Ag}_{97}\text{Pb}_3$ samples annealed at 200°C and those samples annealed at 300°C for less than 10 hours have approximately the same behavior. A typical example is shown in Fig. 28. By careful comparison, for a given sample after normalization, the superconducting volume fraction (SVF) versus temperature curve can be perfectly matched to the I_c versus T curve. This means that the maximum current which the samples can carry without destroying the superconductivity is proportional to the superconducting volume fraction.

The SVF magnitude was found to be sensitive to the amplitude of the a. c. current which flows in the sample coil. The rms value of the a. c. magnetic field inside the sample coil is proportional to the rms value of the driven current. The SVF for quenched $\text{Ag}_{97}\text{Pb}_3$ samples annealed at 200°C for 307 hours for various rms magnetic fields inside the coil is shown in Fig. 29. It can be observed that for a given temperature the SVF decreases with increasing magnetic field in the coil. This is expected for a sample which exhibits the proximity effect. The curve formed by open circles in Fig. 29 is corresponding to the minimum current of which the lock-in amplifier can give a reasonable signal. This corresponds to a 0.9 Gauss magnetic field in the sample coil (including the effect of earth magnetic field). At very low temperature ($T < 1.5^\circ\text{K}$), it can be seen that the SVF gets saturated. The reason is obvious from the graph: the

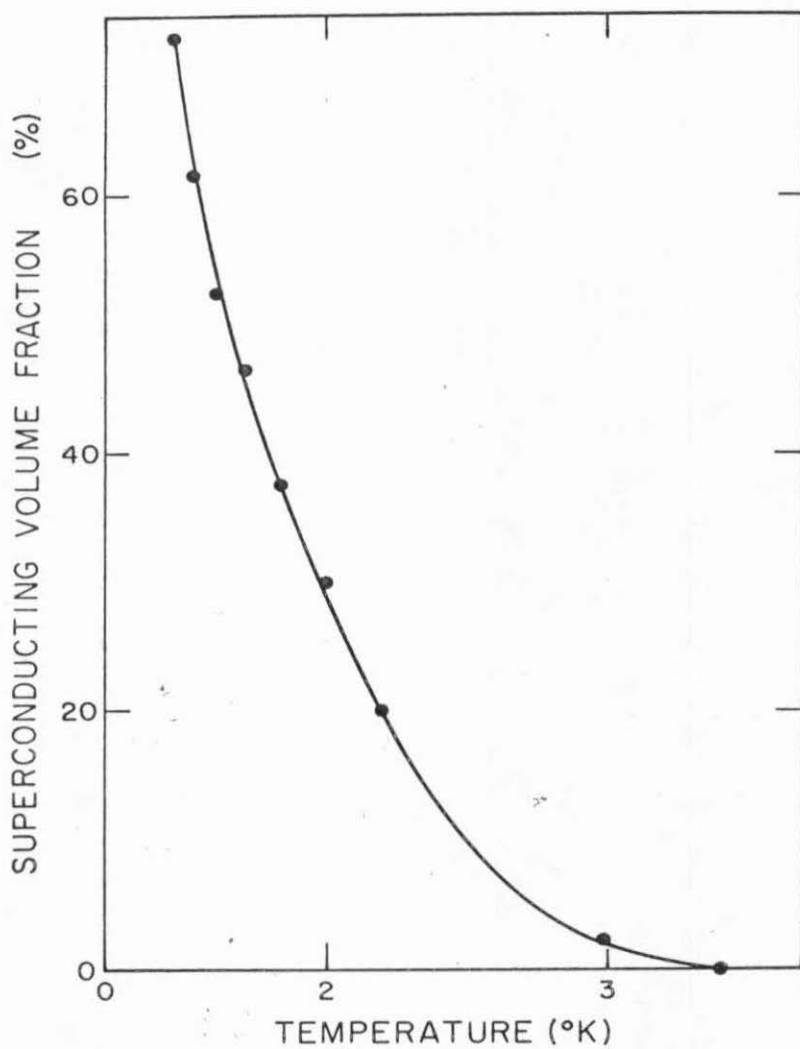


Fig. 28. The superconducting volume fraction versus temperature for the quenched $\text{Ag}_{97}\text{Pb}_3$ alloy annealed at 200°C for 54 hours.

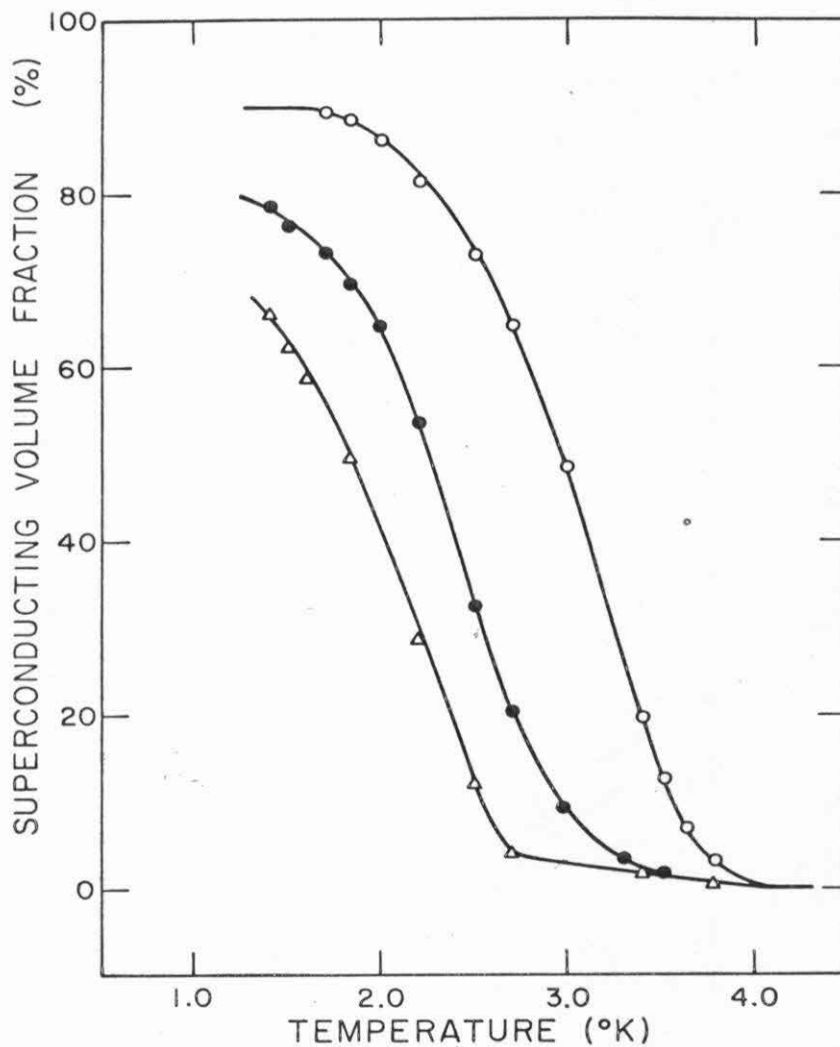


Fig. 29. The superconducting volume fraction versus temperature of a quenched $Ag_{97}Pb_3$ alloy annealed at $200^{\circ}C$ for 307 hours with different rms magnetic fields: \circ $H_{rms} \approx 0.9$ Gauss, \bullet $H_{rms} \approx 5$ Gauss, Δ $H_{rms} \approx 10$ Gauss.

SVF is about 90 per cent with 10 per cent error at $T \sim 1.5^{\circ}\text{K}$; therefore, the whole sample is nearly completely superconducting.

For quenched $\text{Ag}_{97}\text{Pb}_3$ samples annealed at 300°C for relatively long times ($t > 50$ hours), it was observed that the SVF is only about 2 - 3 at. % at low temperature. This agrees with the findings in critical current measurements and microstructure results, that for these samples the superconducting properties are due to the Pb filamentary effect. However, at very low temperature, $T \sim 1.5^{\circ}\text{K}$, for some of those samples the superconducting volume can again rise above the physical volume of Pb. An example is shown in Fig. 30.

2. Magnetization measurement results. From the last few sections and section F in the experimental results, it can be seen that quenched $\text{Ag}_{97}\text{Pb}_3$ samples annealed at 200°C can produce a well-defined geometry to exhibit the three-dimensional proximity effect. A typical example of the magnetization (M) versus field (H) results of these samples is shown in Fig. 31(a). It can be seen that the -M versus H curve is very similar to the behavior of a Type II superconductor except the M versus H at low field is not a straight line. It will be explained and proved in the discussion that each SNS junction in this investigation is actually Type I in nature. The reason that the -M versus H plot looks similar to a Type II superconductor is because the superconducting volume fraction (SVF) is decreasing with field. By using the expression $-4\pi M = (\text{SVF}) \times H$, the SVF versus H for a given temperature can be obtained. The SVF value obtained from Fig. 31(a) is shown in Fig. 31(b). Again similar to the case of SVF versus T which behaves just like I_c versus T, by comparing Fig. 31(b) to Fig.

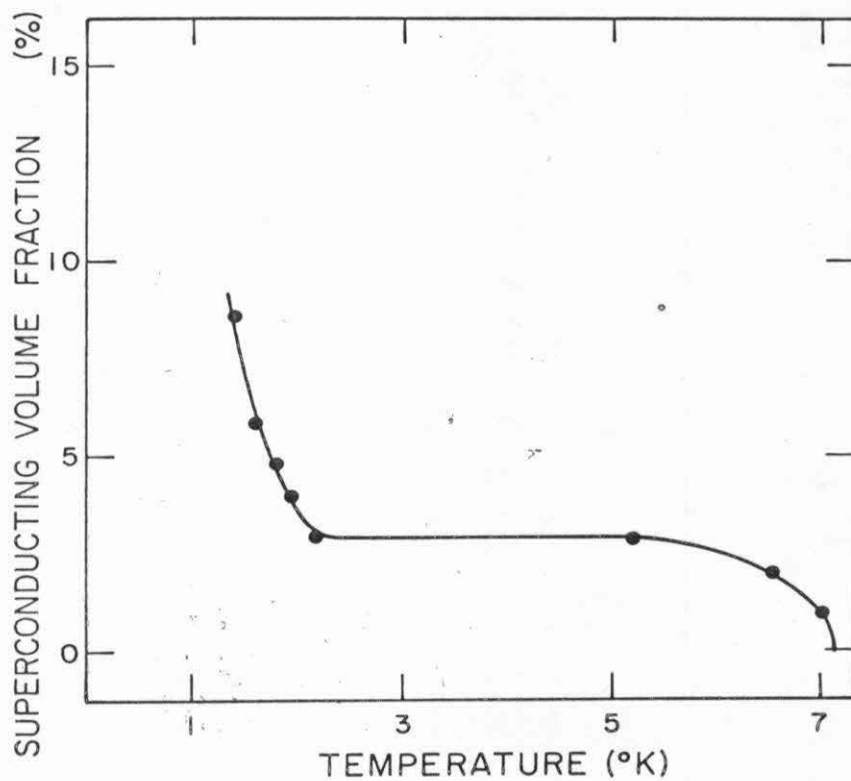


Fig. 30. The superconducting volume fraction versus temperature of a quenched $\text{Ag}_{97}\text{Pb}_3$ alloy annealed at 300°C for 311 hours.

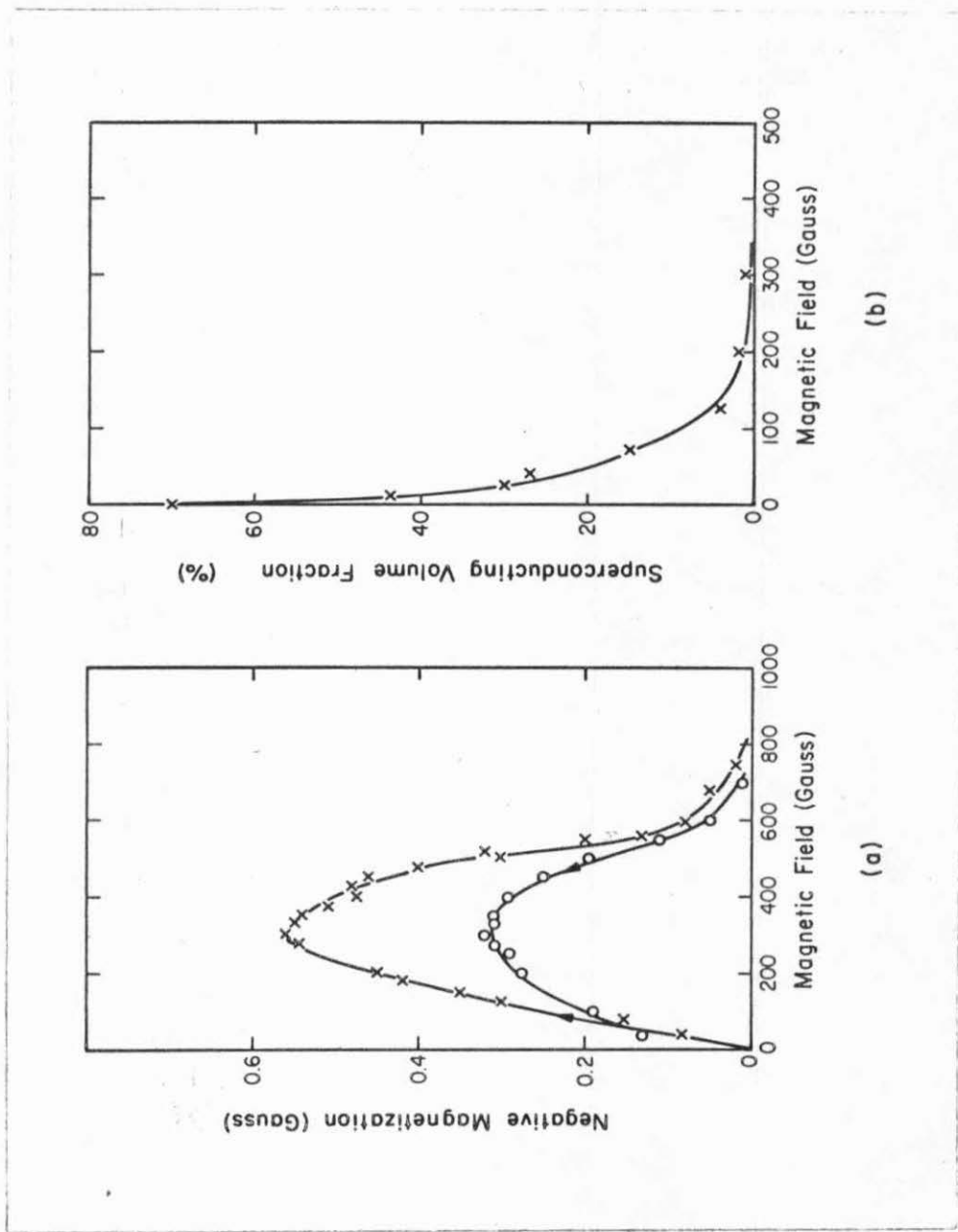


Fig. 31. Magnetization and its corresponding superconducting volume fraction as a function of magnetic field for a quenched $\text{Ag}_{97}\text{Pb}_3$ alloy annealed at 200°C for 307 hours.

24, it can be found that the SVF versus H and J_c versus H behaviors are nearly identical. Therefore, this again proves that the SVF and I_c are proportional.

F. Metallographic Studies

The scanning electron-microscopic (SEM) pictures of the $Ag_{100-x}Pb_x$ samples with $x \leq 3$ immediately after quenching were taken. The results show that the samples are practically single phase with only a few very small Pb-like nuclei distributed through the matrix and they are very far apart. A typical example is shown in Fig. 32 of an as-quenched $Ag_{97}Pb_3$ alloy. It can be observed that there are a few particles with the size of the order of 500 Å or less. The grain sizes are very small too, with average size about 8000 Å. The particle was examined by the EDAX technique. Because of the small size of the particle, an electron beam of the size about 100 Å can melt the particle in a few seconds; therefore, the counter cannot collect enough data from the x-ray emitted by the particle to get a reasonable spectrum. However, some of these particles were able to be identified as the residual Pb nuclei. These residual solvents have been observed in other liquid-quenched solid solutions⁽⁵⁴⁾.

Some of the particle-like images are actually due to the etching effect, polishing roughness, and etch pits, etc. Also, these images might be due to the resolution, which is only about 500 Å for the SEM picture in this particular sample. In conclusion, the sample can be considered as a single phase and practically free from precipitation.

After annealing the quenched $Ag_{97}Pb_3$ samples at 200°C for various times or 300°C for $t < 10$ hours, the SEM picture shows a

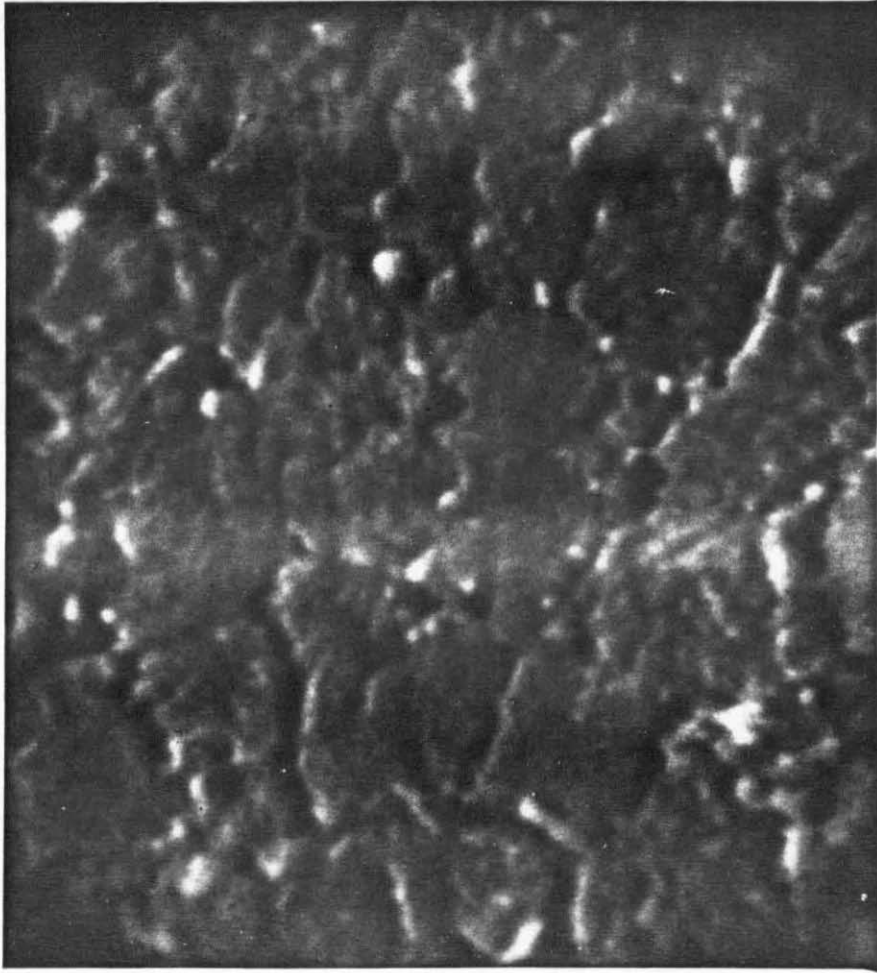


Fig. 32. SEM photomicrograph of an as-quenched Ag₉₇Pb₃ alloy: magnification 27,000 x .

nearly uniform distribution of Pb particles dispersed through the Ag matrix. An example of these samples is shown in Figs. 33 - 35. These figures show a quenched $\text{Ag}_{97}\text{Pb}_3$ sample annealed at 300°C for one hour with different magnifications. The identification of the phases of the background and the precipitates was done by the EDAX technique. The comparison of the characteristic x-ray line emitted by the background and the particle is shown in Fig. 36. The dotted curve (right) is the x-ray intensity collected from the background, and the solid curve (left) is collected from the particle. The dotted curve has a peak around 2.95 Kev to 3 Kev with width ± 0.2 Kev. This peak was identified as the combination of the characteristic $L\alpha$ and $L\beta$ lines of Ag. The solid curve has a peak around 2.35 Kev which was identified as the characteristic M line of Pb. Therefore, the phases were determined. The size of the Pb particle has a distribution in these quenched and annealed samples; for example, the particle size distribution of Fig. 33 is shown in Fig. 37. It can be observed that there is a maximum in the size distribution function; in that particular sample of Fig. 37 the size at which the maximum occurs is around 8300 \AA . By defining the dimension of the particle in a given sample as the size at the maximum of its size distribution function plus or minus its standard deviation, then the experimental result of the dimension of the particle against the annealing time in the quenched $\text{Ag}_{97}\text{Pb}_3$ samples annealed at 200°C and 300°C is shown in Fig. 38. In the cases of annealing at 200°C , it can be observed that the dimension of particle increases rapidly for annealing time less than 25 hours; then the rate of growth becomes gradually slower. The dimension of the particle is

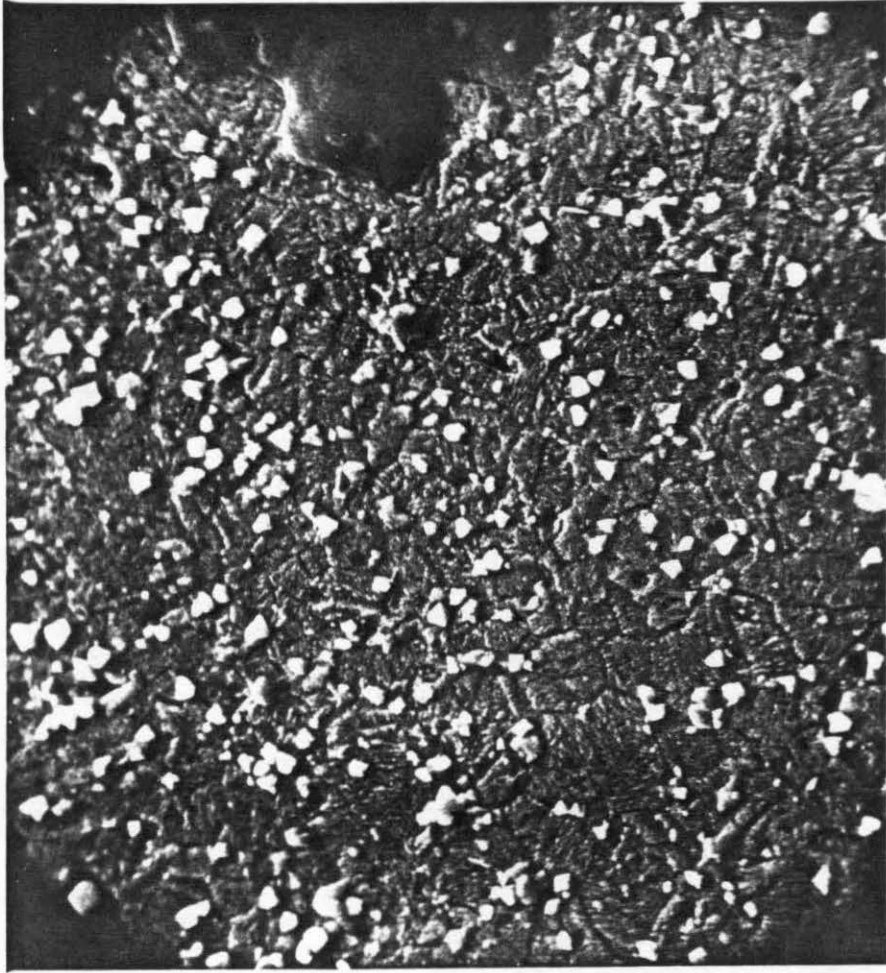


Fig. 33. SEM photomicrograph of a quenched Ag₉₇Pb₃ alloy annealed at 300°C for 1 hour: magnification 3,000X.



Fig. 34. SEM photomicrograph of the same alloy as Fig. 33: magnification 15,500 X .

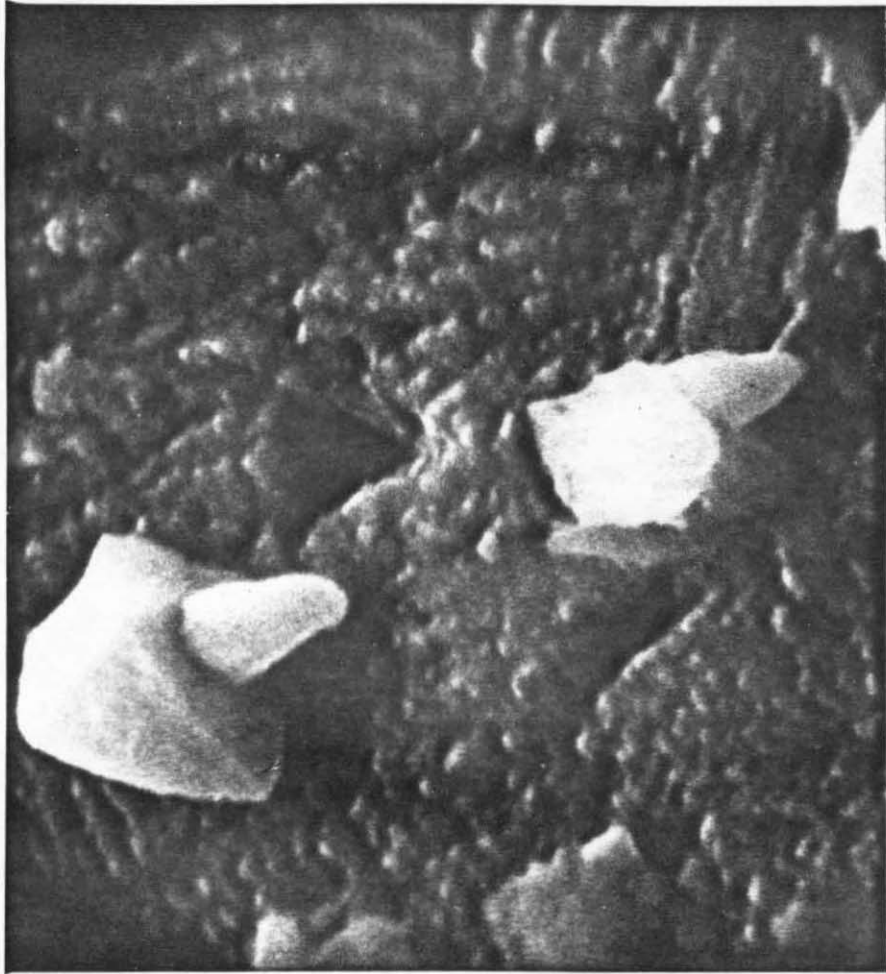


Fig. 35. SEM photomicrograph of the same alloy as in Fig. 33: magnification 30,000 X .

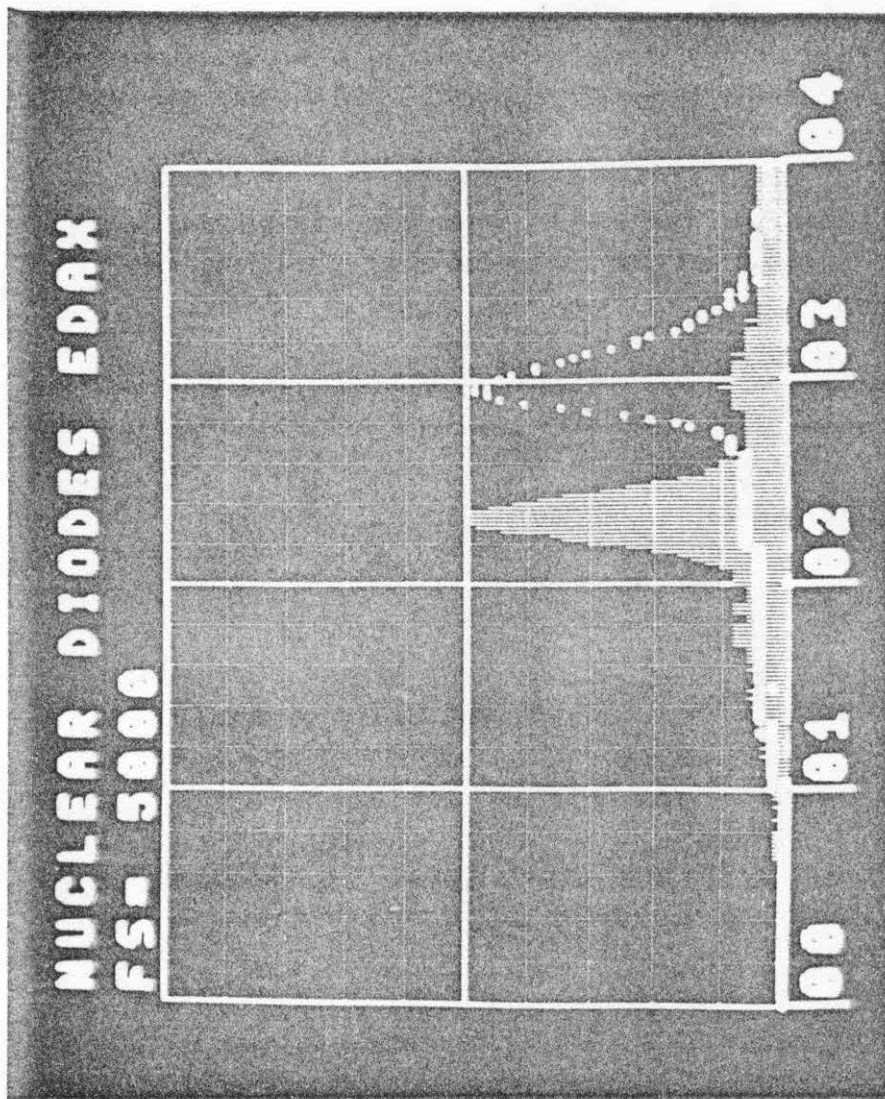


Fig. 36. X-ray spectrum emitted from the background and the precipitate of the alloy in Fig. 33: dotted curve (from the background), solid curve (from a precipitate).

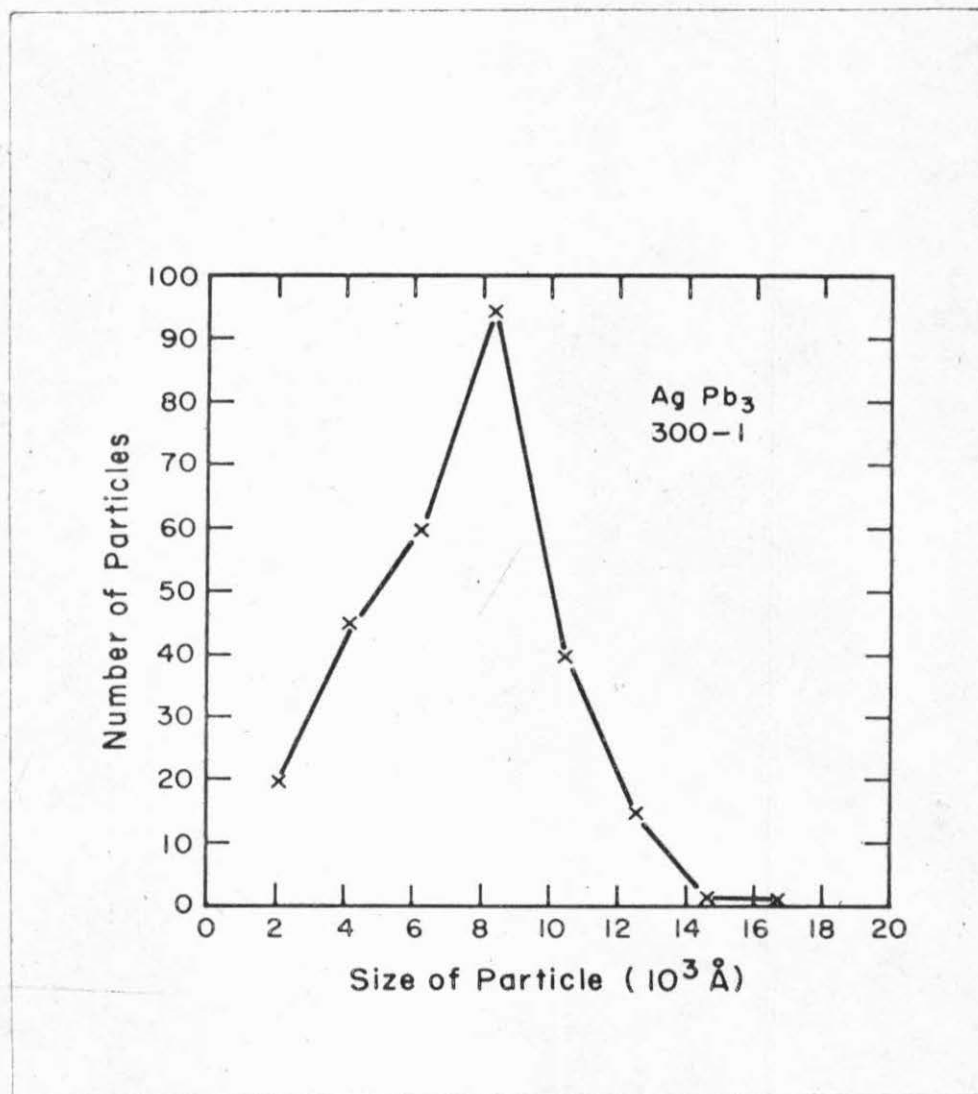


Fig. 37. Size distribution function of the precipitates in Fig. 33.

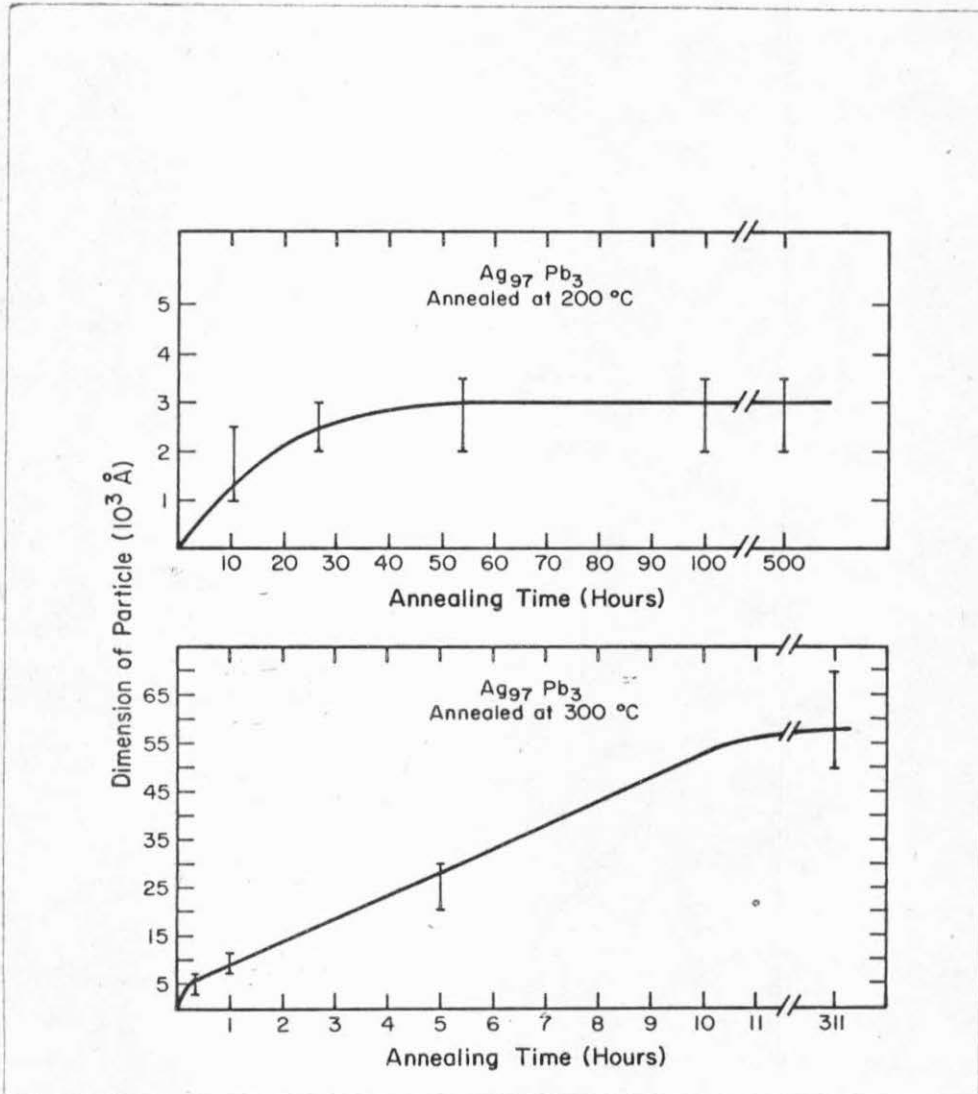


Fig. 38. Dimension of particles (precipitates) as a function of annealing time for the quenched $\text{Ag}_{97}\text{Pb}_3$ alloys annealed at 200 °C and 300 °C.

nearly independent of annealing time after 50 hours of annealing. In the cases of annealing at 300°C , the dimension of the particle increases very fast for annealing time $t < 20$ minutes, then increases nearly linearly but with lower rate until $t \sim 10$ hours. After that, the growth of the dimension of the particle seems stopped.

For quenched $\text{Ag}_{97}\text{Pb}_3$ samples annealed at 300°C for $t > 50$ hours, it was discovered that more than 90 per cent of the Pb precipitates were along the grain boundary, thereby forming continuous Pb filaments across the whole sample. For example, the picture of a quenched $\text{Ag}_{97}\text{Pb}_3$ sample annealed at 300°C for 311 hours is shown in Fig. 39. However, even in these cases, some of the small particles still can remain in the Ag matrix, but this kind of precipitation was usually around the big Pb particles. If a SEM picture was taken around one of the Pb particles in Fig. 39, then Fig. 40 is obtained. It can be observed that many small Pb precipitations were around the big Pb particle which is in the upper half of the picture. The size of the precipitates becomes larger as the distance between the small precipitates and the big one lessens.

For other compositions of the quenched $\text{Ag}_{100-x}\text{Pb}_x$ samples with $x < 3$, after annealing them for the same temperature and the same time as a quenched $\text{Ag}_{97}\text{Pb}_3$ sample, it was found that the dimension of the particles is about the same magnitude. However, the average interparticle distance of those samples becomes larger as the composition of Pb in Ag decreases, as expected.

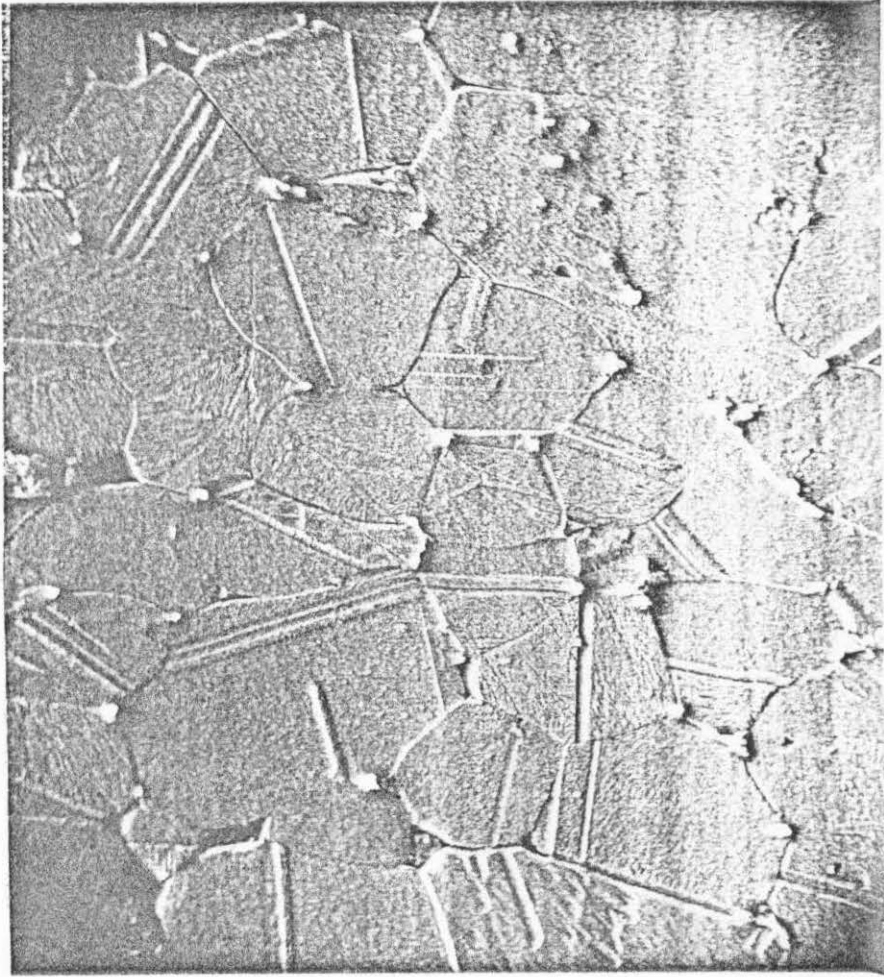


Fig. 39. Photomicrograph of a quenched Ag₉₇Pb₃ alloy annealed at 300°C for 311 hours: magnification 1000 x.

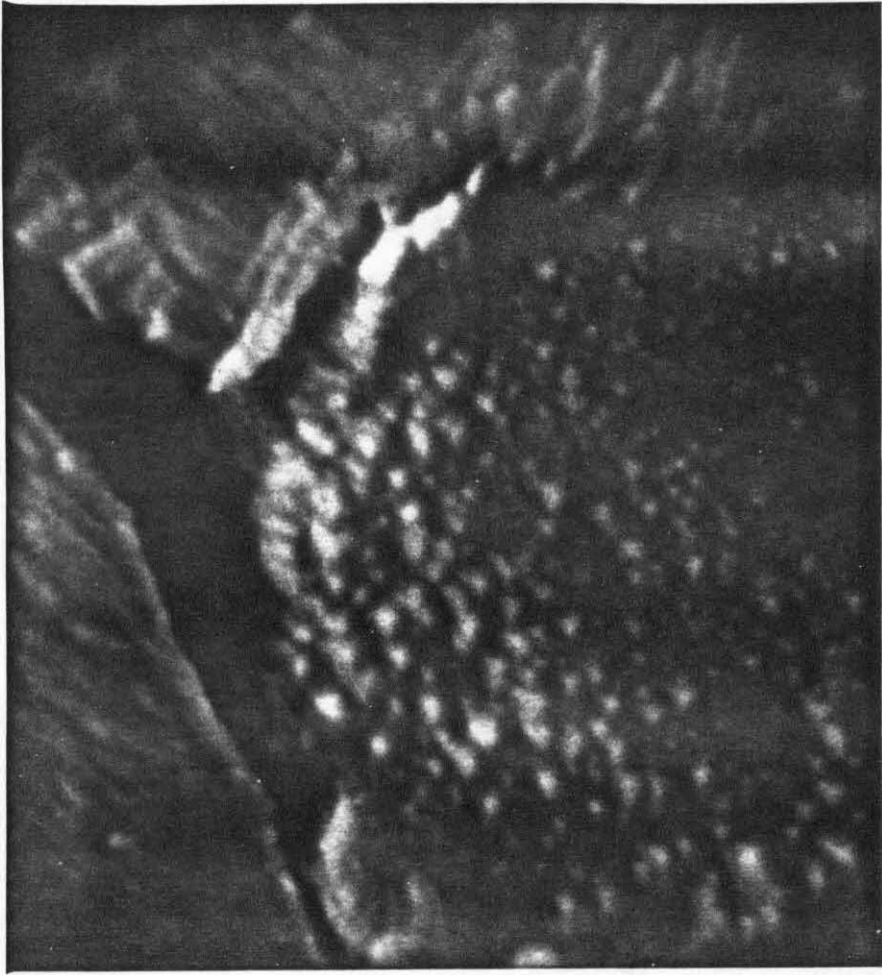


Fig. 40. SEM photomicrograph taken in the vicinity of the big lead precipitates in Fig. 39.

G. Relation between Superconducting Transition Temperature and the Dimension of the Pb Precipitates

It was discussed in the critical current versus temperature result section that it is reasonable to define the superconducting transition as the onset of the resistivity versus temperature transition. By doing that, the experimental relation of the transition temperature and the dimension of the Pb particle for quenched and annealed $\text{Ag}_{97}\text{Pb}_3$ samples can be plotted, and is shown in Fig. 41. It can be seen that the T_c increases from 1.5°K to 7°K as the dimension of the particles increases from 1000 \AA to 10000 \AA . Also by extrapolation, it can be found that T_c would disappear when the dimension of the Pb particle is smaller than 800 \AA . It therefore explains why the as-quenched samples, although they still have some small Pb nuclei, are not superconducting.

Although Fig. 41 is the result for quenched and annealed $\text{Ag}_{97}\text{Pb}_3$ samples, it remains approximately true for the other quenched and annealed $\text{Ag}_{100-x}\text{Pb}_x$ samples with $1 \leq x < 3$.

As mentioned in the resistivity results, the onset of the transition in resistivity versus temperature seems independent of composition ($x \leq 3$) for samples with the same heat treatment. From metallographic studies, the dimension of the precipitates in the sample is independent of composition too, for a given heat treatment. It can therefore be concluded that T_c defined in this section is nearly independent of the average interparticle distance of the Pb particles, and only depends on the dimension of the particles.

One more thing has to be mentioned, that is, that T_c measure-

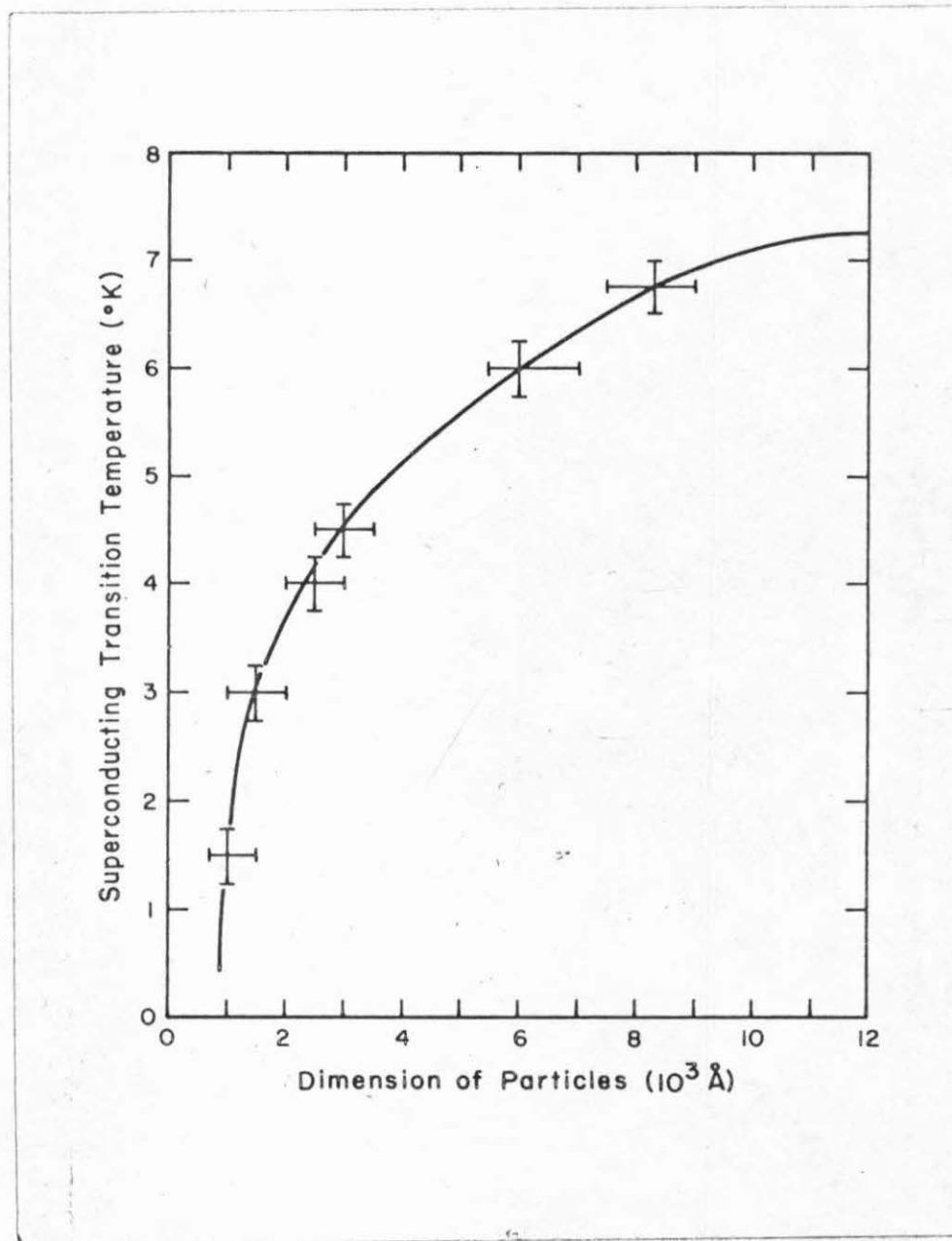


Fig. 41. The superconducting transition temperature versus the dimension of the particle (precipitate) for the quenched and heat-treated $\text{Ag}_{97}\text{Pb}_3$ alloys.

ments on the quenched and annealed $\text{Ag}_{99}\text{Pb}_1$ samples are very difficult to perform, simply because the critical current and the SVF in these samples are too small. Determining T_c by measuring the electrical resistivity versus temperature, the accuracy is limited by the resolution of the digital voltmeter, and the measuring current should be smaller than the critical current of the sample. Since the critical current density in quenched and annealed $\text{Ag}_{99}\text{Pb}_1$ samples is extremely small (normally less than 1 A/cm^2), very small current has to be used. However, if the current is too small, then in the normal state the voltage across the sample is too small to be detectable. Therefore, higher current was used, but this current magnitude might exceed the critical current. That is why the superconductivity in most quenched and annealed $\text{Ag}_{99}\text{Pb}_1$ samples cannot be observed clearly, as was shown in Figs. 15 and 16. Since it is known that SVF is proportional to the critical current, measuring T_c by the a. c. bridge method in the quenched and annealed $\text{Ag}_{99}\text{Pb}_1$ is also very difficult. The T_c determination on the quenched and annealed $\text{Ag}_{99}\text{Pb}_1$ samples was done by combination of the above two methods, but with much larger experimental error than the other compositions.

IV. DISCUSSION

A. Relevant Theory about the Occurrence of Superconductivity for the Samples in this Investigation

The relevant theory which is deduced in this section is based on de Gennes' theory⁽³⁾ and Silvert and Singh's⁽³⁷⁾ theoretical calculation on the "proximity effect" in superconductor.

For a superconductor at normal state ($T > T_c$), the one electron wave function $w_n(r)$ is defined by

$$\left[\frac{p^2}{2m} + u(\vec{r}) \right] w_n = \epsilon_n w_n \quad (4.1)$$

where $p^2/2m$ is the kinetic energy of the electron, $u(r)$ is the effective potential and ϵ_n is the energy eigenvalue.

For $T < T_c$, according to the BCS theory,⁽¹⁾ electrons form pairs when there is an effective attractive interaction obtained by pairing one electron in a state w_n , and another in the time-reversal state w_n . The transition temperature of the superconductor can be characterized by the parameter NV according to the relation

$$T_c = 1.14 \theta_D \exp\left(-\frac{1}{NV}\right) \quad (4.2)$$

where N is the density of states at the Fermi surface, and is always larger than zero, V is the effective electron-electron interaction and θ_D is the Debye temperature of the sample. The criterion for the metal to be a superconductor is therefore $V > 0$. The above relation and procedure in forming pairs work only when the pair potential or the order parameter in the material, $\Delta(r)$, may be taken as independent

of r : in an infinite dimension (or at least the dimension is much larger than the coherence length), pure metals or homogenous alloys. The order parameter $\Delta(r)$ is defined as $F(r)$ which is equal to $\langle \psi_{\uparrow} \psi_{\downarrow} \rangle$, the probability amplitude of the Cooper pair, multiplied by V . Morel and Anderson⁽⁴³⁾ have pointed out that V is essentially a point interaction so that in a system consisting of two different metals, one can suppose that the interaction parameter changes abruptly on the boundary. It is the fact that the condensation amplitude of the superconducting electrons cannot change abruptly at the boundary, but only over a distance of the order of a coherence length, which gives rise to the proximity effect.

In this investigation because NV varies spatially in the sample, the optimum pairing, as in the case of pure metal or homogeneous alloy, is no longer applicable. The Gorkov self-consistent integral equation⁽⁴⁴⁾ has to be used to calculate the spatial variation of $\Delta(r)$.

$$\Delta(\vec{r}) = V(\vec{r}) \sum_{\omega} \int d^3r' \Delta(\vec{r}') H_{\omega}(\vec{r}, \vec{r}') \quad (4.3)$$

and

$$H_{\omega}(\vec{r}, \vec{r}') = T \sum_{\omega} \sum_{nm} \frac{1}{\epsilon_n - i\omega} \frac{1}{\epsilon_m + i\omega} \times w_n(\vec{r}) w_m(\vec{r}) w_n(\vec{r}') w_m(\vec{r}') \quad (4.4)$$

where $\omega = 2\pi T(\nu + \frac{1}{2})$ is the phonon energy and the sum \sum_{ω} represents a sum over all (positive or negative or 0) integers (ν). The function w_n is the one-electron wave function, in the normal state, defined by eq. (4.1). The maximum temperature T at which eq. (4.3) has a nonzero solution $\Delta(r)$ is the transition temperature T_{CNS} of the system.

The symmetric kernel $H_{\omega}(\vec{r}, \vec{r}')$ has some interesting properties. From the orthogonality of the (real) functions w 's, the following relation can be obtained

$$\begin{aligned} \int H_{\omega}(\vec{r}, \vec{r}') d^3 r' &= \sum_n \frac{1}{\epsilon_n^2 + \omega^2} |w_n(\vec{r})|^2 \\ &= N(\vec{r}) \int \frac{d\epsilon}{\epsilon^2 + \omega^2} \\ &= \frac{\pi}{|\omega|} N(\vec{r}) \end{aligned} \quad (4.5)$$

where $N(\vec{r})$ is the local density of states.⁽⁴⁵⁾ Consider the sum

$$\begin{aligned} G_{\Omega}(\vec{r}, \vec{r}') &= \overline{\sum_m w_n(\vec{r}) w_m(\vec{r}) w_n(\vec{r}') w_m(\vec{r}')} \\ &\times \delta(\epsilon_n - \epsilon_m + \Omega) \end{aligned} \quad (4.6)$$

where the average is taken over all states n with a fixed energy ϵ_n . When G is known, $H_{\omega}(\vec{r}, \vec{r}')$ can be derived simply according to (4.4). Now observe that the Fourier transform of $G_{\Omega}(\vec{r}, \vec{r}')$ in eq. (4.6)

$$G(\vec{r}, \vec{r}', t) = \frac{1}{2\pi} \int dt e^{i\Omega t} G_{\Omega}(\vec{r}, \vec{r}') \quad (4.7)$$

is a one-electron correlation function, namely

$$G(\vec{r}, \vec{r}', t) = \overline{[(\vec{r}(0) - \vec{r})][\vec{r}(t) - \vec{r}']} \quad (4.8)$$

where the average is over all one-electron states of energy ϵ_n (in practice at the Fermi energy) and $\vec{r}(t) = e^{iEt} \vec{r} e^{-iEt}$ is the electron position operator in the Heisenberg representation. $E = p^2/2m + U(\vec{r})$ is the Hamiltonian.

In the "dirty" limit in which the mean free path in the material, ℓ , is much smaller than the coherence length in the "clean" limit ($\ell \rightarrow \infty$) $\xi_c = \frac{\hbar v_f}{2\pi k_B T}$, (4.10), as is normally encountered for the samples in this investigation, then the correlation function (4.8) spreads out according to the diffusion equation

$$\begin{aligned} (\partial/\partial|t|) G(\vec{r}, \vec{r}', t) - D\nabla^2 G(\vec{r}, \vec{r}', t) \\ = \text{constant} \times \delta(\vec{r}, \vec{r}')\delta(t) \end{aligned} \quad (4.9)$$

where $D = \frac{1}{3} v_f \ell$ is the diffusion coefficient and v_f is the Fermi velocity. Taking Fourier transform of eq. (4.9), the following equation can be obtained

$$\begin{aligned} G_\Omega(\vec{q}) &= \int G_\Omega(\vec{r}, \vec{r}') e^{i\vec{q} \cdot (\vec{r} - \vec{r}')} d^3 \vec{r}' \\ &= \text{constant} \times \left\{ \frac{1}{i\Omega + Dq^2} + \text{C. C.} \right\} \end{aligned} \quad (4.10)$$

By combining eq. (4.4), eq. (4.6) and eq. (4.10), the function H_ω can be obtained

$$\begin{aligned} H_\omega(\vec{q}) &= \int H_\omega(\vec{r}, \vec{r}') e^{i\vec{q} \cdot (\vec{r} - \vec{r}')} d^3 \vec{r}' \\ &= \text{constant} \times \int d\epsilon d\Omega \frac{1}{\epsilon - i\omega} \frac{1}{\epsilon + \Omega + i\omega} \\ &\quad \times \left\{ \frac{1}{i\Omega + Dq^2} + \text{C. C.} \right\} \\ &= 2\pi N \frac{1}{2|\omega| + Dq^2} \end{aligned} \quad (4.11)$$

where the constant has been obtained from eq. (4.5).

By assuming the solution in eq. (4.3) as $\Delta \sim e^{iqr}$, and using the Fourier transform eq. (4.11) to perform eq. (4.3), then summing over ω , yields the exact solution;

$$\chi(\xi^2 q^2) = \ln(1.14 \theta_D / T_c) - \frac{1}{NV} \quad (4.12)$$

with $\chi(z) = \psi(\frac{1}{2}z + \frac{1}{2}) - \psi(\frac{1}{2})$

and $\psi(z) = [\Gamma'(z)/\Gamma(z)]$ is the digamma function where

$$\begin{aligned} \xi &= \left(\frac{\hbar D}{2\pi k_B T} \right)^{\frac{1}{2}} \\ &= \left(\frac{\hbar v_f \ell}{6\pi k_B T} \right)^{\frac{1}{2}} \end{aligned} \quad (4.13)$$

is the coherence length of the superconductor in the "dirty" limit, \hbar is the Planck's constant and k_B is the Boltzmann constant.

De Gennes⁽³⁾ and Werthamer⁽¹⁶⁾ have derived the boundary conditions on $F(r)$ at the interface between a superconductor and a normal material

$$F_n / N_n = F_s / N_s \quad (4.14)$$

and

$$D_n \frac{\partial F_n}{\partial n} = D_s \frac{\partial F_s}{\partial n} \quad (4.15)$$

Eq. (4.14) implies that the fraction of electrons paired is conserved across the interface. This is so only if the boundary scattering can be completely ignored. The condition eq. (4.15) is characteristic of "dirty" systems. To ignore the boundary scattering, two things have to be done:

1. The electrical contact between N and S must be very good.
2. The atoms of N must not migrate to S and vice versa.⁽⁵⁵⁾

Atomic migrations are dangerous in two respects: (a) A small concentration of N in S lowers the transition temperature of S. This is a weak effect if N is nonmagnetic, but it becomes really catastrophic if N is magnetic. (b) The electron transmission properties at the boundary can be affected: This is probably the most serious effect with nonmagnetic N metals.

Migration effects are minimized by the following procedures: use of N and S metals which are not miscible and do not form intermetallic compounds, and/or use of "dirty" N and S samples. If the mean free paths in N and S are relatively short, they will be insensitive to a small diffusion of N in S and vice versa.⁽³⁾

As described in the material choices in the experimental methods, the Ag-Pb system satisfied the above requirements.

Now, to perform an exact calculation of T_c based on the samples which have the structure as the one shown in Fig. 33, where the superconducting particles are dispersed nearly uniformly throughout the normal matrix, is very complicated if the grain size and boundary effects are included. To simplify this calculation, a few assumptions were made as follows:

1. The grain sizes are so large that the grain size and the grain boundary effects are negligible.
2. All the precipitated particles are of the same size and are spherical with radius a .
3. F and $\frac{\partial F}{\partial n}$ are continuous at the boundary.

The justification of the above assumptions for the samples in this investigation is given in the following:

1. All the interesting proximity effect samples have grains much larger than the individual SNS junctions.
2. For a given quenched and annealed sample there is always a maximum in the size distribution function; in other words, most of the particles are approximately the same size. However, the individual particles are of irregular shape.
3. Because $N_{Pb} \neq N_{Ag}$ and $D_{Pb} \neq D_{Ag}$, therefore, according to eq. (4.14) and (4.15), the functions which are continuous across the SN interface are F/N and $D \frac{\partial F}{\partial n}$, not F and $\frac{\partial F}{\partial n}$. However, the ratios N_{Pb}/N_{Ag} and D_{Pb}/D_{Ag} are constants; it can be expected that, assuming F and $\frac{\partial F}{\partial n}$ continuous, it will not affect the qualitative result.

Since $F = \langle \psi_{\uparrow} \psi_{\downarrow} \rangle$, it can be expected and was shown⁽³⁾ that $F = \frac{\Delta}{V} \propto e^{iqr}$ inside the superconductor and $F \propto e^{-kr}$ in the normal metal in a one-dimensional SN junction or layer structure, where the q and k are real numbers and $k_n^{-1} = \xi_n \left(1 + \frac{2}{2n(T/T_{cn})} \right)^{\frac{1}{2}} = \left(\frac{\hbar v_f \ell_n}{6\pi kT} \right)^{\frac{1}{2}} \times \left(1 + \frac{2}{2n(T/T_{cn})} \right)^{\frac{1}{2}}$ is the penetration depth in the normal region. This means that the pair correlation amplitude is a plane wave inside the superconductor and a damped wave in the normal metal. By extending this idea to three dimensions, it can be expected that F is a spherical wave in the superconductor and a spherically damped wave in the normal metal in a spherically symmetrical system. Therefore by using the three assumptions just described

$$F(r < a) \sim \frac{\sin qr}{r} \quad (4.16)$$

$$F(r > a) \sim \frac{A e^{-k_n r} + B e^{k_n r}}{r} \quad (4.17)$$

where A and B are constants which are determined by the boundary conditions in assumption 3 plus the requirement of $\partial F/\partial r = 0$ at $r = b$, if the interparticle spacing is $2b$.

Now, let T_{c1} be equal to the lead superconducting transition temperature and T_{c2} be equal to the silver superconducting transition temperature. Then from eq. (4.2) and (4.12)

$$\chi(\xi_s^2 q^2) = \ln(T_{c1}/T_c) \quad (4.18)$$

$$\chi(-\xi_n^2 k^2) = \ln(T_{c2}/T_c) \quad (4.19)$$

By using (4.16), (4.17), (4.18), and (4.19) together with the three boundary conditions, the T_c of the system can be determined. Remember this T_c is in the limit that current density is zero in the sample. From Fig. 18, it can be shown that this T_c is the onset of transition in the resistivity versus temperature measurement. This is consistent with the definition of T_c in section G of experimental results.

The penetration depth k_n^{-1} in the normal metal is equal to $\xi_n \left(1 + \frac{2}{\ln(T/T_{cn})}\right)^{\frac{1}{2}}$ (3, 4, 22) According to Matthias,⁽⁴⁶⁾ Ag is not superconducting above 0.35°K and because all the experimental data are taken at $T > 1.2^\circ\text{K}$, therefore $k_{Ag}^{-1} \cong \xi_{Ag} = \left(\frac{\hbar v_f \ell_n}{6\pi k_B T}\right)^{\frac{1}{2}}$. From Table II, it can be seen that $k_{Ag}^{-1} < 1500 \text{ \AA}$. But from the

experimental results, $2b \geq 5000 \text{ \AA}$, and eq. (4.17) is exponentially dependent, then it is a good approximation to assume for the samples in this investigation that

$$F(r > a) \sim \frac{e^{-k_n r}}{r} \quad (4.20)$$

Eq. (4.20) implies that the T_c is independent of b . This is approximately true in this investigation, as discussed in the last part of the section G of experimental results.

From Eq. (4.16), (4.20) and by requiring F and $\frac{\partial F}{\partial r}$ continuous at $r = a$, it can be found

$$q \cot qa = -k_n$$

By defining $Q = q\xi_s$, $K = k_n \xi_n$ and $\alpha = \frac{a}{\xi_s}$ the following system of three equations in three unknowns can be obtained

$$Q \cot Q = -K \quad (4.21)$$

$$\chi(Q^2) = \ln(1/t) \quad (4.22)$$

$$\chi(-K^2) = \ln(\tau/t) \quad (4.23)$$

where $t = T_c/T_{c1}$, and $\tau = T_{c2}/T_{c1}$. From eq. (4.13), $\xi_s = \xi_{os}/t^{\frac{1}{2}}$. Where $\xi_{os} = \xi_s(T = T_{c1})$. As $\alpha \rightarrow \infty$ from eq. (4.21) $Q \rightarrow 0$, $Q\alpha \rightarrow \pi$ and

$$\begin{aligned} t &= \exp(-\chi(Q^2)) \sim \exp(-\frac{1}{4} \pi^2 Q^2) \sim \exp(-\frac{1}{4} \pi^2 (\frac{\pi}{\alpha})^2) \\ &\sim [1 - (\pi^2 \xi_s / 2a)^2] \end{aligned}$$

This result, aside from geometrical factors, has the same size

dependence as found for layered system.⁽³⁾

Theoretically, if silver is superconducting at T_{c2} , then the lower limit for the transition temperature of the whole system is T_{c2} . Matthias⁽⁴⁶⁾ has shown experimentally that silver is not superconducting above 0.35°K. Deutscher⁽³⁰⁾ has shown that the effective interaction parameter in Ag is very weak although attractive. Therefore it is a good approximation to assume $T_{c2} = 0$. From eq. (4.23) as $t \rightarrow \tau$, $K \rightarrow 0$ and from eq. (4.21) $Q\alpha \rightarrow \pi/2$. It is interesting to observe as $t \rightarrow \tau \rightarrow 0$ eq. (4.22) becomes

$$\chi(\xi_{os}^2 q^2/t) = \ln(1/t)$$

Because $\chi(z) \sim \ln(2z) + \gamma$ as $z \rightarrow \infty$ so

$$\chi(\xi_{os}^2 q^2/t) \sim \ln(2 \xi_{os}^2 q^2/t) + \gamma \quad \text{as } t \rightarrow 0$$

where γ is the Euler's constant, $\gamma = 0.577$. Therefore

$$1/t \sim e^\gamma 2 \xi_{os}^2 q^2/t$$

or

$$q = \frac{1}{\xi_{os} \sqrt{2 e^\gamma}} \quad (4.24)$$

since $Q\alpha \rightarrow \pi/2$ or $qa \rightarrow \pi/2$, eq. (4.24) becomes

$$a \rightarrow \frac{\pi}{2} \sqrt{2 e^\gamma} \xi_{os} = 2.965 \xi_{os}$$

This means that in the "dirty" limit, when the superconducting particle radius drops to less than $2.965 \xi_{os}$, the superconducting properties of the system disappear. The result of the calculation

with different $\tau = T_{c2}/T_{c1}$ is shown in Fig. 42.

The T_c versus dimension of the particle has already been presented in Fig. 41. In that plot, the dimension of the particle is equivalent to the diameter of the spherical particle, or $2a$, in the above calculations. Before making a comparison between the theoretical and experimental results (Fig. 41 and Fig. 42), two things have to be obtained, namely the value of T_{c2} and ξ_{os} .

As mentioned in the previous page, it is reasonable to assume that the $\tau = T_{c2}/T_{c1} = 0$ curve is the one which can be used to compare with the experimental result.

About the value of ξ_{os} , according to eq. (4.13)

$$\xi_{os} = \left(\frac{\hbar v_{fs} \ell_s}{6\pi k_B T_{cs}} \right)^{\frac{1}{2}}$$

If the free-electron theory can be applied, then the mean free path can be calculated from the normal residual resistivity by the following formulas,

$$\sigma = \frac{1}{\rho} = \frac{ne^2\tau}{m} = \frac{ne^2\ell}{m v_f} \quad (4.25)$$

Where n is the number of free electrons per unit volume in the sample, e is the electron charge which is equal to 4.8×10^{-10} esu, m is the electron mass which is equal to 9.11×10^{-28} gram and σ is the conductivity. The free electron theory can be applied to Ag, but not to Pb.⁽⁵⁶⁾ To calculate the mean free path in Pb, the Pippard relations should be used, e. g.

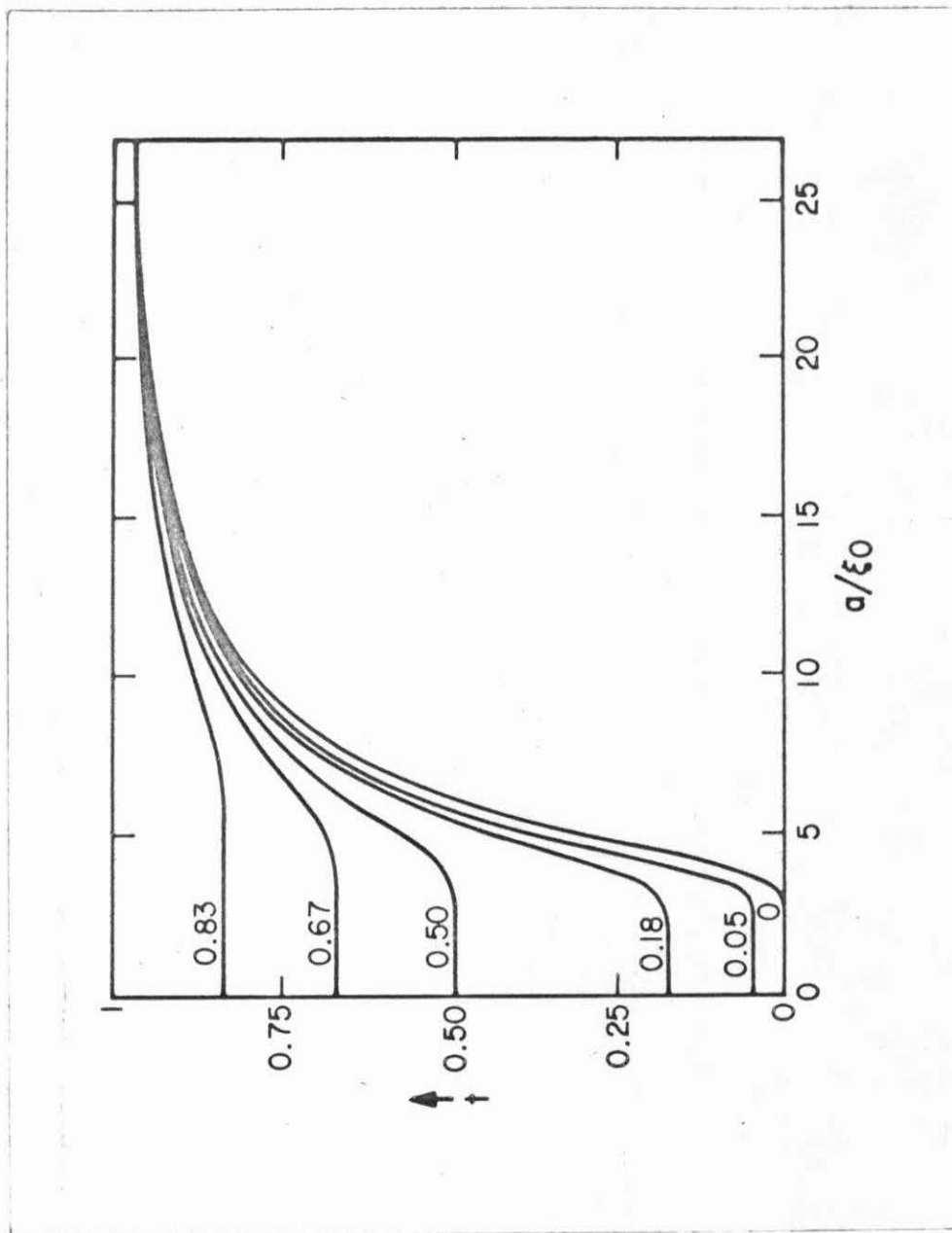


Fig. 42. Normalized and superconducting transition temperature as a function of the size of the particle (calculated by Silvert and Singh).

$$\sigma = \frac{e^2 S \langle \ell \rangle}{12\pi^3 \hbar}, \quad \Gamma = k_B^2 S / 12 \pi \hbar \langle v_f \rangle \quad (4.26)$$

where S is the Fermi surface area, Γ is the coefficient of normal electron specific heat, and the brackets mean that the parameter is averaged over the Fermi surface. Combining relations (4.26)

$$v_f \ell = (\pi k_B / e)^2 (\sigma / \Gamma) \quad (4.27)$$

which makes it possible to estimate $v_f \ell$ from the experimentally measured quantities σ and Γ . The substitution of relation (4.27) in eq. (4.13) yields a result which actually is general for any Fermi surface. By combining (4.27) and (4.13)

$$\xi_{os} = \left(\frac{\hbar \pi k_B}{6 \Gamma_{cs} e^2 \rho \Gamma} \right)^{\frac{1}{2}} \quad (4.28)$$

In all samples performed in this study the normal residual resistivity of Pb is $\rho_{Pb} = 1.5 \times 10^{-5} \Omega \text{-cm}$ and $\Gamma_{Pb} = 1.72 \times 10^3 \text{ ergs/cc } ^\circ\text{K}^2$. Therefore for Pb, $\xi_{os} = 126.5 \text{ \AA}$. If $v_f = 1.82 \times 10^8 \text{ cm/sec}$ ⁽⁵⁶⁾ was used, then the mean free path of Pb is only 15.6 \AA. This value is much smaller than the coherence length, therefore the "dirty" limit in Pb is justified. Fig. 43 was obtained by replotting Fig. 41 with T_c against $D/2\xi_{os}$ which is equivalent to plotting T_n against a/ξ_{os} in Fig. 42. By comparing Fig. 43 with the case of $\tau = 0$ in Fig. 42, it can be found that these two graphs are qualitatively, although not quantitatively, similar. Because of the simplified assumptions in the calculated curve, this result was expected. It is interesting to observe that the T_c in the experimental curve Fig. 43

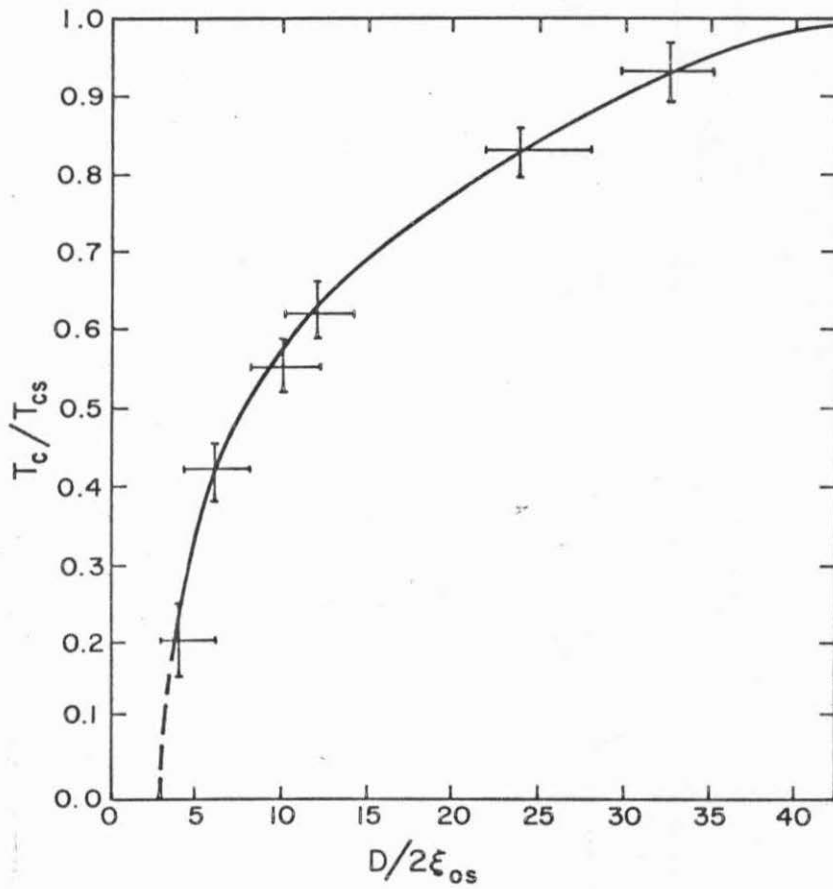


Fig. 43. Normalized superconducting transition temperature as a function of the normalized dimension of the particles (precipitates) in the quenched and heat-treated $\text{Ag}_{97}\text{Pb}_3$ alloys.

did go to zero at about $D/2\xi_{OS} = 3$ as the eq. (4.24) predicted (2.965). This numerical value may be just a coincidence, but it is important to know that for superconducting particles smaller than certain critical size the superconductivity in the sample disappears.

For quenched $Ag_{97}Pb_3$ samples annealed at $200^{\circ}C$ for various times, the superconductivity behavior in Fig. 9 is now obvious. For samples annealed less than 1 hour the precipitated Pb particle size is less than the critical size. That is why they are not superconducting. For samples annealed more than 1 hour but less than 50 hours the size of the Pb precipitated particle grows with annealing time. Therefore the T_c increases as annealing time increases. However, for samples annealed at $200^{\circ}C$ for more than 50 hours the size of the particles does not increase very much, in fact it is nearly independent of annealing time, but the T_c still increases. This is because the mean free path of the sample is still increasing with annealing time and the "dirty" approximation ($l \ll \xi$) in the sample (especially in Ag matrix) is gradually breaking down. The penetration depth $k_n^{-1} \cong \xi_n$ is then longer than eq. (4.13) predicts,⁽⁴⁾ so more Cooper pairs can be tunneling through the normal barrier; therefore, the transition temperature keeps increasing.

For quenched $Ag_{97}Pb_3$ samples annealed at $300^{\circ}C$ for $0 < t < 10$ hours the T_c goes up with annealing time, because the size of the precipitated particle increases as annealing time increases. For samples annealed more than 10 hours, the metallographic studies have already shown that the Pb precipitation gets into the grain boundary and forms continuous paths in the sample. Therefore,

the T_c 's are equal to 7.2°K .

For other compositions of $\text{Ag}_{100-x}\text{Pb}_x$, $1 \leq x \leq 3$, metallograph studies have already shown that for a given heat treatment the particle size is nearly independent of compositions. Therefore, the T_c can be explained in exactly the same way as $\text{Ag}_{97}\text{Pb}_3$ samples were.

The T_c , mean free path, coherence length of quenched $\text{Ag}_{97}\text{Pb}_3$ samples and their annealing times and temperatures are listed in Table II.

B. Critical Current and Superconducting Volume Fraction

1. Model and experimental results of critical current versus temperature

According to Josephson,⁽⁷⁾ the supercurrent across the normal boundary is a natural consequence of phase locking due to the minimization of the barrier free energy in the superconducting side. The free energy of the system contains a contribution from the barrier region which depends on the relative phases of the values of the wave function on the two sides of the barrier, and whose magnitude becomes greater as the barrier is made thinner. This term is analogous to the 'kinetic energy term'

$$\frac{1}{2m} \left| i\hbar\nabla\psi + \frac{e}{c} A\psi \right|^2$$

in the Ginsburg-Landau expression for the free energy density. With very thick barriers the free energy contribution from the barrier is negligible and the phases are able to vary arbitrarily with respect to each other. As the barrier is made thinner, however, the barrier

Table II

Superconducting transition temperature T_c , mean free path in Ag l , coherence length in Ag, ξ_{Ag} and the mean interparticle distance $2b$ of the quenched $Ag_{97}Pb_3$ alloys annealed at $200^\circ C$ and $300^\circ C$.

Anneal- ing tem- perature ($^\circ C$)	Anneal- ing time (hours)	Super- conducting transition tempera- ture ($^\circ K$)	Mean free path (l) (\AA)	Coher- ence length (ξ_{Ag}) at $7.2^\circ K$ (\AA)	Coher- ence length (ξ_{Ag}) at $1.3^\circ K$ (\AA)	Mean Inter- particle distance ($2b$) (\AA)
200	0	< 1.2	80	235	569	
200	0.33	< 1.2	95	255	616	
200	2	~ 2.5	121	289	699	
200	7	~ 3.5	154	325	788	
200	20	~ 4	188	360	872	
200	35	~ 4.2	211	383	925	
200	54	4.5	273	434	1050	5940
200	102	5.2	368	506	1225	5631
200	225	5.8	483	579	1401	5190
200	500	6	604	647	1567	4324
300	0.33	6	187	360	872	
300	1	6.4	210	382	922	
300	3	7.2	225	395	955	

energy begins to exert an influence, tending to fix the phase relationships at those values which minimize the barrier energy. As the barrier thickness is reduced further, this influence becomes stronger until eventually any possibility of changing the phase relationships becomes completely suppressed. The above description is equivalent to saying that Cooper pairs can penetrate through a barrier if it is thin enough. Bound pairs of electrons do not have any scattering across the boundary, therefore no resistance appears. As the boundary becomes thinner and thinner, more Cooper pairs can penetrate through the barrier thereby increasing the critical current density. In this investigation, although samples are three-dimensional, but for a given sample, supercurrent flows through the precipitated particles can be expected dominantly to go from one particle to another one dimensionally without too much dispersion in the other directions. This is because the distances between precipitated particles are different so the current will flow dominantly from a given lead particle to the next nearest particles (Ref. Fig. 33). Therefore, a quasi-one dimensional model can be assumed in order to calculate the critical current in the sample. To simplify the calculation five additional assumptions were made in the following:

1. Each particle is spherical in shape with radius a ; 2. The inter-particle distance between two particles is $2b$ and is the same for all particles; 3. The probability amplitude of Cooper pair $F(r)$ linearly drops in the S region near the SN boundary with a characteristic distance ξ_{GL} (3, 28) as shown in Fig. 44(a); 4. $F(r)$ is proportional to $\frac{e^{-k_n r}}{r}$ in the N region; (3, 4, 28, 31, 37) and 5. The critical current

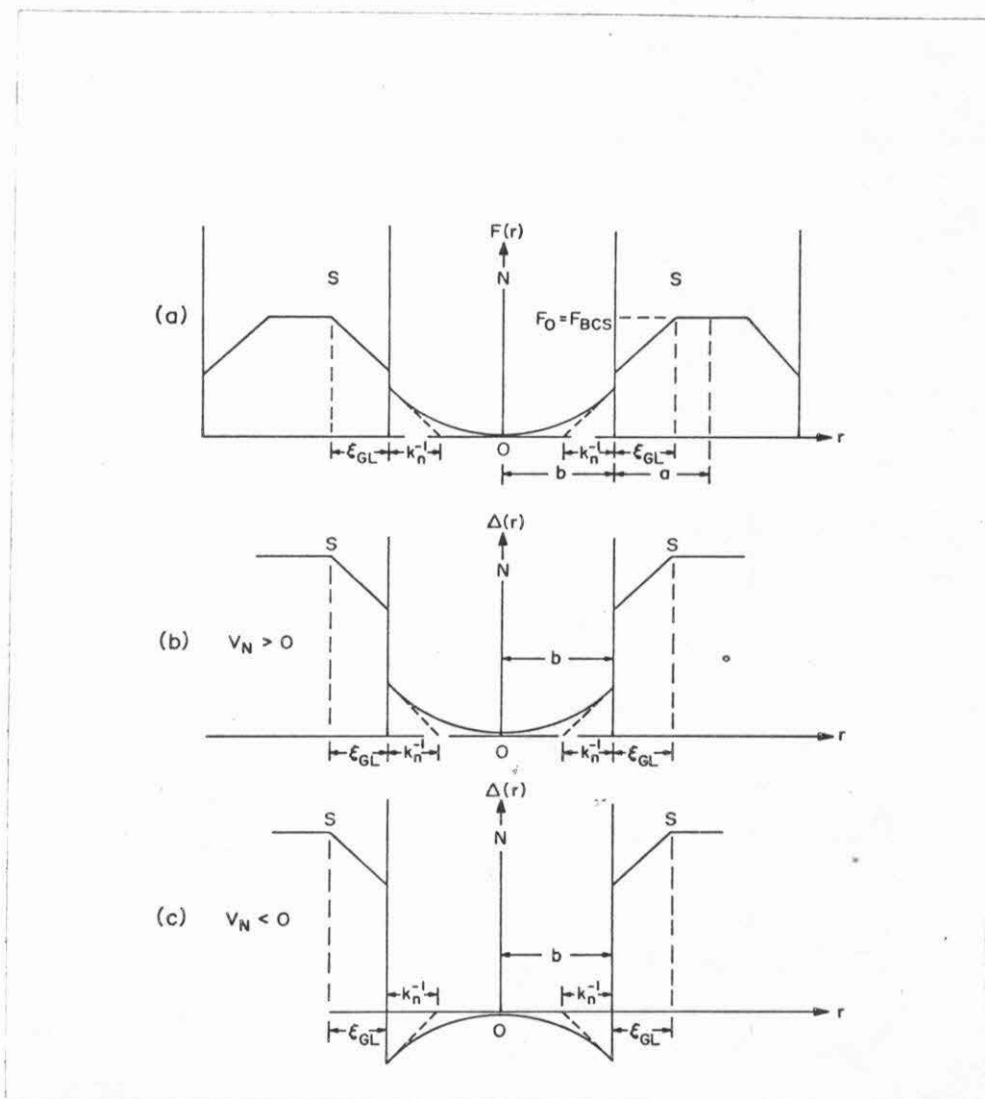


Fig. 44. (a) Simple model of the Cooper pair amplitude $[F(r)]$ for calculating the critical current in a SNS junction. (b) The corresponding pair potential $[\Delta(r)]$ of (a) for the case of $V_N > 0$. (c) The corresponding pair potential $[\Delta(r)]$ of (a) for the case of $V_N < 0$.

in the samples is so small that it affects only the phase, but not the amplitude of the order parameter. This simplified model used to calculate the critical current in a given junction is shown in Fig. 44(a). From the definition $\Delta(r) = F(r) \times V(r)$, the $\Delta(r)$ in this SNS junction for the cases of $V_N > 0$ and $V_N < 0$ are shown in Fig. 44(b) and 44(c).

In Fig. 44 the ξ_{GL} is the Ginsburg-Landau coherence length, in the case of Pb in the dirty limit $\xi_{GL}(T) \sim \xi_{os} \left(1 - \frac{T}{T_{cs}}\right)^{-\frac{1}{2}}$ where ξ_{os} was defined in eq. (4.28). Assumptions 1, 2 and 4 can be justified in the same way as the assumptions in the last section. Strictly speaking assumption 3 requires only that $\xi_{GL} \gg \xi_n$ which is strictly valid only near T_{cs} , but even if $\xi_{GL} \sim \xi_n$ this approximation would not affect the temperature dependence of I_c much because of the exponential term of $F(r)$ dominants as will be seen in eq. (4.29) and Fig. 46. Since for quenched and annealed $Ag_{100-x}Pb_x$, $x \leq 3$, the average interparticle distance is larger than 5000 \AA and k_n^{-1} , the penetration depth of the Cooper pair is less than 1500 \AA , it can therefore be expected that the number of Cooper pairs that can penetrate the barrier is low. Experiments have shown that J_c is normally smaller than 10^3 A/cm^2 which is much less than the normal critical current density of bulk Pb which is 10^5 A/cm^2 . Therefore, assumption 5 is justified.

Let two SN boundaries be at $r = -b$ and $r = +b$ and φ_b and φ_{-b} be the values of $\arg F$ at the boundary as shown in Fig. 44(a). From all the above assumptions and eq. (4.14), the probability amplitude of Cooper pairs $F(r)$ can be written as follows:

$$F(r) = \left[\left(\frac{N_s}{N_n} k_n^{-1} \right) F_0 \right] \times \left(\frac{N_n}{N_s} \right) \times \left[\frac{\exp\{(r-b)/k_n^{-1} + i\varphi_b\}}{|r - (a+b)|} + \frac{\exp\{(-r-b)/k_n^{-1} + i\varphi_{-b}\}}{|r + (a+b)|} \right] \quad (4.29)$$

The first term on the right hand side of eq. (4.29) is the F value at the S side of the boundary. The product of the first term and the second term is the F value at the N side of the boundary. The third term is the exponentially decaying term of F inside the normal barrier in terms of a three dimensional spherical coordinate system together with the phase term.

The supercurrent is calculated from the expression

$$I_c \propto \left(F^* \frac{\partial F}{\partial r} - F \frac{\partial F^*}{\partial r} \right)_{r=b \text{ or } r=-b}$$

giving

$$I_c(T) = A \frac{(F_0(T))^2}{(k_n^{-1} + \xi_{GL})^2} (k_n^{-1})^2 \exp(-2b/(k_n^{-1})) \sin \varphi \times \left[\frac{1}{k_n^{-1} a(2b+a)} + \frac{(a+b)}{b^2 a(2b+a)} \right]$$

where A is a constant independent of temperature, $\varphi = \varphi_b - \varphi_{-b}$ and $F_0(T)$ is the bulk Cooper pair amplitude in Pb at temperature T . Since $k_n^{-1} \cong \xi_n = \left(\frac{\hbar v_{fn} l_n}{6\pi k_B T} \right)^{\frac{1}{2}}$, therefore,

$$I_c(t) \cong \frac{A(F_0(T))^2}{(\xi_n + \xi_{GL})^2} \xi_n^2 \exp(-2b/\xi_n) \sin \varphi \left[\frac{1}{\xi_n a(2b+a)} + \frac{a+b}{b^2 a(2b+a)} \right] \quad (4.30)$$

This equation is very similar to Clarke's⁽²⁸⁾ result in the case of one-dimensional SNS junctions except with one more term, because the $F(r)$ is a damped spherical wave instead of a damped plane wave.

Between 1 and 4°K ξ_{GL} and $\Delta_{Pb}(\alpha F_0)$ are nearly constant and ξ_n changes only by a factor of 2. Consequently, the exponential term dominates the temperature dependence of $I_c(T)$ and one may write

$$I_c(T) \cong A' \exp(-CT^{\frac{1}{2}}) \quad (4.31)$$

where A' and C are constants with respect to temperature, and

$$C = \left(\frac{6\pi}{\hbar v_{fn} \ell_n} \right)^{\frac{1}{2}} \times 2b \quad (4.32)$$

A graph of $\log I_c$ against $T^{\frac{1}{2}}$ of quenched $Ag_{97}Pb_3$ annealed at 200°C for various times is shown in Fig. 45. For $T < 2.5^\circ K$, it can be observed that the dependence of $\log I_c$ versus $T^{\frac{1}{2}}$ is indeed linear. In this linear region, the slope is the constant C which in turn yields the average interparticle distance $2b$. These values of $2b$ are summarized in Table II. The magnitude of these $2b$'s is quite close to the mean value of the observed interparticle distance from the SEM pictures.

At higher temperatures, the ξ_{GL} gets larger and $F_0(T)$ also decreases, so that the critical current decreases faster as temperature increases, as eq. (4.30) predicted.

By taking the b value and the value of the mean free path from Table II and the a value from Fig. 38 (note $a = \text{dimension}/2$) for a given sample, one can perform calculations of eq. (4.30) and

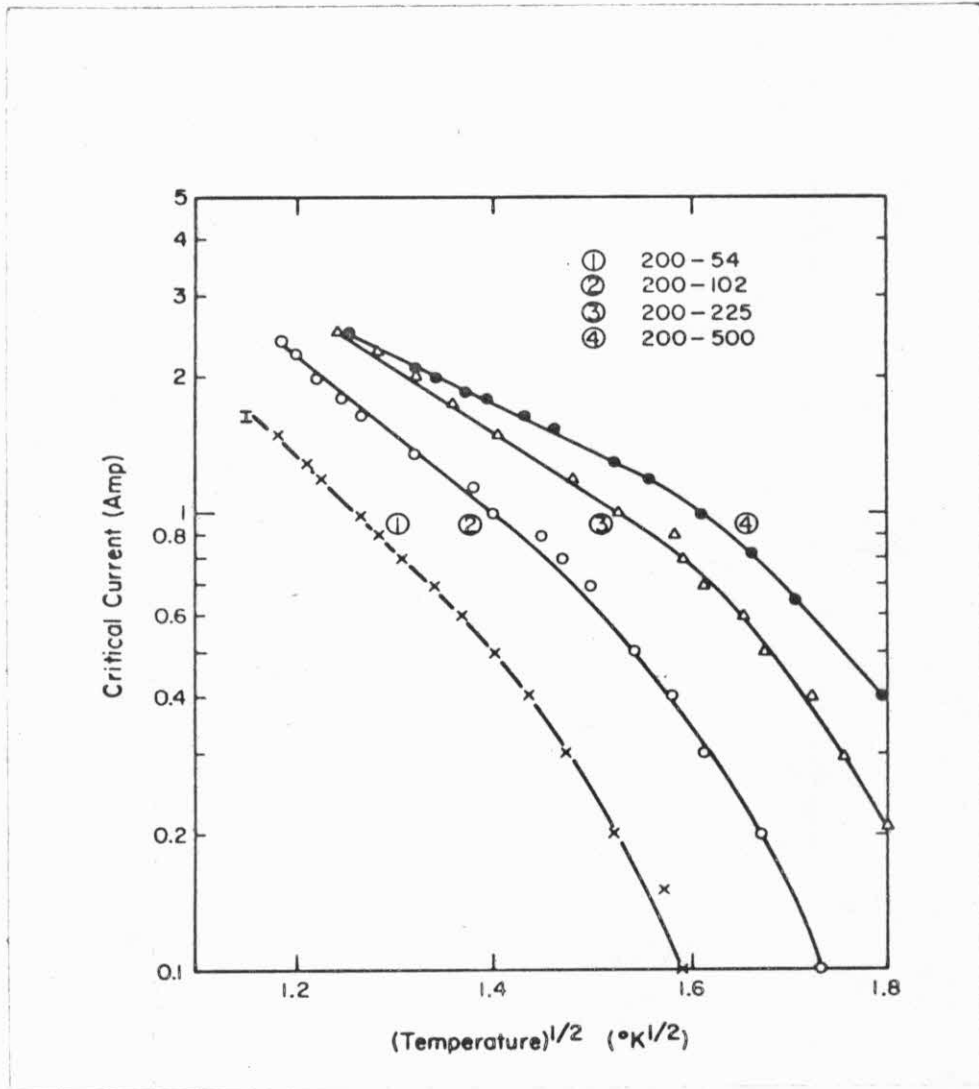


Fig. 45. $\log I_c$ versus $T^{\frac{1}{2}}$ for the quenched $Ag_{97}Pb_3$ alloys annealed at $200^\circ C$.

compare it with the experimental results for $1.5^{\circ}\text{K} < T < 7.2^{\circ}\text{K}$. A typical result is shown in Fig. 46. In that plot, the solid curve is obtained from eq. (4.30) and the points are obtained from the experiment. These two values were normalized at $T = 2^{\circ}\text{K}$. It can be observed that the model explains the experimental data reasonably well.

The quenched $\text{Ag}_{97}\text{Pb}_3$ samples annealed at 200°C for various times show different mean free paths and $2b$ values. This particular composition ($\text{Ag}_{97}\text{Pb}_3$) is of special interest because of its higher critical current density. According to eq. (4.30) for a given temperature, $\log(I_c) \propto \ell_n^{-\frac{1}{2}} \times 2b$. By plotting the $\log I_c$ of these samples against the values $\ell_n^{-\frac{1}{2}} \times 2b$, the results indeed show a linear correspondence as seen in Fig. 47. The samples annealed for 500 hours, which is the only exception to this behavior, can be accounted for as follows:

1. By annealing the sample for such a long time the mean free path becomes comparable to the coherence length as seen in Table II; therefore, the "dirty" limit on which the calculation was based might not be valid any longer; and 2. Due to the saturation effect.⁽⁴⁹⁾

The saturation effect is explained as follows: At low temperature for a sample with long mean free path, the penetration depth can be very long. When the penetration depth is so long that the superconducting volume fraction approaches 100% then the critical current will not increase as fast as eq. (4.30) indicates. At very low temperature, when the SVF is approaching 100% the critical current tends to reach a finite limit. This effect is called the saturation effect.

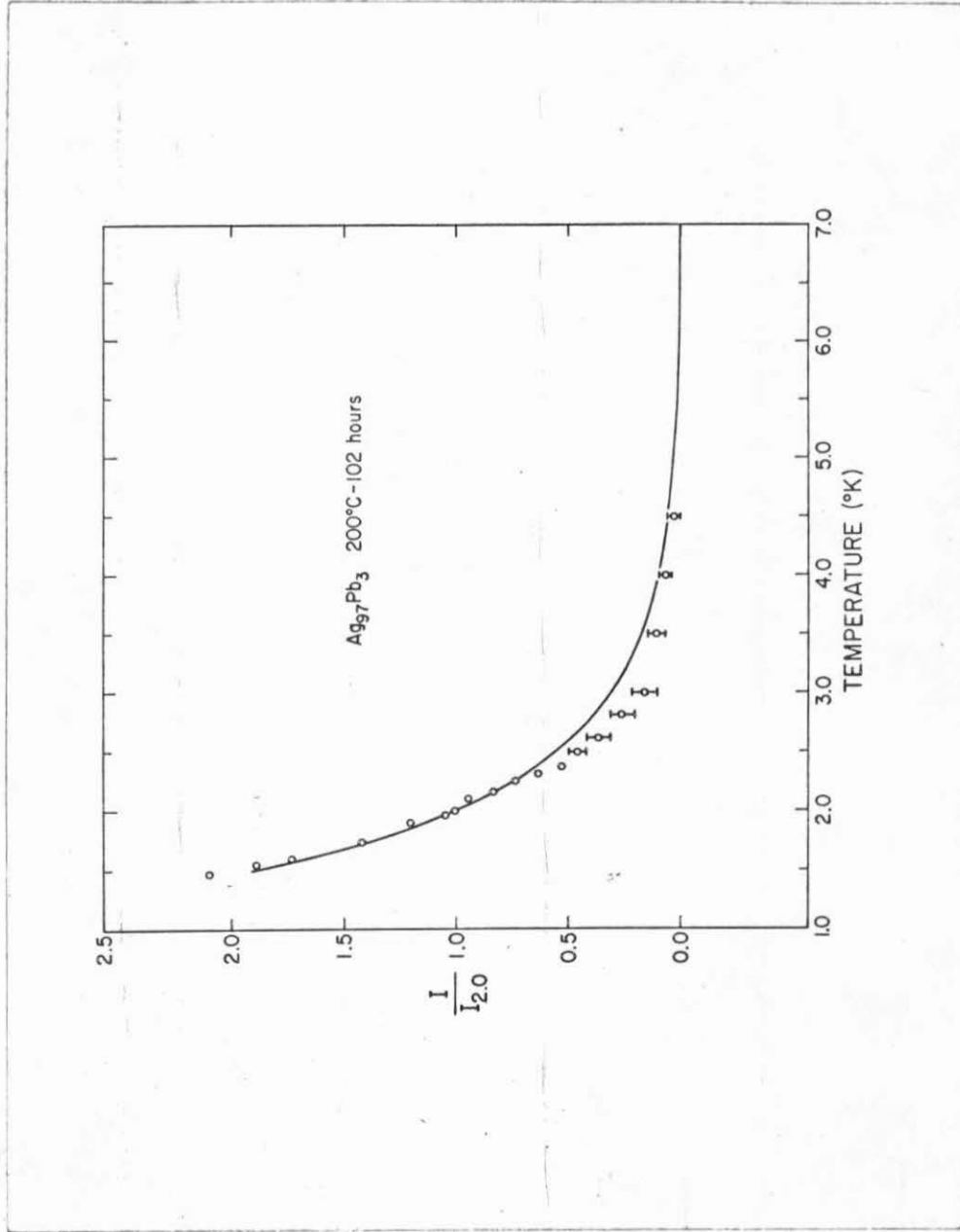


Fig. 46. Experimental results (points) and theoretical calculation (solid curve based on eq. (4.30)) of the normalized critical current versus temperature for the quenched Ag₉₇Pb₃ alloy annealed at 200°C for 102 hours.

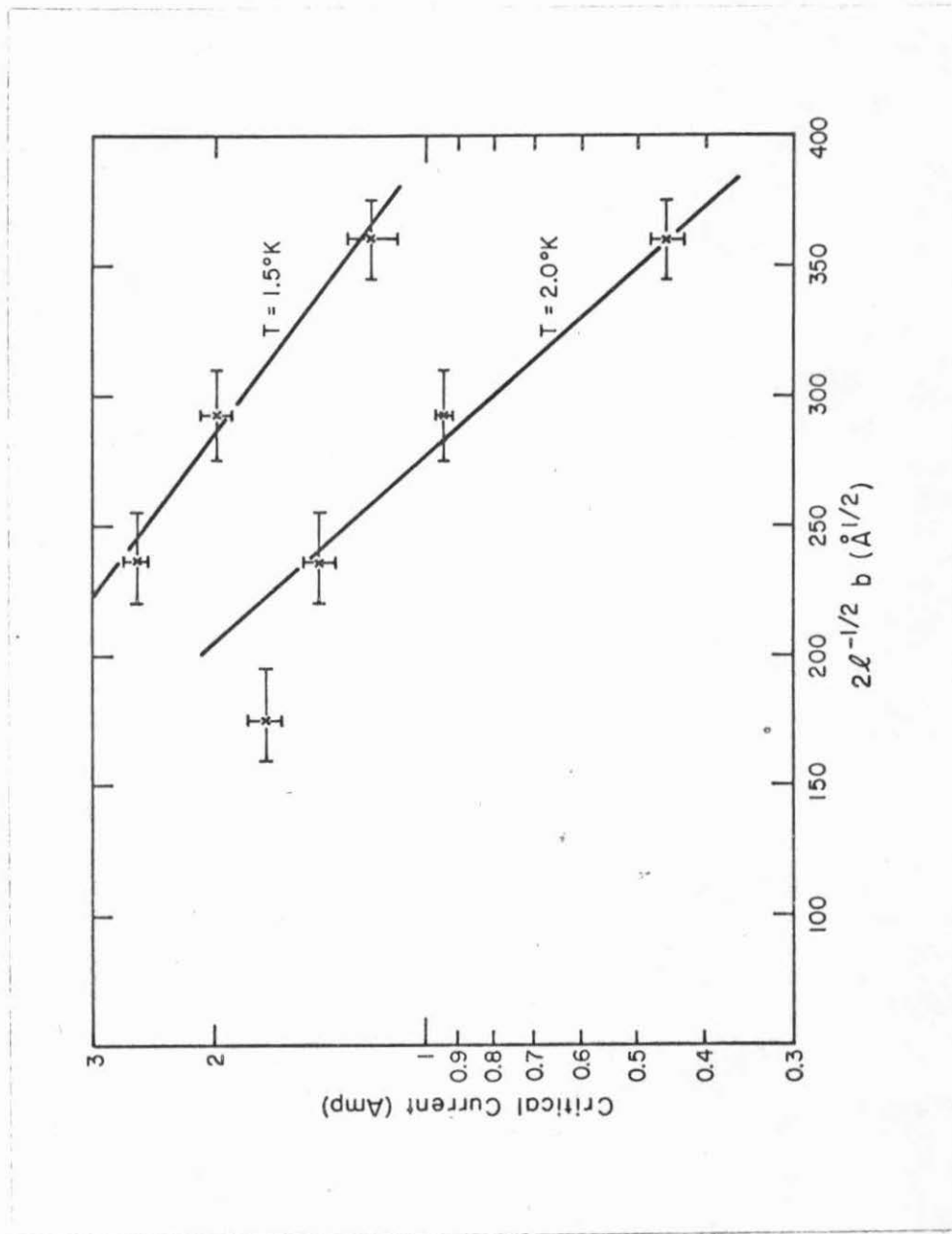


Fig. 47. $\log I_c$ versus $2L^{-1/2}b$ for the quenched $Ag_{97}Pb_3$ alloy annealed at $200^\circ C$ at two different temperatures: points on each curve from right to left are for samples annealed for 54 hours, 102 hours, 225 hours, and 500 hours.

An example of this effect has been shown in Fig. 30. This effect was observed in a one-dimensional proximity junction, for example see Fig. 1 in the paper by Romagnan et al. (31)

It is now time to discuss why quenched $\text{Ag}_{97}\text{Pb}_3$ samples annealed at 200°C for various times are the most important samples in this investigation. Back in the experimental results, it has been discovered that samples with Pb content higher than the TSSE (Terminal Solid Solubility Extension) can give an inconsistent result in the proximity effect studies. From the discussion given in this section the dominant term in the critical current is $\exp(-2b/\xi_n)$. Therefore, the critical current is strongly dependent on the value of b which in turn depends on the content of Pb in the sample. Also, by annealing samples with different compositions for a given time at a given temperature, the ξ_n values are approximately constant. It can therefore be concluded from eq. (4.30) that the critical current density decreases very fast as the Pb content in the samples decrease. Low critical current density makes the measurement difficult. It is therefore to be expected that samples with the highest Pb content without exceeding TSSE can give the most pronounced and consistent proximity effect. In this investigation this is $\text{Ag}_{97}\text{Pb}_3$. Also from the microstructure studies it is shown that samples annealed at 200°C can give the most reasonable rate of precipitation. Judging from the reasons stated above, it can be concluded that $\text{Ag}_{97}\text{Pb}_3$ samples annealed at 200°C for various times are the most important samples in this investigation.

From the metallographic studies it was found that, for quenched $\text{Ag}_{97}\text{Pb}_3$ samples annealed at 300°C for $t > 50$ hours, continuous superconducting short circuits which were formed by the Pb precipitations, laid across the samples. Therefore, for these samples the I_c versus T behavior is about the same as bulk lead samples. It was known^(10,59,60) that for a type I superconductor the critical current behavior is approximately the same as the order parameter Δ which goes to the value at $T = 0$ very fast as the temperature decreases ($\Delta = \Delta_0 (1 - \frac{T}{T_{cs}})^{\frac{1}{2}}$). Therefore it is not surprising to observe the apparent saturation of critical current in Fig. 23 at low temperature ($T < 4^\circ\text{K}$).

2. The effect of external magnetic field on critical current

It was predicted by Josephson⁽⁵⁾ in 1962 and demonstrated by Rowell⁽⁵⁰⁾ that the magnetic field dependence of the critical current for a one dimensional SNS junction which was not self-field limited was of the following form

$$I_c(H) \propto \frac{(\sin[\pi\Phi/\Phi_0])}{(\pi\Phi/\Phi_0)} \quad (4.33)$$

The N is an insulator in this case. A section of a one dimensional tunneling junction is shown in Fig. 48 which was used to explain the parameters in eq. (4.33). Φ is equal to $2(b + \lambda)wH$ where λ is the penetration depth of the superconductor, H is the magnetic field strength with direction at right angles to the page in Fig. 48, and Φ_0 is the flux quantum which is equal to $2 \times 10^{-7} \text{ G}_{\text{cm}}^2$. The current will flow uniformly not self-field limited through the junction

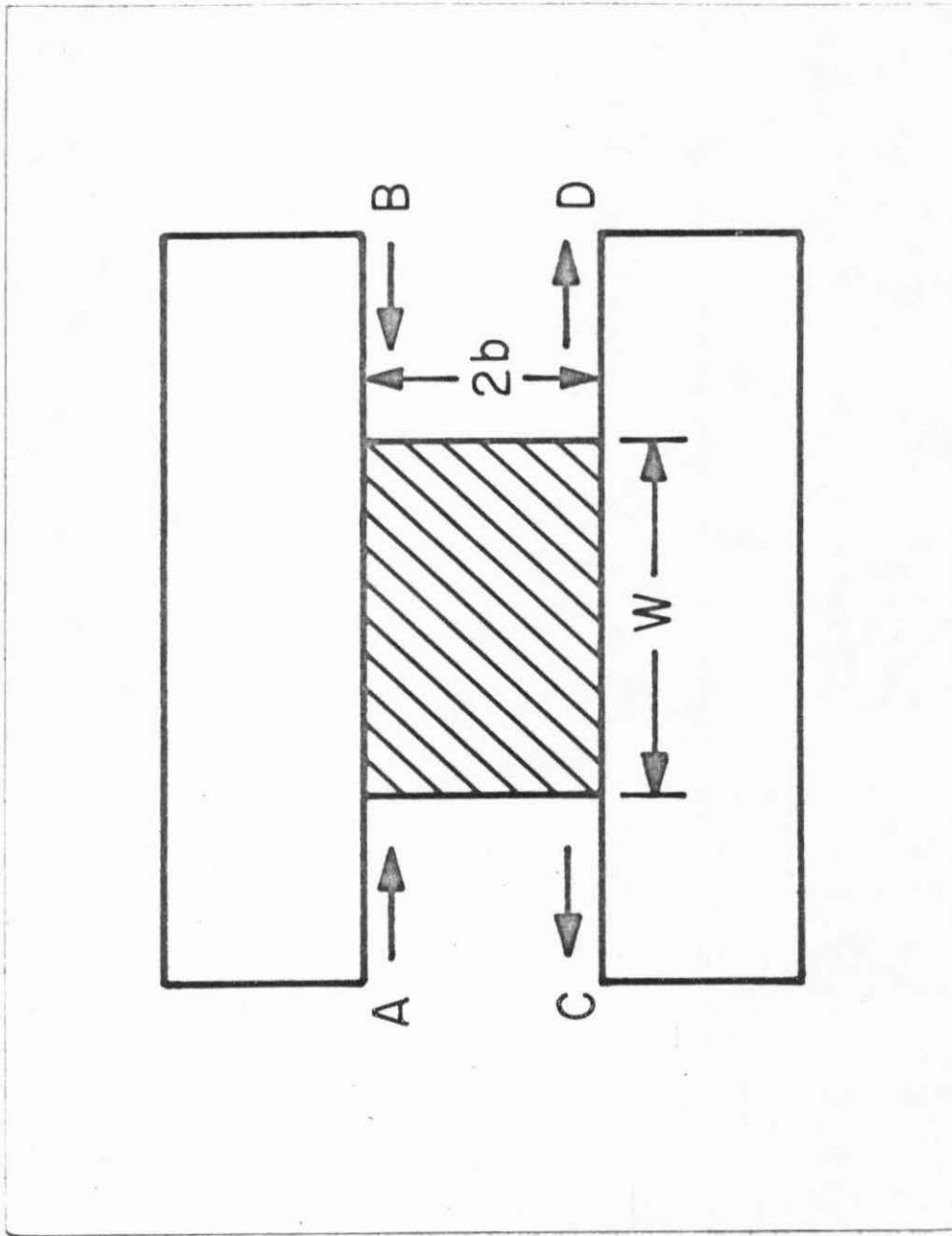


Fig. 48. Section of a one-dimensional tunneling junction. Two superconductors, AB and CD, are separated by a barrier of thickness $2b$ and width w .

if w is small compared with the junction penetration given by^(6,51,52)

$$\lambda_J = \left(\frac{\hbar c^2}{16\pi(b+\lambda)eJ_c} \right)^{\frac{1}{2}}$$

where J_c is the critical current density in the junction and c is the speed of light. In this investigation, the junction width w is effectively limited by the dimensions of the particles, or D , which is less than a micron for quenched $Ag_{97}Pb_3$ samples annealed at $200^\circ C$ and λ_J is larger than 20 microns, with the typical value of $b + \lambda \sim 5000 \text{ \AA}$ and $J_c < 100 \text{ A cm}^{-2}$ per junction. Therefore, $\lambda_J \gg w$ and the junction is not self-field limited. However, as pointed out by de Gennes,⁽¹⁰⁾ eq. (4.33) has to be modified for the case that N of the SNS junction is a metal instead of an insulator. In the case of an S-insulator-S junction the order parameter of the superconductor near the insulator side is not affected by the presence of the insulator,⁽¹⁰⁾ while in the case of an S-Normal metal-S junction the order parameter of the superconductor near the normal metal side was greatly affected by the normal metal. By using the Ginsburg-Landau equation which works especially well in the "dirty" limit ($l \ll \xi$) of which samples in this investigation belong, the modified equation of (4.33) for a one-dimensional SNS junction of which N is a normal metal can be obtained as⁽¹⁰⁾

$$I_c(H) \propto \psi_S \psi_{S'} \frac{(\sin[\pi\Phi/\Phi_0])}{\pi\Phi/\Phi_0} \quad (4.34)$$

where ψ_S and $\psi_{S'}$ are the Ginsburg-Landau wave functions of the superconductors at $r = +b$ and $r = -b$ in Fig. 45. The wave function

ψ is related to the order parameter Δ by

$$\psi_S(r) = \frac{(2mC)^{\frac{1}{2}}}{\hbar} \Delta(r) \quad (4.35)$$

with $C \cong N(0)\xi_0^2$ and ξ_0 is the coherence length. If the dimension of the superconductor (D) is within $\sqrt{5}$ times its magnetic field penetration depth, λ , then the function ψ will change from its zero field value to its critical field value gradually. But if $D > \sqrt{5} \lambda$ then the function ψ will change abruptly at the critical field.^(10, 58) For D not significantly larger than $\sqrt{5} \lambda$ the function ψ will fall gradually as the field increases, but at the critical field the ψ will drop abruptly to zero.⁽⁵⁸⁾ It is therefore a good approximation to assume that in this case

$$\psi_S(T) = (1 - BH)\psi_{oS}(T) \quad (4.36)$$

for $H < H_c(T)$ with $B \ll 1/H$ where ψ_{oS} is the Ginsburg-Landau wave function for the superconductor at zero magnetic field and B is a constant for a given sample. In all the samples which show a pronounced proximity effect, for example quenched $Ag_{97}Pb_3$ samples annealed at $200^\circ C$ for various times, the λ value at low temperature ($T < 2^\circ K$) is of the order of 500 \AA , and D is of the order of 3000 \AA (Fig. 41). Therefore, D is larger than $\sqrt{5} \lambda$, but not much larger, and eq. (4.36) can be used for the ψ_S in eq. (4.33). Now for those samples $\Phi \sim 2D(b + \lambda)H$ but b has a wide range and D also has a distribution, for example see Fig. 36 and Fig. 40. Therefore, the $\frac{\sin(\pi\Phi/\Phi_0)}{\pi\Phi/\Phi_0}$ function in eq. (4.34) was smoothed out. It can be expected that only the envelope of that function will show up in the

experimental results. For $\Phi > \Phi_0$ or H approximately larger than 50 Gauss, the envelope function is approximately $\frac{1}{(\pi\Phi/\Phi_0)}$ which is proportional to $1/H$. By gathering all the above information, the I_c versus H at a given temperature is expected to be

$$I_c(H) \cong D_T \psi_{oS} (1 - BH) \psi_{oS'} (1 - B'H) \frac{1}{H}, \quad H \geq 50G$$

where D_T , B and B' are constants. Since B and B' are much less than $1/H$, then

$$I_c(H) \cong D_T \psi_{oS} \psi_{oS'} (1 - (B+B')H) \frac{1}{H}, \quad H \geq 50G$$

or

$$\begin{aligned} I_c(H) &\cong D_T \psi_{oS} \psi_{oS'} \left(\frac{1}{H} - (B+B') \right) \\ &= E_T \left(\frac{1}{H} - (B+B') \right), \quad H \geq 50G \end{aligned}$$

where E_T , which is equal to $D_T \psi_{oS} \psi_{oS'}$, is a new constant.

By replotting the experimental result in Fig. 24 of I_c versus H into I_c versus $1/H$, Fig. 49 can be obtained. It can be observed that eq. (4.37) is a very good approximation. By fitting the experimental value with eq. (4.37), the parameter can be obtained for each sample. For example, for the quenched $Ag_{97}Pb_3$ sample annealed at $200^\circ C$ for 102 hours, the $E_T = 56$ Amp-Gauss and $(B+B') = 0.004$ Gauss $^{-1}$. Therefore $(B+B') \ll 1/H$ for $H \geq 50$ Gauss, just as eq. (4.36) predicts. It was found that all the samples of the quenched $Ag_{97}Pb_3$ annealed at $200^\circ C$ above 50 hours have approximately the same $(B+B')$ values. Judging from the above discussions that $(B+B')$ is only a function of the dimension of particles and all the quenched $Ag_{97}Pb_3$ samples annealed at $200^\circ C$ above 50 hours have approximately

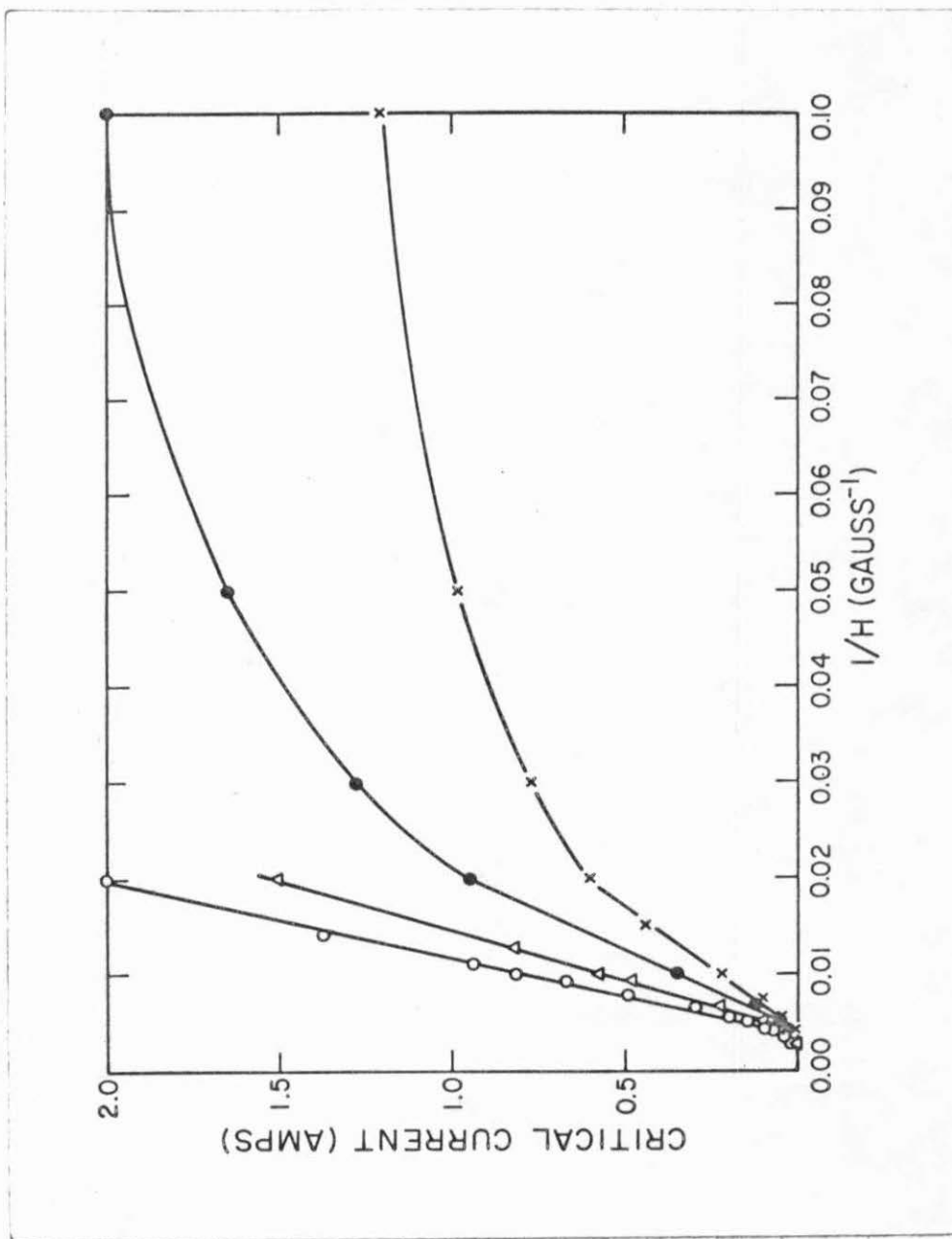


Fig. 49. Critical current versus the reciprocal of magnetic field for the quenched $\text{Ag}_{97}\text{Pb}_3$ alloy annealed at 200°C . x 50 hours, ● 102 hours, Δ 225 hours, o 500 hours.

the same dimension, this result is expected. For a given field, according to the last section, the $\log(I_c)$ and the $\log(E_T)$ values are dependent on $l^{-\frac{1}{2}} \times 2b$. The experimental result of the E_T value shows that it is indeed approximately true except for the quenched $Ag_{97}Pb_3$ sample annealed at $200^\circ C$ for 500 hours in which the "dirty" limit approximation is not totally correct. This result is shown in Fig. 50.

For the case in which the field is less than 50 Gauss, eq. (4.37) is not correct. The critical current will still increase as the field decreases but it will eventually reach a limit set by the supercurrent carrying capacity of the sample at zero field.

As discussed in the last section for the quenched $Ag_{97}Pb_3$ samples annealed at $300^\circ C$ for $t > 50$ hours, the critical current is expected to behave like bulk Pb because of the filamentary effect. It is therefore not surprising to observe the saturation of J_c at H less than 150 Gauss, as shown in Fig. 26.

3. Superconducting volume fraction (SVF)

The superconducting volume fraction measurement gives the percentage of the volume in the sample which is superconducting. The supercurrent can only flow through the superconducting region in the sample. It is therefore to be expected that the critical current density is proportional to the SVF. Based on this idea, it is not surprising to observe that for a given sample the SVF as a function of temperature for a given magnetic field and as a function of field for a given temperature have the same dependence as I_c .

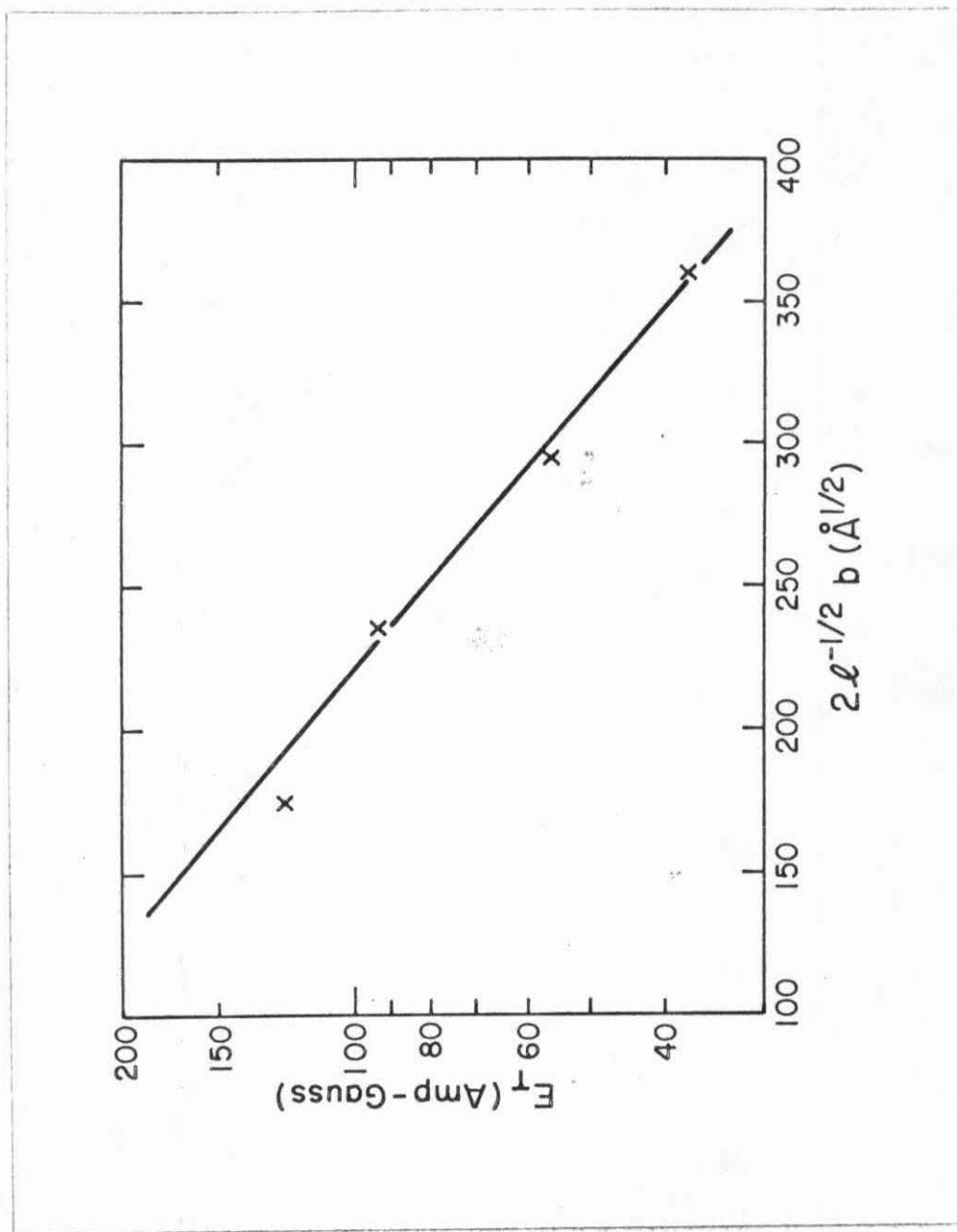


Fig. 50. $\log(E_T)$ versus $2L^{-1/2}b$ for the quenched $\text{Ag}_{97}\text{Pb}_3$ alloy annealed at 200°C . Points from right to left are for samples annealed for 54 hours, 102 hours, 225 hours, and 500 hours.

For the quenched $\text{Ag}_{97}\text{Pb}_3$ samples annealed at 200°C for various times the temperature dependence of SVF for a given field will follow the temperature dependence of eq. (4.30), and the field dependence of SVF for a given temperature will follow eq. (4.37) for $H \geq 50$ Gauss. As a typical example, for the case of the SVF versus T , the experimental result in Fig. 28 for the quenched $\text{Ag}_{97}\text{Pb}_3$ samples annealed at 200°C for 54 hours was replotted with $\log(\text{SVF})$ against T 's. The result is shown in Fig. 51. It was discovered that the $\log(\text{SVF})$ is indeed linearly dependent on T 's at low temperature ($T < 2^\circ\text{K}$) just like the behavior of the same sample in the $\log(I_c)$ versus T 's as shown in Fig. 45. For a given temperature, since the $\log(\text{SVF})$ is proportional to $\ell_n^{-\frac{1}{2}} \times 2b$, according to eq. (4.30), it can be expected that for samples annealed at 200°C the SVF goes up with the annealing time until SVF reaches 100%. For samples with the same heat treatment the SVF goes up as the Pb content in the sample increases. For quenched samples annealed at 300°C for $t > 50$ hours, it has been shown that Pb precipitations form a continuous path along the grain boundaries of Ag in the sample. It is therefore to be expected that for those samples the SVF is about the same as the volume percentage of Pb. In the case of $\text{Ag}_{97}\text{Pb}_3$ samples, Fig. 30 has already shown that the SVF is about 2 to 3 percent between 2°K and 7°K . However, for $T < 2^\circ\text{K}$ the SVF can go beyond the physical volume of the Pb. This can be explained by the SEM picture of that particular sample, as shown in Fig. 40. It is obvious from the picture that part of the Pb precipitations are

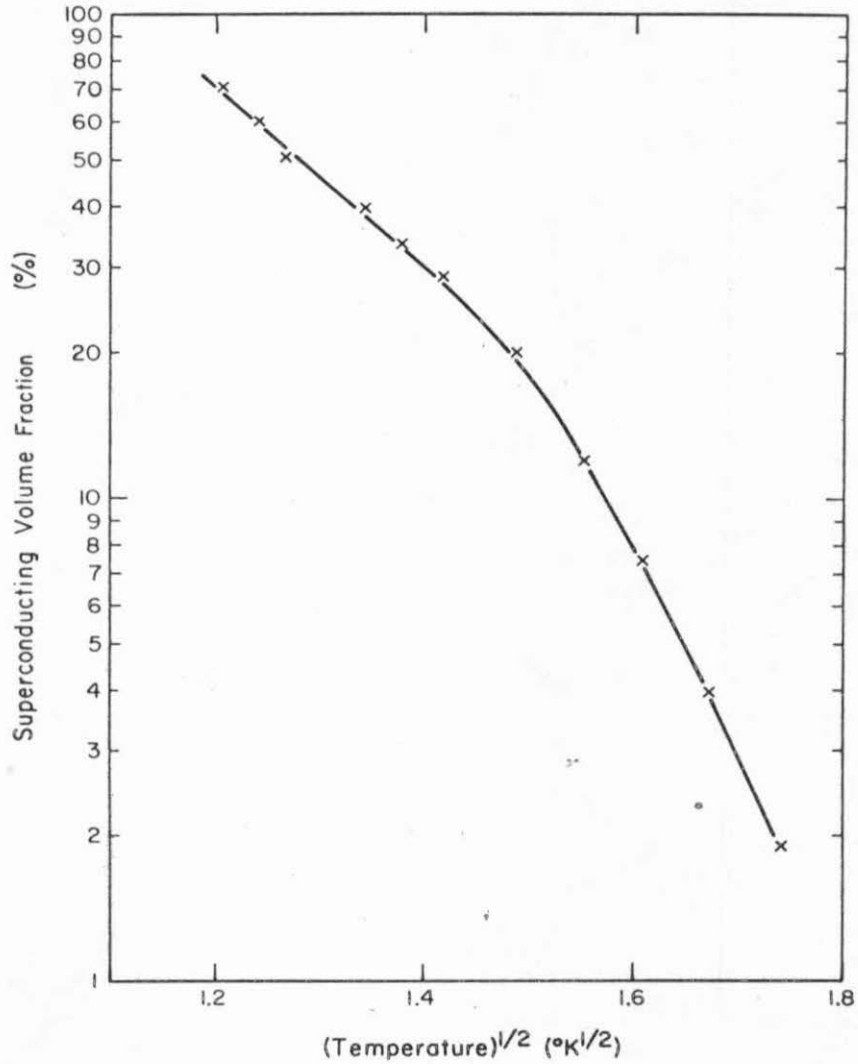


Fig. 51. $\log(\text{SVF})$ versus $T^{\frac{1}{2}}$ for the quenched $\text{Ag}_{97}\text{Pb}_3$ alloy annealed at 200°C for 54 hours.

still in the form of small particles as described in the experimental result previously. The region in which the particles exist can exhibit proximity effect at low temperature. It therefore explains why the SVF goes up at $T < 2^{\circ}\text{K}$.

As a typical example, for the case of the SVF versus H , the experimental result in Fig. 31(b) for the quenched $\text{Ag}_{97}\text{Pb}_3$ samples annealed at 200°C for 307 hours was replotted with SVF against $1/H$. This result is shown in Fig. 52. It was discovered that this result shows the same behavior as the I_c versus $1/H$ of those samples shown in Fig. 49. The $(B+B')$ value in eq. (4.37) obtained from Fig. 50 is also 0.004 Gauss^{-1} .

C. Demagnetization Effect and Critical Magnetic Field

1. Demagnetization effect in H_c measurement

By measuring the critical magnetic field electrically (from magnetoresistivity), it has been discovered that at low temperature, $T < 2^{\circ}\text{K}$, the magnetic field H at which the ρ drops to zero is different between the cases of longitudinal and transverse magnetic fields, but the onset of the ρ versus H curve is not. A typical result has been shown in Fig. 18. This effect can be explained by the demagnetization effect in the sample as follows:

For an SNS junction if κ , the Ginsburg-Landau parameter, is much less than 1, it behaves like a type I superconductor, and each junction has a characteristic magnetic field called H_b in which a first order transition of magnetic field into N region occurs. (4,19,20).

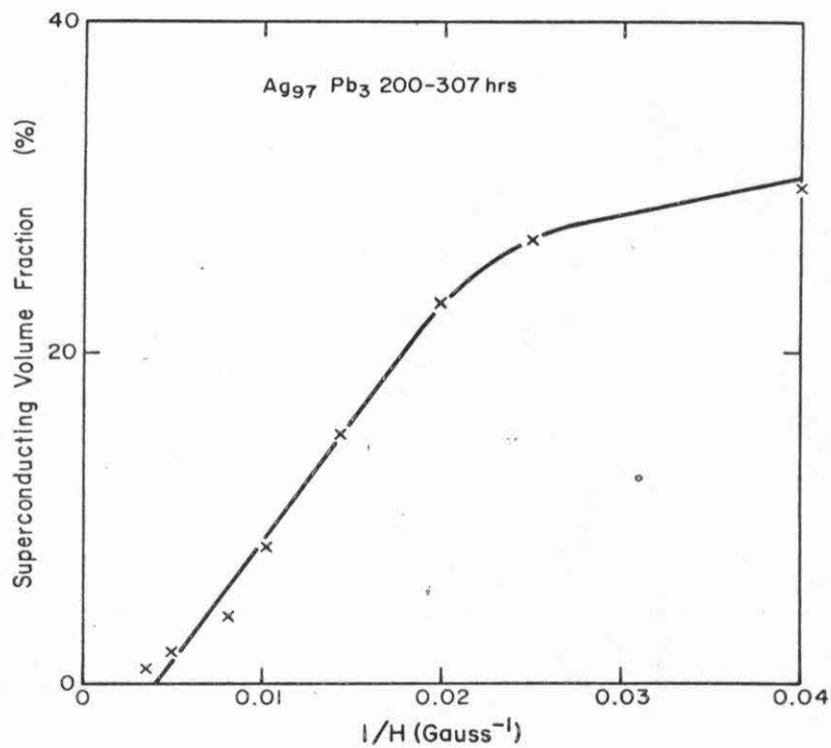


Fig. 52. SVF versus $1/H$ for the quenched $\text{Ag}_{97}\text{Pb}_3$ alloy annealed at 200°C for 307 hours.

For a given geometry, a superconductor can have a demagnetization effect; the macroscopic field that the material actually sees is of the following form

$$H_{\text{mac}} = H_{\text{app}} - 4\pi MD_m \quad (4.38)$$

where H_{app} is the applied magnetic field, M is the magnetization in the samples and D_m is the demagnetization in the direction of the applied magnetic field. The values of D_m are between zero and one and for the ellipsoid case the values were tabulated. (61, 62) Samples used in this investigation, as described before, is a rectangular shape with length a , width b and thickness c . Normally $a \sim 0.1$ cm and $c \sim 0.005$ cm so $a \gg b \gg c$. The sample shape can be replaced approximately by an ellipsoid. For the case of longitudinal field magnetic field, D_m is very small (normally less than 0.1), while in the case of transverse magnetic field D_m is near 1. It is therefore a good approximation to use $D_m = 0$ in the longitudinal field case and $D_m = 1$ in the transverse field case.

If each Ag-Pb-Ag SNS junction behavior is like type I, then the R versus H transition normally starts from point 1 to point 2 as the field increases, as shown in Fig. 53 I(b). At point 1, M is not zero. Therefore, from eq. (4.38) the sample in a transverse magnetic field sees a magnetic field

$$\begin{aligned} H_{\text{mac}} &= H_{\text{app}} - 4\pi MD_m \\ &\cong H_{\text{app}} + XH_{\text{in}} \end{aligned}$$

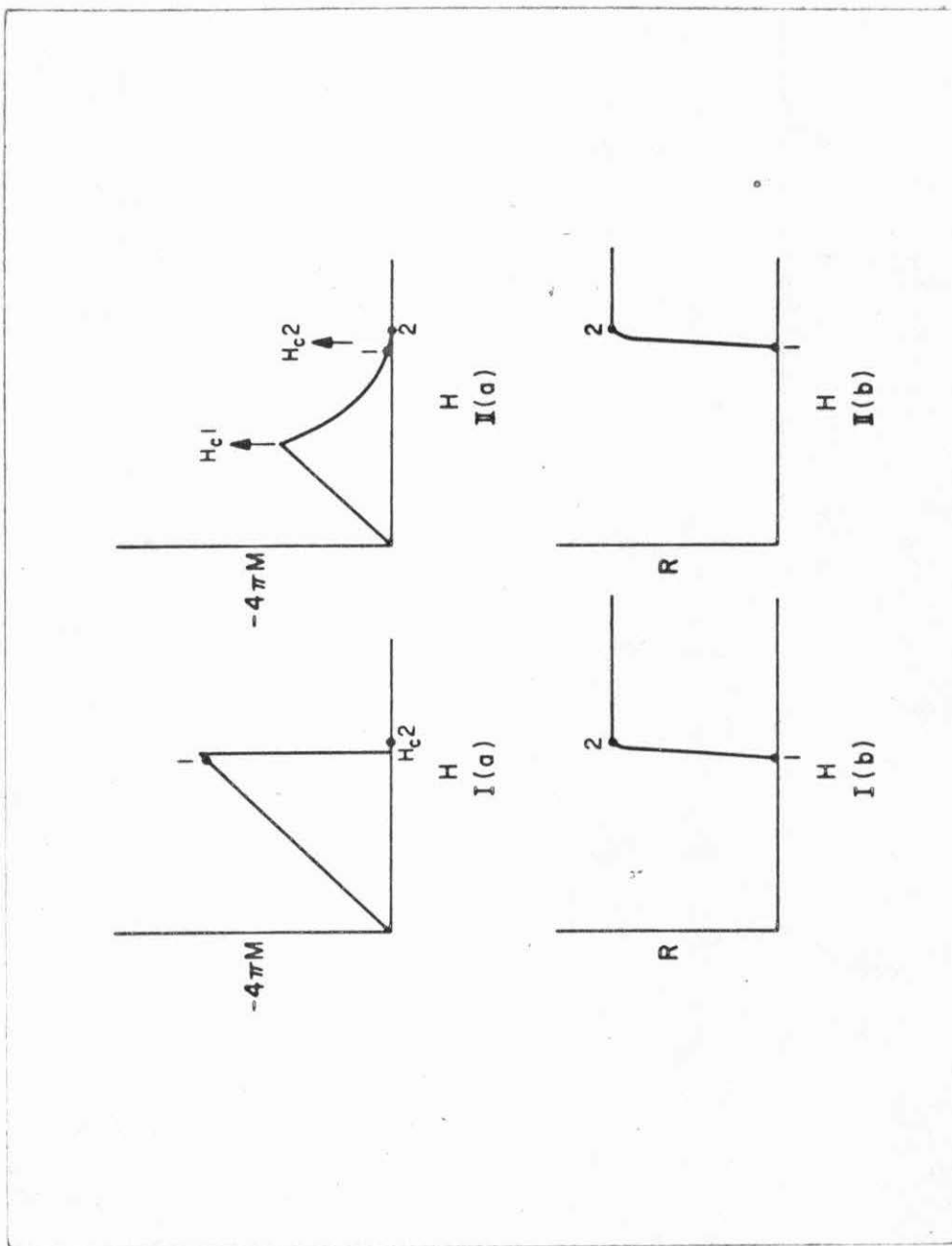


Fig. 53. I(a) - $4\pi M$ versus H for an ideal Type I superconductor; I(b) R versus H curve corresponding to the superconductor in I(a); II(a) - $4\pi M$ versus H for an ideal Type II superconductor; II(b) R versus H curve corresponding to the superconductor in II(a).

or
$$H_{\text{mac}} = \frac{H_{\text{app}}}{1-X} \quad (4.39)$$

and the sample in a longitudinal field sees a magnetic field

$$H_{\text{mac}} = H_{\text{app}} - 4\pi MD_m \cong H_{\text{app}} \quad (4.40)$$

where X is the superconducting volume fraction of the sample. Since $X > 0$, the sample sees a higher magnetic field than the actual applied field in the transverse field case. Therefore, by defining point 1 in Fig. 53 I(b) as the critical field H_b , the critical field for the transverse field case is $H_{\text{app}}^c \cong (1-X)H_b$ which is smaller than $H_{\text{app}}^c \cong H_b$ in the longitudinal case. At point 2 in Fig. 58 I(b), the onset point in the R versus H curve, M is zero. From eq. (4.38), there will be no difference between the H_{in} and H_{app} for all cases; therefore, no demagnetization effect can be observed.

If the SNS junction is a type II superconductor, then from Fig. 51 II(a) and II(b), it can be observed that M is nearly zero for either the point 1, the "finish" point of R versus H , or point 2, the "onset" point of R versus H . Therefore, from eq. (4.38), there will be no difference between H_{mac} and H_{app} for all cases, so no demagnetization effect can be observed.

Since the quenched $\text{Ag}_{97}\text{Pb}_3$ annealed at 200°C for various times shows the demagnetization effect in the transverse magnetoresistivity measurements, for example Fig. 18, it can be concluded from the above discussions that most of the SNS junctions in the sample at $T < 2^\circ\text{K}$ are Type I in nature, and measuring the sample in longitudinal magnetic field is the best method to get rid of the

demagnetization effect. The reason one confines this measurement below 2°K is because as T increases the κ value increases, so the demagnetization effect in the sample will become less obvious.^(19, 20) The experimental results also show this fact.

2. Critical magnetic field (H_b)

It can be expected and has been theoretically proven that it is a good approximation to have the following form for H_b ⁽⁴⁾

$$H_b \propto \exp(-k_n d_n) \quad (4.41)$$

and in the "dirty" limit

$$k_n^{-1} = \left(\frac{\hbar v_{fn} \ell_n}{6 \pi \kappa_B T} \right) \left(1 + \frac{2}{2m(T/T_{cn})} \right)^{\frac{1}{2}}$$

where d_n is the thickness of the normal metal film.

In this investigation the d_n corresponds to the interparticle distance $2b$ and $k_n^{-1} \cong \xi_n = \left(\frac{\hbar v_{fn} \ell_n}{6 \pi \kappa_B T} \right)^{\frac{1}{2}}$. Therefore, for a given temperature it can be expected that $\log(H_b)$ is linearly dependent on the product of $2b$ and $\ell_n^{-\frac{1}{2}}$.

In determining the value of H_b , the longitudinal magnetoresistivity data were used because of the reasons given in the last section. However, besides the demagnetization effect, the critical current effect should also be considered. Because the critical current decreases with field rapidly, it can be expected and was observed that the ρ versus H curve depends on the magnitude of the applied current density as was discussed in the critical current section in the discussion. Because the onset point of ρ versus H , as in the case of the onset point of ρ versus T , is independent of the magnitude of

the applied current, the onset field was used as H_b .

By using the $2b$ values which were obtained from the slope in Fig. 45 and the measured ℓ_n 's in Table II, the result of $\log(H_b)$ versus $2\ell_n^{-\frac{1}{2}} b$ of the quenched $Ag_{97}Pb_3$ samples annealed at $200^\circ C$ for various times is shown in Fig. 54. It can be seen that the above prediction is correct with the exception of the sample which was annealed for more than 500 hours. As discussed before, this is because in this sample, the "dirty" approximation is no longer correct.

D. Determination of the Superconducting Transition Temperature and the Effective Electron-Electron Interaction Parameter in Ag

It has been shown from eq. (4.30) that the critical current density (J_c) is proportional to $e^{-2k_n b}$ for a given SNS junction.

Ideally, if the b and J_c for each junction are known the parameter

k_n can be obtained by plotting $\log(J_c)$ versus b . Since $k_n^{-1} = \xi_n \left(1 + \frac{2}{\ln(T/T_{cn})}\right)^{\frac{1}{2}}$ and ξ_n is only dependent on temperature

and the mean free path of the sample; therefore, the T_{cn} of the sample can be obtained. Clarke⁽²⁸⁾ has obtained the T_{cn} for Cu

this way. However, for the samples in this investigation, the b values in a given sample have a very wide range, and there is no way to obtain the critical current density for each junction. Therefore, it is impossible to obtain the T_{cn} by this method. In 1962,

Hilsch⁽¹²⁾ introduced an empirical relation to determine the value of

k_n^{-1} in the sample for a one dimensional SNS junction. The relation

is

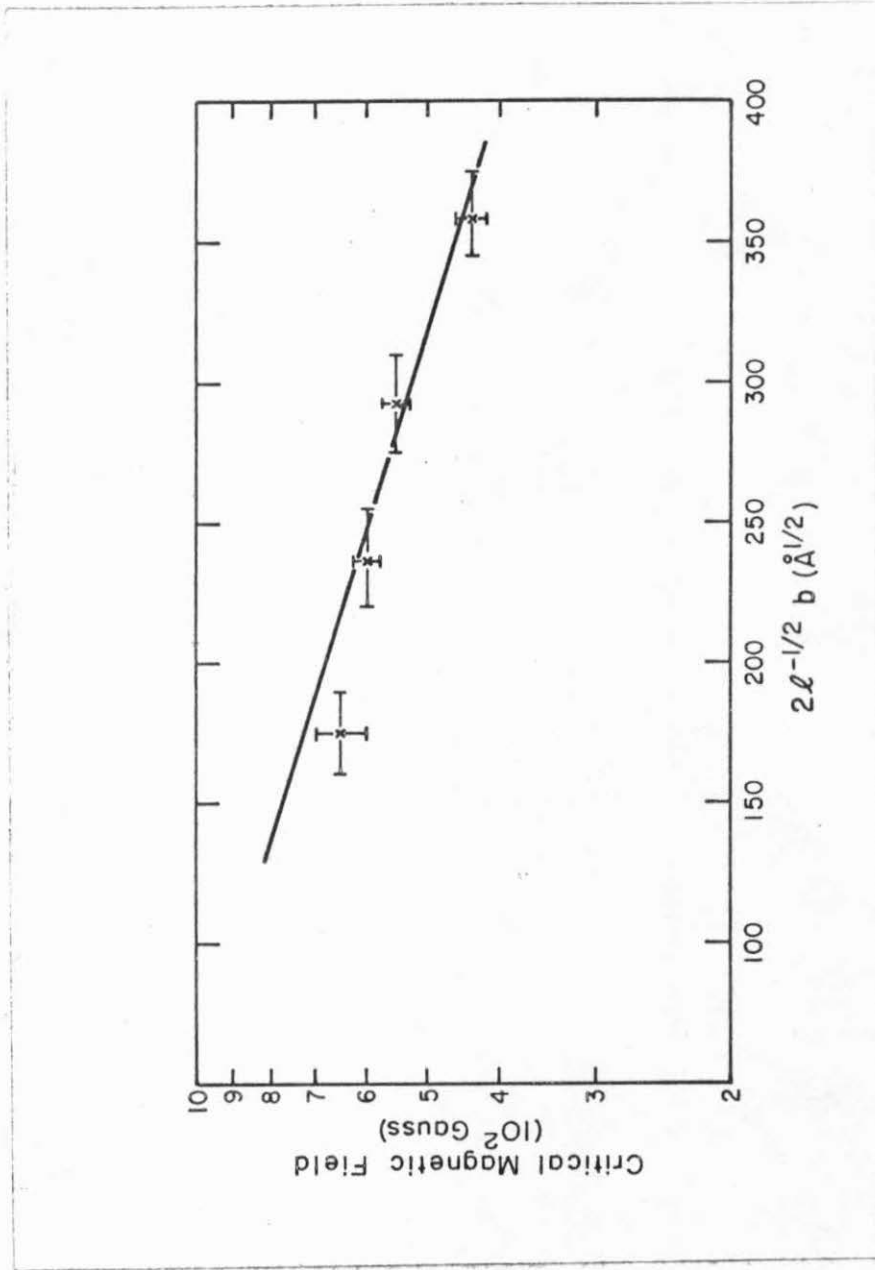


Fig. 54. $\log(H_c)$ versus $2\ell^{-1/2}b$ for the quenched Ag₉₇Pb₃ alloy annealed at 200°C: points from right to left are for samples annealed for 54 hours, 102 hours, 225 hours, and 500 hours.

$$a^2 \rho_n = 1.7 \times 10^{-7} \Omega - \text{cm}^3 \quad (4.42)$$

and

$$a = 2k_n^{-1} = 2 \left(\frac{\hbar v_{fn} \ell_n}{6\pi k_B T} \right)^{\frac{1}{2}} \left(1 + \frac{2}{\ln(T/T_{cn})} \right)^{\frac{1}{2}} \quad (4.43)$$

where ρ_n is normal residual resistivity in Ag. These empirical relations were then theoretically supported by de Gennes.⁽³⁾ The de Gennes' theory seems applicable to any dimension. Therefore, eq. (4.42) and eq. (4.43) were used to the best examples in this investigation, namely quenched $\text{Ag}_{97}\text{Pb}_3$ samples annealed at 200°C for various times. The value of $T_c(\text{Ag})$ is of the order of 10^{-5}K which by using eq. (4.2) would lead to 0.06 for the value of the interaction parameter NV in Ag.

Table III compares the present value of NV and T_{cn} in silver with those obtained by other authors. However, because k_n^{-1} is only a weak function of T_{cn} , as seen in eq. (4.43), small experimental discrepancies can give rise to large errors in the estimation of NV. Besides, it seems doubtful whether the theory is sufficiently advanced to allow a meaningful value of NV to be deduced from the data. For example, Jacobs⁽²⁶⁾ has pointed out that in the vicinity of the SN interface, where the kernel $H_\omega(\vec{r}, \vec{r}')$ in eq. (4.3) contains contributions from both materials, it is not clear how one should treat the cutoff of the electron-phonon interaction. He has shown further that different methods of performing the cutoff in the superconductor gave rise to markedly different values of NV for copper; this is because lead, which was used as the superconductor in all the experiments, is strong-coupling.

Table III

Values of NV and the corresponding T_{cn} obtained by various authors for silver. The NV and T_{cn} values in the present work are presented for the quenched $Ag_{97}Pb_3$ samples annealed at $200^{\circ}C$ for 54 hours, 102 hours, 225 hours and 500 hours in the respective order.

Author	NV	Corresponding T_{cn} ($^{\circ}K$)
Krätzig ⁽⁷²⁾	0.072	2.36×10^{-4}
Valette ⁽⁷⁰⁾	0.06	1.46×10^{-5}
Deutscher & Valette ⁽⁷¹⁾	0.05	5.2×10^{-7}
	0.08	10^{-3}
present work	0.0636	3.79×10^{-5}
	0.0620	2.5×10^{-5}
	0.0624	2.78×10^{-5}
	0.0621	2.57×10^{-5}

Despite all the difficulties, hardly any doubt remains that NV is positive for silver. By observing Table III even the quantitative agreement is quite good, in view of the widely different experimental approaches. It is amazing to observe that the value of NV or T_{cn} obtained for quenched $Ag_{97}Pb_3$ annealed at $200^{\circ}C$ at various times is nearly identical. The odds that this can happen are very small.

The NV values obtained in this investigation are in moderately good accordance with other determinations.^(30,70,71,72) This causes one to believe that the Hilsch empirical relation is indeed applicable to all dimensions and is really quite accurate.

E. Kinetics of Transformation of the Ag-Pb Metastable Solid Solution

1. Amount of transformation and the activation energy

Since for different samples, the sample surface roughness and thickness are not exactly equal, therefore in determining the amount of transformation the normalized intensity $I_{Pb(111)}/I_{Ag(111)}$ line was always used to compare samples with different heat treatment. The (111) line was used because this is the strongest x-ray peak in the Pb and Ag phases. It can be expected that for a perfect Ag-Pb solid solution in the Ag rich side the $I_{Pb(111)}/I_{Ag(111)}$ is equal to zero. For a completely transformed sample, that is the Ag and Pb phases are completely separated from each other, then $I_{Pb(111)}/I_{Ag(111)}$ is approximately equal to $3\% \times (Z_{Pb}/Z_{Ag})^2$ or about 0.1 in the case of $Ag_{97}Pb_3$ samples. Here, Z is the atomic number. By defining the amount of transformation as

$$f = \frac{(I_{\text{Pb}}(111)/I_{\text{Ag}}(111))(t)}{(I_{\text{Pb}}(111)/I_{\text{Ag}}(111))(t=\infty)}$$

the result of the quenched $\text{Ag}_{97}\text{Pb}_3$ samples annealed at 200°C is shown in Fig. 55. It can be observed for $t = 100$ hours that nearly 95% of the samples have been transformed.

The time which is required for the sample to have 95% transformation against the reciprocal annealing temperature is shown in Fig. 56. This figure indicates that the transformation is a typical diffusion-controlled process. The time required for 95% transformation can be fitted by an equation as follows:

$$t = A e^{E/kT} \quad (4.44)$$

The E corresponds to the "activation energy," T is the absolute temperature, k is the Boltzmann constant and A is a constant. From the slope of the curve in Fig. 56, $E = 1.1 \pm 0.2$ ev or in metallurgical terms $E = 25000 \pm 5000$ cal/gram-mole.

An attempt was made to fit the raw x-ray diffraction data with the transformation equation in the quenched $\text{Ag}_{97}\text{Pb}_3$ samples annealed at 200°C for various times. The approximated equation used was of Johnson-Mehl type⁽⁶³⁾ in which the relationship between the amount of transformation or precipitated state and the time t is as follows:

$$f = 1 - \exp(-(\frac{t}{\tau})^n) \quad (4.45)$$

where n is a number independent of the initial number of the solute

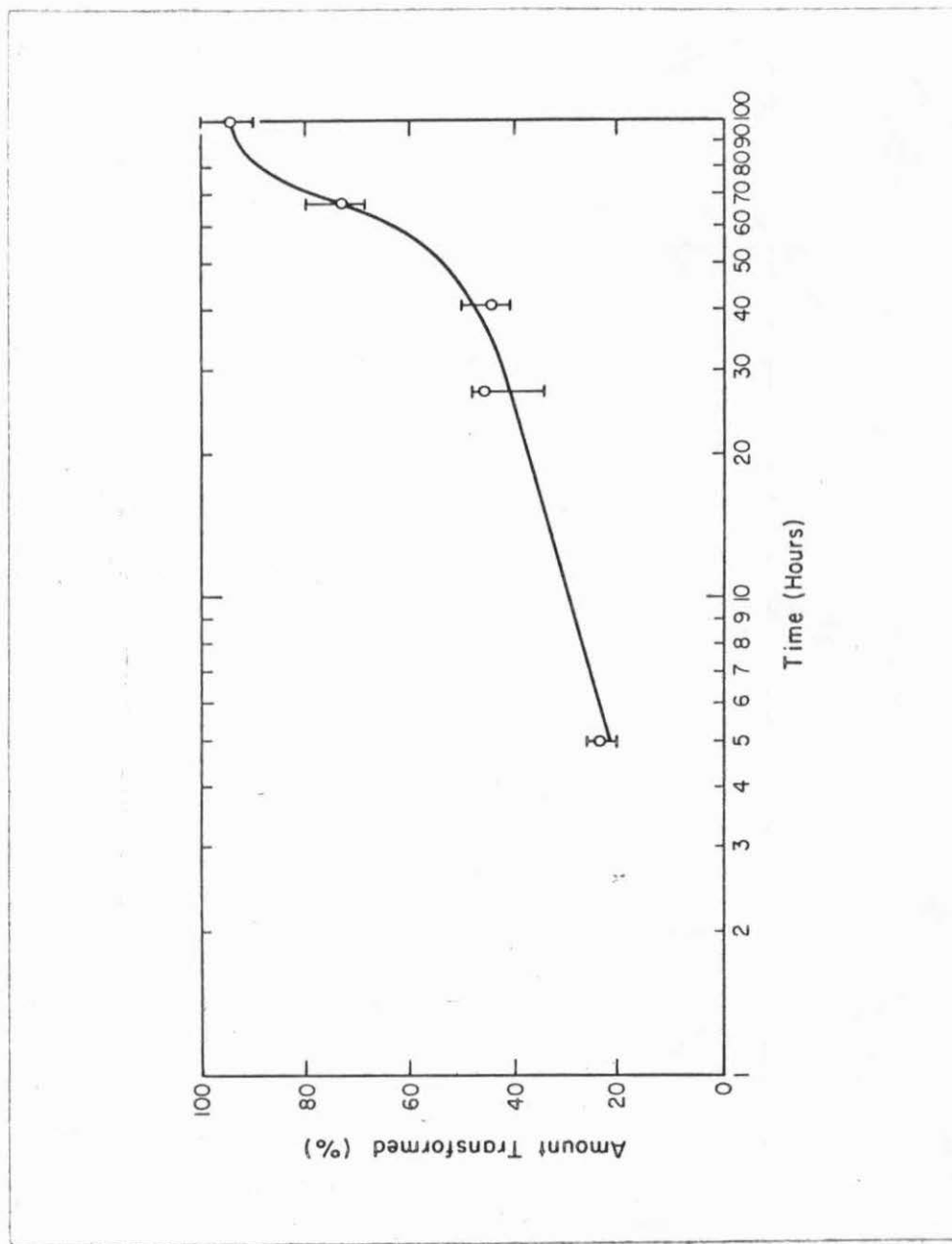


Fig. 55. Amount of transformation versus annealing time for the quenched $Ag_{97}Pb_3$ alloy annealed at $200^{\circ}C$.

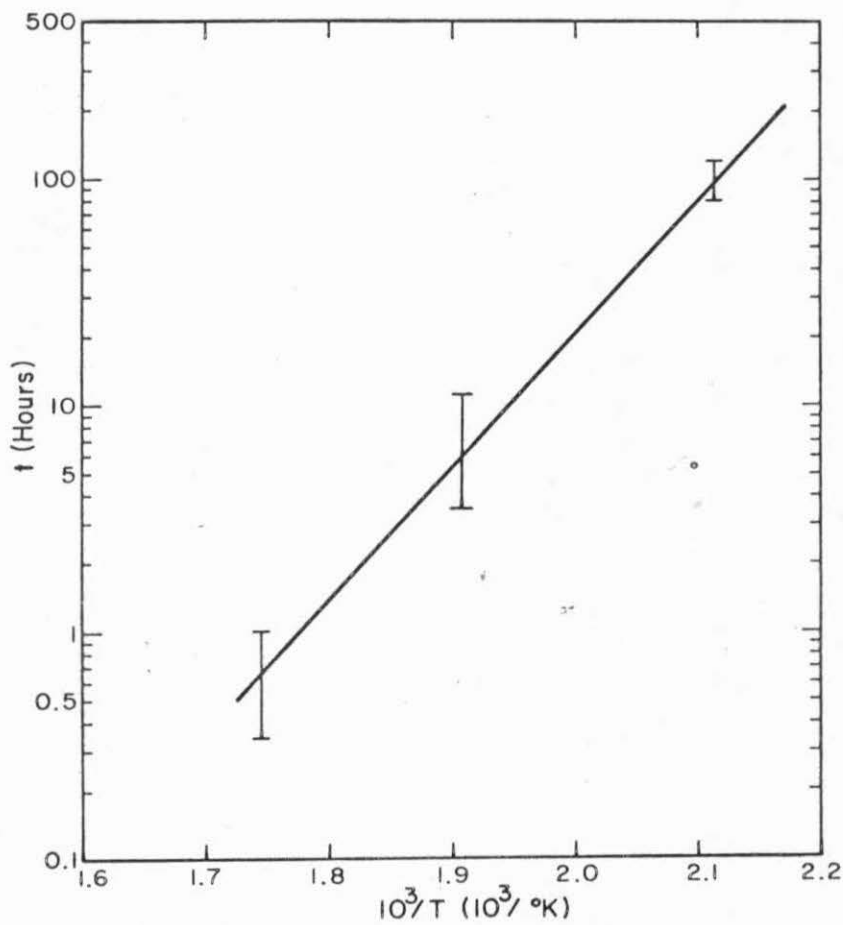


Fig. 56. $\log(t)$ versus $10^3/T$ for the quenched $\text{Ag}_{97}\text{Pb}_3$ alloy to have 95% transformation after annealing.

atoms while τ is dependent of it. However, for a given composition and annealing temperature, both n and τ are constants.

By defining

$$I(t) = \frac{I_{\text{Pb}}(111)}{I_{\text{Ag}}(111)} (t)$$

and

$$I_f = \frac{I_{\text{Pb}}(111)}{I_{\text{Ag}}(111)} (t \rightarrow \infty)$$

eq. (4.45) can be rewritten as

$$\ln\left(1 / \left(1 - \frac{I}{I_f}\right)\right) = \left(\frac{t}{\tau}\right)^n \quad (4.46)$$

By plotting eq. (4.46) on log-log paper, the n and τ can be readily obtained. In the case of quenched $\text{Ag}_{97}\text{Pb}_3$ samples annealed at 200°C for various times, the result is shown in Fig. 57. From the slope of the straight line and from the time at which $\ln\left(1 / \left(1 - \frac{I}{I_f}\right)\right) = 1$ in Fig. 57, $n = 0.61$ and $\tau = 50$ hours was obtained. The value of n has been shown theoretically to vary with the mechanism of nucleation and precipitate shape. For homogeneous nucleation this value ranges between 1 and 2.5.^(64, 65) For heterogeneous nucleation, theoretical values between 0.5 to 1 have been reported.⁽⁶⁶⁾ In the present work, because of the nature of the rapidly quenched samples, high density dislocations, vacancies and small grains are present. It is therefore to be expected that in this case the heterogeneous nucleation occurs. Therefore, the value of n obtained is reasonable.

The physical meaning of τ is that it equals the time at which the total volume of the precipitation is rising from effectively zero to its equilibrium value.

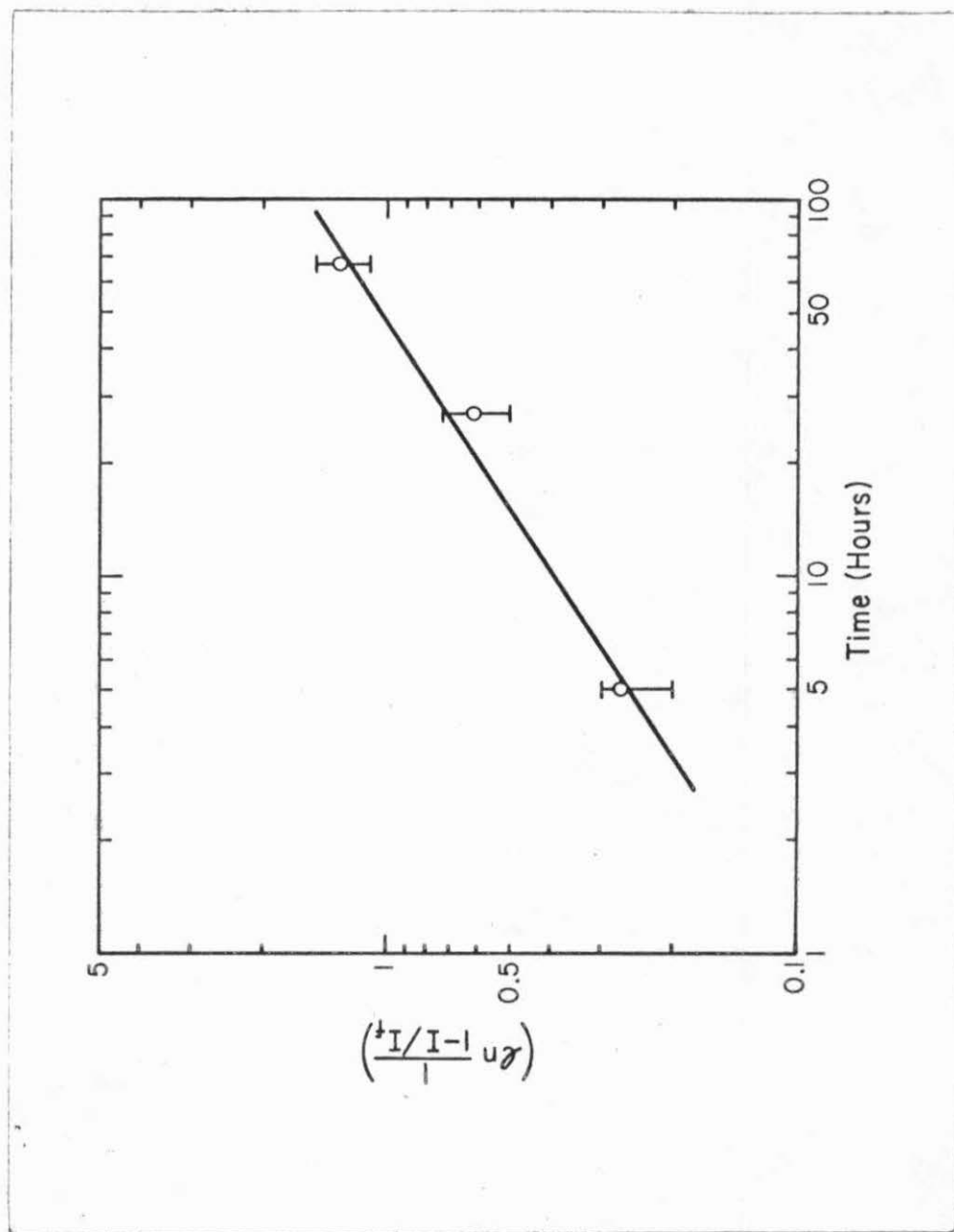


Fig. 57. $\log\left(\frac{1}{1 - I/I_f}\right)$ versus annealing time for the quenched $\text{Ag}_{97}\text{Pb}_3$ alloy annealed at 200°C .

2. The precipitation process of the phase from the Ag-Pb supersaturated solid solution

The growth of the Pb precipitate at two different annealing temperatures for the quenched $\text{Ag}_{97}\text{Pb}_3$ samples, as shown in Fig. 38, can be explained in the ordinary way.⁽⁴⁰⁾ The size of the precipitations normally grows very fast in the first stage of growth in which the precipitation process was governed by the nucleation and growth processes. At longer aging times, when the equilibrium volume fraction is approached, growth of the particle can only take place by the selective coarsening process termed Ostwald ripening.^(41, 42) This Ostwald ripening process required that the solute has some solubility in the solvent. This process arises because of the Gibbs-Thompson effect,⁽⁶⁷⁾ which requires that the concentration of solute in the solvent phase adjacent to a small particle is higher than that in a region adjacent to a larger particle. There is thus a diffusional flow of solute in the matrix from small particles to large particles, and this flux is maintained by the progressive dissolution of the small particles. The net driving force for the reaction is the decrease in the solute-solvent interface area, and hence, in the surface-free energy with this approximation the total amount of precipitation remains constant.

For quenched $\text{Ag}_{97}\text{Pb}_3$ samples annealed at 200°C , the equilibrium volume reached for annealing time t approaches the value of τ which is 50 hours in this case, as obtained from the last section. Therefore, before 50 hours the growth of the particle was dominated by the nucleation and growth process. As $t > 50$ hours, the growth

of the particle can only take place by the Ostwald ripening process which requires Pb to have some solubility in Ag. At 200°C the solubility of Pb in Ag is less than 0.1 at. %. This makes the Ostwald ripening process nearly impossible. Therefore, the growth of the size of the precipitated particles stops.

For quenched $\text{Ag}_{97}\text{Pb}_3$ samples annealed at 300°C, the equilibrium volume is reached in a very short time, namely, $t = 20$ minutes. With annealing time shorter than this value, the growth of the particle was dominated by the nucleation and growth process. The size of the precipitate at which the equilibrium volume is reached is higher for samples annealed at 300°C. ⁽⁶⁸⁾ As $t > 20$ minutes, the growth of the particle by the Ostwald ripening process is possible because at 300°C the solubility of Pb in Ag is about 0.8 at. %. Therefore, it can be observed that the particle keeps growing until $t = 10$ hours. Grain boundaries can provide nucleation sites for the Pb which will precipitate there and eventually grow by the Ostwald process.

After $t > 10$ hours, the Pb precipitate was found to form a continuous path along the grain boundary. In fact, it is sometimes completely surrounding the grain. Therefore, it is hard to define the size of the precipitate. That is why the growth of the size of the precipitation stops. This phenomenon is also supported by the fact that all samples annealed longer than 10 hours show the continuous filamentary effect of Pb in the measurements of their superconducting properties.

It is expected, and was observed experimentally, that the distribution of defects, dislocations, and nuclei are uniformly distributed through the sample in the as-quenched state. From the kinetics of the transformation analysis given in the last section, it was concluded that after annealing, the heterogeneous nucleation occurs in these quenched samples. This heterogeneous precipitation can therefore explain why the uniform precipitation, as in Fig. 33, can occur in the quenched $\text{Ag}_{100-x}\text{Pb}_x$ samples, $1 \leq x \leq 3$, annealed at 200°C for various times and at 300°C for less than 10 hours. For quenched samples annealed at 300°C for longer than 10 hours but less than 50 hours, discontinuous filaments of Pb along the grain boundary sometimes occur. Therefore, the proximity effect in these samples can still exist. After annealing more than 50 hours, nearly all the filaments of Pb joined together, so the filamentary effect always dominated in the superconducting properties of the sample.

V. SUMMARY AND CONCLUSIONS

The results of this investigation can be summarized as follows:

- (1) The solid solubility of Pb in Ag can be extended from less than 0.1 at. % to 3.2 at. % by quenching from the liquid state.
- (2) After heat treatment, the precipitation process of Pb in Ag was found to be heterogeneous and diffusion-controlled.
- (3) Three-dimensional proximity effects can be observed and controlled in quenched $\text{Ag}_{100-x}\text{Pb}_x$ samples, $1 \leq x \leq 3$, which were annealed at 200°C and 300°C for various times. The best composition to observe the proximity effect was found to be $x = 3$.
- (4) The superconducting transition temperature of samples which show the proximity effect increases from below 1.2°K to 7.2°K as the average size of the precipitated particles increases from zero to $2\ \mu\text{m}$. This effect can be qualitatively explained by the theoretical calculation developed by Silvert and Singh⁽³⁷⁾.
- (5) The temperature dependence of the critical current at a given external magnetic field for samples which show the proximity effect is dominated by a term, $\exp(KT^{\frac{1}{2}})$, where K is a factor proportional to $\ell^{-\frac{1}{2}} \times 2b$, T is the temperature, ℓ is the mean free path, and $2b$ is the average interparticle distance. This fact can be explained by a simple model in which the Cooper pair amplitude in the normal metal (Ag) is in the form of a damped spherical wave.
- (6) The magnetic field dependence of the critical current at a given temperature is found to be proportional to $(\frac{1}{H} - B)$, in which H is the applied magnetic field and B is a constant which depends only on the average size of the precipitated particles. This behavior can be de-

rived by summing over the Josephson supercurrent from all the small SNS junctions in the alloy, and the modification of the order parameter at the Pb side of the Pb-Ag interface by the applied magnetic field.

(7) The superconducting volume fraction was observed to be larger than the physical volume of Pb in the alloy. This result shows that the Meissner effect can appear in the normal region (Ag) of the alloy as in the case of layer structures.

(8) At a given temperature, the logarithm of the critical magnetic field is proportional to $\ln^{-\frac{1}{2}} \times 2b$. This fact can be explained by the theory of proximity effect.

(9) The superconducting volume fraction was found to be proportional to the critical current. This indicates that the increase in the critical current with the decreasing temperature or magnetic field is due to the increase in the superconducting volume in the sample.

(10) The Hilsch empirical relations [Equations (4.42) and (4.43)] were applied to estimate the interaction parameter NV in Ag. The NV value obtained is approximately 0.06, which corresponds to a superconducting transition temperature for Ag of the order of 10^{-5} °K. This value is in satisfactory agreement with other determinations made on vapor-deposited metallic film sandwiches. Hence, the Hilsch empirical relation valid for layer structure is also applicable to the three-dimensional case.

References

1. J. Bardeen, L. N. Cooper, and J. R. Schrieffer, Phys. Rev. 108, 1175 (1957).
2. P. G. de Gennes and E. Guyon, Phys. Letters, 3, 168 (1963)
3. P. G. de Gennes, Rev. Mod. Phys. 36, 225 (1964).
4. G. Deutscher and P. G. de Gennes, in Superconductivity, edited by R. D. Parks (Marcel Dekker, New York, 1969), vol. 2, Chap. 17.
5. B. D. Josephson, Phys. Letters, 1, 251.
6. B. D. Josephson, Rev. Mod. Phys., 36, 216.
7. B. D. Josephson, Adv. Phys. 14, 419.
8. J. E. Zimmerman and J. E. Mercereau, Phys. Rev. Letters, 14, 887.
9. J. Clarke, Phil. Mag. 13, 115 (1966).
10. P. G. de Gennes, Superconductivity of Metals and Alloys, page 234.
11. H. Meissner, Phys. Rev. 117, 672 (1960).
12. P. Hilsch, Z. Physik 167, 511 (1962).
13. R. H. Parmenter, Phys. Rev. Letters, vol. 7, no. 7, p. 274 (1961).
14. Paul H. Smith et al., Phys. Rev. Letters, vol. 6, no. 12, p. 686 (1961).
15. D. H. Douglass, Jr., Phys. Rev. Letters, vol. 9, no. 4, p. 155 (1962).
16. H. R. Werthamer, Phys. Rev., vol. 132, no. 6, p. 2440 (1963).

References (Cont'd)

17. J. J. Hauser et al., *Phys. Rev.*, vol. 136, no. 3A, p. A637 (1964).
18. J. J. Hauser et al., *Phys. Rev.*, vol. 142, no. 1, p. 118 (1966)
19. J. P. Burger et al., *Phys. Letters*, vol. 17, no. 3, p. 180 (1965).
20. P. G. de Gennes and J. P. Hurault, *Phys. Letters*, vol. 17, no. 3, p. 181 (1965).
21. G. Fischer, R. Klein and J. P. McEvoy, *Phys. Letters*, vol. 19, no. 3, p. 193 (1965).
22. J. Clarke, *J. de Physique*, Colloque C2, p. C2-3 (1968).
23. J. P. Burger, *J. de Physique*, Colloque C2, p. C2-17 (1968).
24. F. Meunier, *J. de Physique*, Colloque C2, p. C2-21 (1968).
25. H. T. Yeh, *Ann. Phys.*, vol. 46, p. 546 (1968).
26. H. E. Jacobs, *Phys. Rev.*, vol. 162, no. 2, p. 375 (1967).
27. W. L. McMillan, *Phys. Rev.*, vol. 175, no. 2, p. 559 (1968).
28. J. Clarke, *Proc. Roy. Soc. A* 308, p. 447 (1969).
29. J. Clarke et al., *Solid State Comm.*, vol. 11, p. 689 (1972).
30. G. Deutscher et al., *Phys. Rev. B*, vol. 8, no. 11, p. 5055 (Dec. 1973).
31. J. P. Romagnan, A. Gilabert and J. C. Noiray, *Solid State Comm.*, vol. 14, p. 83 (1974).
32. A. Martinet, Thesis (1966).
33. C. J. Adkins and B. W. Kington, *Phys. Rev.* 177, 777 (1969).

References (Cont'd)

34. Pol Duwez and R. H. Willens, *Trans. AIME*, 227, p. 362 (1962).
35. P. Pietrokowski, *J. Sc. Instrum.*, 34, p. 445-6 (1962).
36. Ch. J. Raub and Z. Raub, *Z. Physik* 186, 1, 210 (1965).
37. W. Silvert and A. Singh, *Phys. Rev. Letters*, vol. 28, no. 4, p. 222 (1972).
38. C. C. Tsuis and L. R. Newkirk, *J. Mat. Sci.* 8, p. 1307-1314 (1973).
39. J. F. Allen, *Phil. Mag.* 16, p. 1005 (1933).
40. See for example, M. Jovanović, *Fizika* 2, Suppl. 2 (1970).
41. C. Wagner, *Z. Electrochem.*, 65, 581, (1961).
42. J. M. Lifshitz and V. V. Slyozov, *J. Phys. Chem. Solids*, 19, 35, (1961).
43. P. Morel and P. W. Anderson, *Phys. Rev.* 125, 1263, (1962).
44. L. P. Garkov, *JETP (U.S.S.R.)* 37, 1407 (Trans. 1960 JETP 10, 998).
45. C. Carols, P. G. de Gennes, and J. Matricon, *J. Phys. Rad.*, 23, 707 (1962).
46. B. T. Matthias, T. H. Gaballe, and V. B. Compton, *Rev. Mod. Phys.* 35, p. 1-22 (1963).
47. J. Bardeen and J. R. Schrieffer, *Progress in Low Temperature Physics*, Vol. III (ed. C. J. Torter), Amsterdam, North-Holland.

References (Cont'd)

48. G. Deutscher, Solid State Comm. 9, 891 (1971).
49. G. Deutscher, P. Lindenfeld and S. Wolf, Phys. Rev. Lett. 23, 1102 (1969).
50. J. M. Rowell, Phys. Rev. Lett., 11, 200.
51. P. W. Anderson, Lectures on the many-body problem (ed. E. R. Caianiello) New York and London, Academic Press (1964).
52. R. A. Ferrell and R. E. Prange, Phys. Rev. Lett. 10, 479.
53. P. Ramachandrarao, M. G. Scott, and G. A. Chadwick, Phil. Mag. 25, 961 (1972).
54. R. K. Linde, Trans. of the Metallurgical Society of AIME 236, p. 58-64 (1966).
55. A. C. Rose-Innes and B. Serin, Phys. Rev. Lett. 7, 278 (1961).
56. See for example, C. Kittel, Introduction to Solid State Physics 4th ed. 1970.
57. A. B. Pippard, Rept. Prog. Phys. 23, 176 (1960).
58. D. Douglas, Jr., IBM J. Res. Develop., 6, 47 (1962).
59. W. A. Harrison, Solid State Theory, McGraw Hill Inc. (1970).
60. J. M. Ziman, Physics of Solids, 2nd ed. (1972).
61. J. A. Osborn, Phys. Rev. 67, 351 (1945).
62. E. C. Stoner, Phil. Mag. 36, 803 (1945).
63. W. A. Johnson and R. F. Mehl, AIME Trans., vol. 135, p. 416-58 (1939).

References (Cont'd)

64. J. Burke, *Phil. Mag.*, 6, 1439 (1961).
65. C. A. Wert and C. Zener, *J. Appl. Phys.*, 21, 5 (1950).
66. R. Bullough and R. C. Newman, *Phil. Mag.*, 6, 403 (1961).
67. R. W. Cahn, *Physical Metallurgy*, 2nd ed. (1970).
68. A. H. Cottrell, *Theoretical Structural Metallurgy*, 2nd ed. (1955).
69. C. Syryanarayana and T. R. Anantharaman, *J. of Material Sciences* 5, pp. 992-1004 (1970).
70. C. Valette, Thesis (Orsay, 1971) (unpublished).
71. G. Deutscher and C. Valette, in *proc. of the 13th International Conference on Low Temp. Physics, Boulder, Colo., 1972*, ed. by R. H. Kropschot and K. D. Timmerhaus (Univ. of Colorado Press, Boulder, Colo., 1973).
72. E. Krätzig, *Solid State Comm.* 9, 1205 (1971).

APPENDIX 1

Dimensional Dependence of the Volume Fraction of the
Superconducting Element for a Given Critical Current
Density Induced by the Proximity Effect

The advantage of using higher dimensions in minimizing the volume fraction of the superconducting element in the sample with a given critical current density can be demonstrated by a special example shown in Fig. 58. In this figure, the size of the superconducting elements is fixed, with a constant value a . In the one-dimensional case, the size is defined as the width of the superconducting element. In the two-dimensional case, it is defined as the diameter of the superconducting cylinder. And in the three-dimensional case, it is defined as the diameter of the superconducting sphere. The minimum distance between two superconductors is always $2a$, because the critical current density induced by the proximity effect is a function of the minimum distance between superconductors only, at $T \ll T_{cs}$, where T_{cs} is the superconducting transition temperature of the superconductor (S). Thus, in Figs. 58(a), (b), and (c), the critical current density should be the same at a given temperature. However, the volume fraction of the superconducting element, as seen in Fig. 58, is completely different. In the one-dimensional case, it can be seen that the volume of the superconducting element (V_S) versus the total volume of the sample (V_{S+N}) is 50 per cent. In the two-dimensional case, this ratio decreases to

$$\frac{V_S}{V_{S+N}} = \frac{\pi \left(\frac{a}{2}\right)^2}{(3a)^2} \cong 8.7 \text{ percent ;}$$

and in the three-dimensional case, the ratio is only

$$\frac{V_S}{V_{S+N}} = \frac{\frac{4}{3} \left(\frac{a}{2}\right)^3}{(3a)^3} \cong 1.94 \text{ per cent.}$$

In the real world, the example in Fig. 58 may be somewhat idealized. In a real sample, the distance between superconducting particles in the two- and three-dimensional cases may be different, and the size of the superconducting particles may not be the same as in the case of the present investigation. The V_S/V_{S+N} ratio may be somewhat higher than the value obtained by assuming equal particle size and interparticle distance, but at least Fig. 58 demonstrates that there is a definite advantage in using higher dimensionality to achieve the minimization of the superconducting element used.

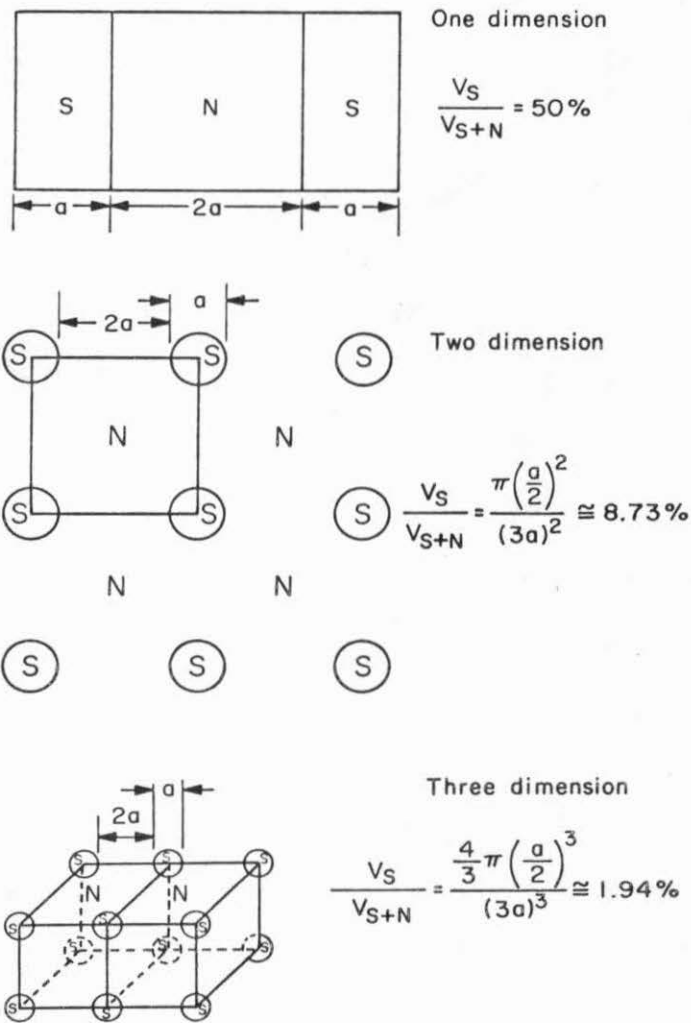


Fig. 58. Demonstration of the effect of dimensionality in minimizing the amount of superconducting element without decreasing the critical current density.

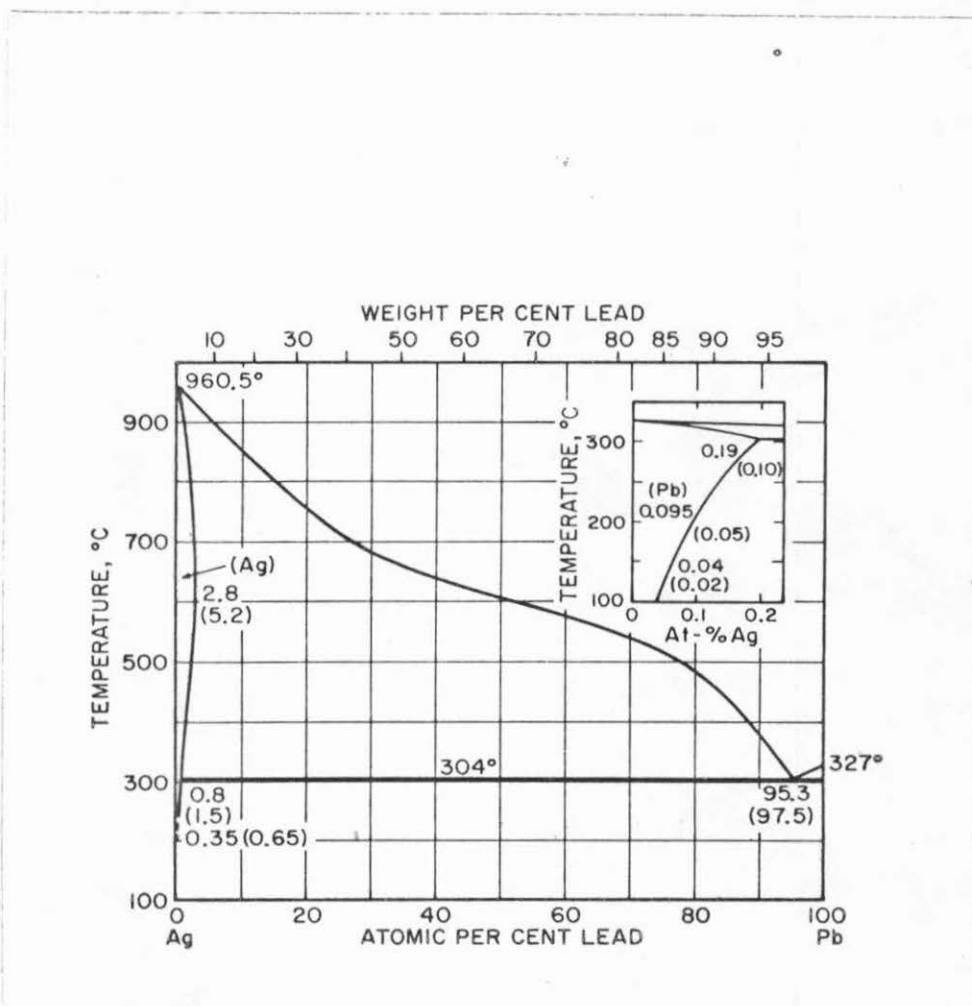


Fig. 59. Phase diagram of the Ag-Pb binary system.